Universidade do Minho
Escola de Ciências

Sónia Catarina Silva Pinto

BODIPY derivatives: design, synthesis, and evaluation as chemosensors, probes for bioimaging, and photosensitizers for PDT

December 2021

BODIPY derivatives: design, synthesis, and evaluation as chemosensors, probes for bioimaging, and photosensitizers for PDT
Sónia Catarina Silva Pinto

UMinho | 2021


FCT
Fundação para a Ciência e a Tecnologia
PORTUGAL
2020
UNIÃO EUROPEIA
Fundo Europeu de
Desenvolvimento Regional
NORTE
2020

Universidade do Minho
Escola de Ciências

Sónia Catarina Silva Pinto

BODIPY derivatives: design, synthesis, and evaluation as chemosensors, probes for bioimaging, and photosensitizers for PDT

Master Thesis
Master in Chemical Analysis and Characterization Techniques

Work done under the supervision of
Professor Maria Manuela Marques Raposo
and
Professor João Manuel Ferreira Pita Batista Pina

December 2021

DIREITOS DE AUTOR E CONDIÇÕES DE UTILIZAÇÃO DO TRABALHO POR TERCEIROS

ACKNOWLEDGMENTS

The accomplishment of this project would not be possible without the help of several people who, directly or indirectly, were essential for the elaboration of this dissertation.

Firstly, I would like to thank Professor Manuela Raposo and Professor Susana Costa who have accompanied me since my first steps in research. I appreciate the opportunity to carry out this complete and diversified project, which contributed to my professional and personal growth. I am grateful for the knowledge and help provided and for their support and encouragement, which always motivated me all over these years.

I would like to thank the Department of Chemistry / Chemistry Center at the University of Minho, for allowing this project to be carried out in their laboratories, and the Fundação para a Ciência e Tecnologia (FCT) for funding the project where this work was inserted, project PTDC/QUI-COL/28052/2017.

I would like to thank Professor João Pina and Doctor Lígia Silva, for their willingness to welcome me to the University of Coimbra to perform the photophysical and biological studies. I am very grateful for the support, the time spent, and the countless lessons that allowed me to enrich this project. These were months of inspiration and full of learning.

I would like to thank Doctor Manuel Bañobre-López, Doctor Juan Gallo, and AmTheNa group, for their welcome to the International Iberian Nanotechnology Laboratory and the opportunity to perform biological studies. Special thanks to Milene for monitoring these studies and sharing her knowledge.

I would like to thank Dr. Elisa Pinto for her commitment to preparing NMR spectra.

I would also like to thank all my laboratory colleagues for the pleasant work environment provided and for the help given when I needed it most, especially to Raquel Rainha, who accompanied me in this project and helped me tirelessly.

A very special thank you to my parents, who are my inspiration and without them, I would never have achieved everything I have achieved so far. Thank you for the love, for the good mood, for the motivating words that always gave me strength in all stages of my life, and, mainly, for believing in me like no one else.

A sincere thank you to everyone for having contributed to another great step of my life.

STATEMENT OF INTEGRITY

I hereby declare having conducted this academic work with integrity. I confirm that I have not used plagiarism or any form of undue use of information or falsification of results along the process leading to its elaboration. I further declare that I have fully acknowledged the Code of Ethical Conduct of the University of Minho.

ABSTRACT

BODIPY derivatives: design, synthesis, and evaluation as chemosensors, probes for bioimaging, and photosensitizers for PDT

4,4-Difluoro-4-bora-3a,4a-diaza-*s*-indacene derivatives, commonly referred as BODIPYs, constitute a class of fluorophores that has been arousing great curiosity in the scientific community. The excellent photophysical properties, the accessible synthesis, and the chemical versatility of BODIPY derivatives explain the growing interest in this class of compounds in recent years, as well as its demand for application in the most diverse areas of research.

Thus, this dissertation was based on several objectives: the design, synthesis, and photophysical characterization of BODIPY derivatives functionalized with distinct groups at the *meso* position of the BODIPY core and the evaluation of the capacity of these compounds for different applications, namely, as optical chemosensors, fluorescent probes for bioimaging, aggregation-induced emission (AIE) fluorophores and photosensitizers for photodynamic therapy.

In order to evaluate the application of these derivatives as optical chemosensors, spectrofluorimetric titrations were carried out in the presence of Pd^{2+}, Hg^{2+}, Fe^{3+}, and Al^{3+}, since the preliminary study of sensing capacity revealed a selectivity for these cations. On the other hand, the potential application as a fluorescent probe in bioimaging was evaluated in HeLa cancer cells using fluorescence techniques and confocal microscopy, with promising results. In the evaluation as a AIE fluorophore, the influence of solvent polarity on the spectroscopic and photophysical properties of one of the BODIPY derivatives under study and its emissive behavior in the aggregation state in an aqueous medium was also studied. Finally, for potential application as a photosensitizer for photodynamic therapy, the sensitization of singlet oxygen in solution was evaluated by spectroscopy, and the internalization and cytotoxicity performance of one BODIPY derivative was studied in 4T1 cancer cells using fluorescence techniques and flow cytometry, giving promising results.

Keywords: AIE Fluorophores, Bioimaging, BODIPY, Optical Chemosensors, Photodynamic therapy.

RESUMO

Derivados de BODIPY: *design*, síntese e avaliação como sensores químicos, sondas para bioimagem e fotossensibilizadores para PDT

Os derivados de 4,4-difluoro-4-bora-3a,4a-diaza-*s*-indaceno, designados usualmente como BODIPYs, constituem uma classe de fluoróforos que tem vindo a despertar grande curiosidade na comunidade científica. As ótimas propriedades fotofísicas, a síntese acessível e a versatilidade química dos derivados de BODIPY explicam o crescente interesse por esta classe de compostos nos últimos anos bem como a sua procura para aplicação nas mais diversas áreas de investigação.

Assim, esta dissertação baseou-se em vários objetivos: o *design*, síntese e caraterização fotofisica de novos derivados de BODIPY e a avaliação da capacidade destes compostos para diversas aplicações, nomeadamente, como sensores químicos óticos de iões, sondas fluorescentes para bioimagem, fluoróforos com emissão induzida por agregação (AIE) e fotossensibilizadores para terapia fotodinâmica.

Com o objetivo de avaliar a aplicação destes derivados como sensores químicos óticos, efetuaram-se titulações espetrofluorimétricas na presença de Pd^{2+}, Hg^{2+}, Fe^{3+} e Al^{3+}, uma vez que o estudo preliminar de capacidade sensora revelou seletividade para estes catiões. A potencial aplicação como sonda fluorescente em bioimagem foi avaliada em células cancerígenas HeLa recorrendo a técnicas de fluorescência e microscopia confocal, tendo-se obtido resultados promissores. Na avaliação como fluoróforos AIE, estudou-se a influência da polaridade do solvente nas propriedades espectroscópicas e fotofísicas de um dos derivados em estudo bem como o seu comportamento emissivo no estado de agregação em meio aquoso. Por fim, tendo como objetivo a aplicação como fotosensibilizador para terapia fotodinâmica avaliou-se a sensibilização de oxigénio singleto em solução por espetroscopia e a capacidade de internalização e a citotoxicidade de um derivado de BODIPY num estudo com células cancerígenas 4T1 recorrendo a técnicas de fluorescência e citometria de fluxo, tendo-se obtido resultados promissores.

Palavras-chave: Bioimagem, BODIPY, Fluoróforos AIE, Sensores óticos, Terapia fotodinâmica.

CONTENTS

LIST OF ABBREVIATIONS, ACRONYMS, AND SYMBOLS

AAS	Atomic absorption spectroscopy
Abs	Absorbance
ACN	Acetonitrile
ACQ	Aggregation-caused quenching
AIE	Aggregation-induced emission
a.u.	Arbitrary units
BDP	BODIPY
BODIPY	4,4-Difluoro-4-bora-3a,4a-diaza-*s*-indacene
BSA	Bovine serum albumin
CE	Capillary electrophoresis
CHEF	Chelation enhancement of fluorescence
CHEQ	Chelation enhancement of quenching
CT	Charge transfer
d	Duplet
DCM	Dichloromethane
DDQ	2,3-dichloro-5,6-dicyano-*p*-benzoquinone
dH_2O	Distilled water
DME	Dimethoxyethane
DMEM	Dulbecco's modified eagle's medium

DMSO	Dimethylsulfoxyde
eqv	Equivalent
ESI	Electrospray ionization
FBS	Fetal bovine serum
FLIM	Fluorescence lifetime imaging microscopy
FRET	Fluorescent resonance energy transfer
HeLa	Human cervical cancer epithelial cell line
HMBC	Heteronuclear multiple bond correlation
HMQC	Heteronuclear multiple quantum correlation
HOMO	Highest occupied molecular orbital
HPS	Hexaphenylsilole
IC	Internal conversion
ICP-MS	Mass spectroscopy coupled with inductive plasma
ICT	Intramolecular charge transfer
IC_{50}	Half maximal inhibitory concentration
ISC	Intersystem crossing
J	Coupling constant
LE	Locally excited state
LED	Light-emitting diode
LUMO	Lowest unoccupied molecular orbital

m	Multiplet
MCF-7	Human breast cancer cell line
MFI	Mean fluorescence intensity
mSLN	Magnetic solid lipid nanoparticles
MTR	MitoTracker® Deep Red FM
m/z	Mass to charge ratio
NIR	Near-infrared
NMR	Nuclear magnetic resonance
ns	Not significant
OLEDs	Organic light-emitting diodes
PBS	Phosphate-buffered saline
PDI	Photodynamic inactivation
PDT	Photodynamic therapy
PET	Photoinduced electronic transfer
PS	Photosensitizer
RIM	Restriction of intramolecular movement
RIR	Restriction of intramolecular rotation
RIV	Restriction of intramolecular vibration
ROS	Reactive oxygen species
RPMI	Roswell Park Memorial Institute

r.t.	Room temperature
s	Singlet
S_EAr	Aromatic electrophilic substitution
SLN	Solid lipid nanoparticles
S_NAr	Aromatic nucleophilic substitution
S_N	Nucleophilic substitution
TEA	Triethylamine
TFA	Trifluoroacetic acid
THF	Tetrahydrofuran
TICT	Twisted intramolecular charge transfer
TLC	Thin-layer chromatography
TPA	Triphenylamine
TPAN	2,3,3-Triphenylacrylonitrile
TPE	Tetraphenylethylene
TPPy	Tetraphenylpyrazine
TPPh	Triphenylphosphine
TPPo	Tetraphenylporphyrin
UV	Ultraviolet
UV-vis	Ultraviolet–visible
^{13}C NMR	Carbon 13 nuclear magnetic resonance

^{1}H NMR	Proton nuclear magnetic resonance
4T1	Mouse breast cancer cell line
δ	Chemical shift
ε	Molar absorption coefficient
ϕ_F	Relative quantum fluorescence yield
ϕ_Δ	Singlet oxygen quantum yield
Δ_{ss}	Stokes' shift
λ_{em}	Emission wavelength
λ_{abs}	Absorption wavelength
λ_{exc}	Excitation wavelength

LIST OF FIGURES

LIST OF SCHEMES

LIST OF TABLES

SCIENTIFIC COMMUNICATIONS/PROCEEDINGS

Part of the work developed during this dissertation gave rise to national and international communications and a proceeding in an international congress:

Proceeding in international congress

Pinto, S. C. S.; Gonçalves, R. C. R.; Costa, S. P. G.; Raposo, M. M. M. Synthesis and characterization of a *meso*-anthracene-BODIPY derivative for colorimetric recognition of Cu^{2+} and Fe^{3+}. Proceedings of the 24th International Electronic Conference on Synthetic Organic Chemistry. *Chem. Proc.* **2021**, *3*(1), 79. Seijas, J. A. and Tato, M. P. V. (Eds), MDPI, Basel, Switzerland. https://doi.org/10.3390/ecsoc-24-08292

International Poster Communication

Pinto, S. C. S.; Gonçalves, R. C. R.; Pina, J.; Costa, S. P. G.; Raposo, M. M. M. Synthesis and photophysical characterization of BODIPY dyes. Iberian Symposium of Young Photochemists 2021, Virtual Conference: https://isyp.web.uah.es/; 18-22 October 2021.

National Oral Communication

Pinto, S. C. S.; Gonçalves, R. C. R; Silva, M. C.; Gallo, J.; Costa, S. P. G.; Raposo, M. M. M. A fluorescent probe based on a BODIPY derivative to study cellular ingestion and internalization of Solid Lipid Nanoparticles. F16 (Flash oral communication), XXVII Encontro Nacional da Sociedade Portuguesa de Química, Braga, Portugal, 14-16 July 2021.

THESIS OVERVIEW

Motivation and objective of this dissertation

Currently, there is a wide variety of fluorescent organic compounds, but 4,4-difluoro-4-bora-3a,4a-diaza-*s*-indacene, better known as BODIPY, has stood out among the rest. This compound was discovered by Treibs and Kreuzer in 1968, but it was only after the 1980s that it gained greater recognition in the scientific community. In fact, after realizing the potential of this class of compounds in terms of chemical versatility and excellent photochemical and photophysical properties, the design and synthesis of new BODIPY derivatives with the most varied applications grew exponentially.

The search for new multifaceted compounds continues, so the main reason for this thesis was not only the synthesis of new BODIPY derivatives but also the evaluation of their potential for application in the most diverse areas.

Therefore, this dissertation focuses on several objectives: the design, synthesis, and photophysical characterization of BODIPY derivatives functionalized with distinct groups at the *meso* position of the BODIPY nucleus and, additionally, the ability of these compounds to be used in four distinct applications (optical chemosensors, bioimaging probes, AIE fluorophores and photosensitizers for photodynamic therapy).

Dissertation structure

The dissertation presented is divided into five chapters: introduction, experimental section, results and discussion, conclusions and perspectives and references.

Chapter 1 presents the introduction based on a literature review, which supports the work to be developed. In this section, important concepts about the BODIPY derivatives are presented. In a general way, the main characteristics of these derivatives are mentioned, as well as the different synthesis methodologies for the structural modification of the BODIPY core and the consequent photophysical modulation. Furthermore, some applications of these versatile derivatives are presented, accompanied by practical examples from the literature.

Chapter 2 describe the materials and methods used while Chapter 3 presents the experimental results obtained during the work development and the respective interpretation and discussion.

Chapter 4 includes the main conclusions of the developed research as well as suggestions for future work.

Finally, Chapter 5 presents the references cited throughout this work.

Chapter 1

Introduction

1. Introduction

1.1 Synthesis and functionalization of BODIPY derivatives

Research in the field of fluorescent dyes is extensive and there are already several fluorophores such as fluorescein, rhodamine, coumarins, and cyanines with applicability in the most diverse areas. However, currently, the 4,4-difluoro-4-bora-3a,4a-diaza-*s*-indacene, called BODIPY, has deserved greater prominence in the scientific community due to the combination of its remarkable physical-chemical characteristics and ease of synthesis and functionalization. This compound was discovered by Treibs and Kreuzer in 1968 and is evidenced by high molar absorption coefficients (ε), high quantum fluorescence yields (ϕ_F), intense and narrow absorption/emission bands in the visible region of the electromagnetic spectrum, chemical and photochemical stabilities both in solution and in the solid-state. In spectroscopic terms, this compound has maximum absorption and emission wavelengths of approximately 500 nm, but it is an extremely versatile compound in the sense that substituents can be introduced in various positions of the BODIPY core in order to adjust its spectroscopic and photophysical characteristics.[1–3]

Functionalization aims to modify the BODIPY core and, consequently, to modulate its photophysical properties considering the intended applications. The BODIPY core can be obtained through several synthesis routes, which allow the formation of a wide variety of derivatives, from the simplest to the most complex.[4–6]

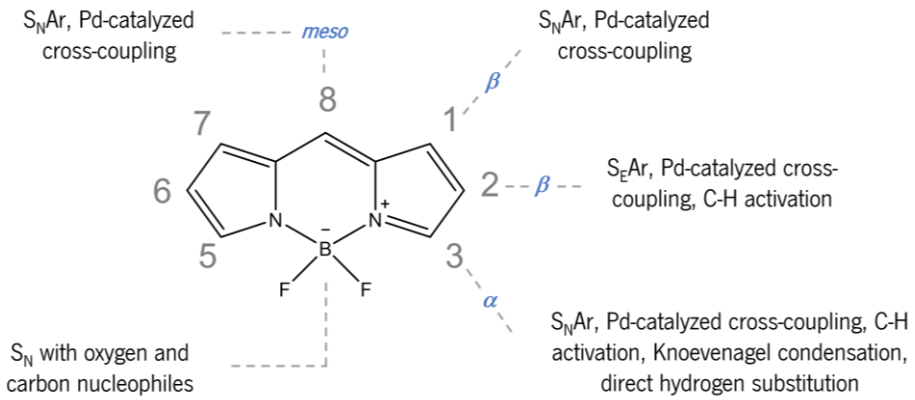

***Figure 1**. Possible chemical reactions for the BODIPY core functionalization. (Figure adapted from reference 5).*

Thus, the BODIPY core can be functionalized at the *meso* (8), α (3 and 5), β (1, 2, 6, and 7) positions and at the central boron atom. The introduction of functional groups in these different positions is achieved through various reactions, such as aromatic electrophilic and nucleophilic substitutions, Suzuki and Sonogashira cross-coupling reactions, Knoevenagel condensations, among others, as illustrated in **Figure 1**.[4–6]

In geometric terms, the aromatic groups inserted at the *meso* position appear twisted concerning the BODIPY core and favor the orthogonal geometry between these two subunits. In this way, the electronic coupling is minimized and, therefore, functionalization in this position has little effect on the variation of absorption and emission wavelengths. In contrast, the functionalization of the *meso* position enabled the improvement of other properties of BODIPY, for example, the increase in water solubility through the introduction of appropriate hydrophilic groups, such as sulfonate and carboxylate. On the other hand, several studies have also been carried out with BODIPY derivatives functionalized with aggregation-induced emission fluorophores at the *meso* position to promote the formation of emissive aggregates in aqueous media.[7,8]

The functionalization of α and β positions of the BODIPY core has been chosen to increase the fluorescence emission and the absorption and emission wavelength once the insertion of suitable substituents in the various positions of the pyrrole allows coplanar geometry between the substituents and the BODIPY core and maximizes electronic coupling. Thus, the halogenation of positions 2 and 6 is one of the strategies to achieve greater absorption and emission wavelengths (**Figure 2**).[7–10]

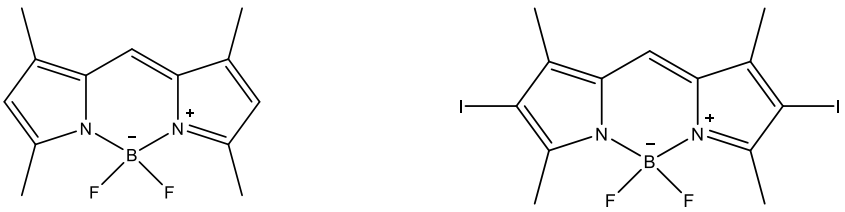

EtOH

λ_{abs} 505 nm

λ_{em} 516 nm

MeOH

λ_{abs} 534 nm

λ_{em} 548 nm

***Figure 2**. Red shift of the maximum absorption and emission wavelength caused by iodine substitution in the BODIPY core. (Figure adapted from reference 10).*

Nevertheless, the most usual strategy has been the introduction of aromatic substituents at positions 3 and 5 of the BODIPY core, simply because it extends the conjugation of the aromatic rings linked to the BODIPY core having a great effect on the photophysical properties of this heterocyclic system. Therefore, the appropriate design of the BODIPY structure leads to longer emission wavelengths, greater quantum fluorescence yields, and greater Stokes' shifts. Besides, the combination of the extension of the conjugation with the introduction of electron donor groups in these same positions causes a more significant bathochromic deviation, reaching the near-infrared (NIR) region of the electromagnetic spectrum (**Figure 3**).[7–9,11]

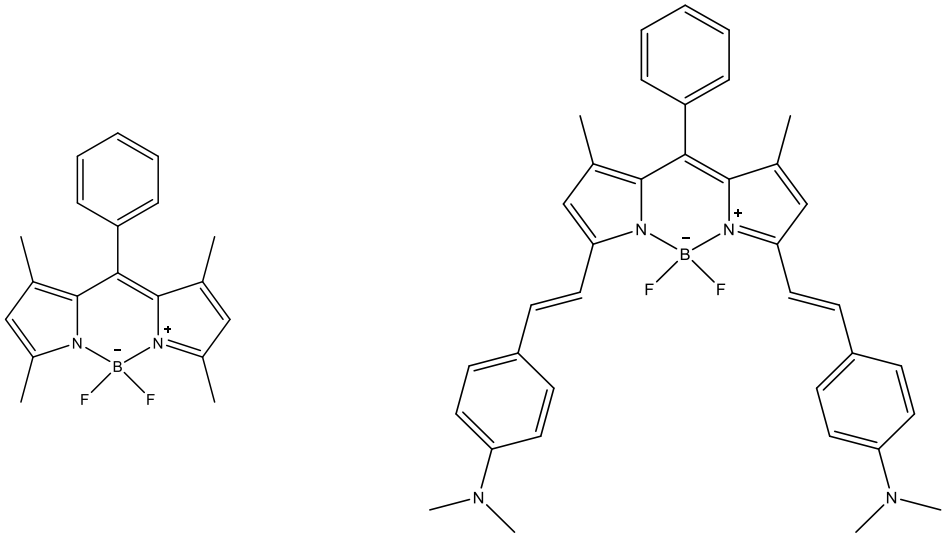

Figure 3. *Variation of the maximum absorption and emission wavelength for the red zone of the electromagnetic spectrum after functionalization at the 3,5-positions and incorporation of electron-donating substituents in the BODIPY core. (Figure adapted from references 8).*

Different and more challenging strategies have been implemented to achieve this same objective, that is, the fusion of aromatic units with pyrrolic rings to increase the emission and absorption wavelengths, once the rotation of the aromatic units is avoided (**Figure 4A**). Aza-BODIPY derivative (B), with a nitrogen atom in place of *meso* carbon, also proved to be a promising option because the non-binding electron pair in the nitrogen atom contributes to reducing the difference of energy between the highest occupied molecular orbital (HOMO) and lowest unoccupied molecular orbital (LUMO) of the BODIPY derivative (**Figure 4B**).[7–9,11–13]

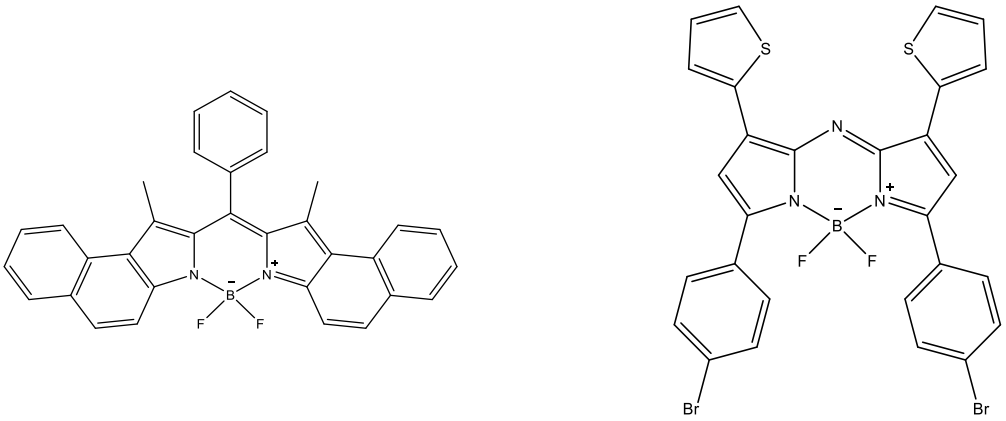

A

CH_2Cl_2

λ_{abs} 630 nm

λ_{em} 640 nm

B

CH_2Cl_2

λ_{abs} 694 nm

λ_{em} 729 nm

Figure 4. *Example of (A) fused BODIPY and (B) aza-BODIPY with maximum absorption and emission wavelength in the red region of the electromagnetic spectrum. (Figure adapted from references 9 and 13).*

Finally, the functionalization of the central boron atom allows the formation of many BODIPY derivatives with modulated properties, such as fluorescent quantum yield, redox behavior, and aggregation behavior, without significantly affecting the spectral maxima of the absorption and emission. Functionalization at this position of the BODIPY core has been one of the strategies to increase the biocompatibility and water solubility of the BODIPY core. For this purpose, solubilization groups and/or bulky groups have been introduced that prevent the aggregation of the BODIPY core and make it more emissive.[7,13]

As it was possible to verify by all the examples mentioned above, there are several hypotheses regarding the modification of the BODIPY core and, consequently, of its spectroscopic properties. It is also important to note that BODIPY derivatives are extremely versatile compounds having in mind that the same substituent gives rise to different spectroscopic properties when introduced in different positions of its core. An example of this statement is presented in **Figure 5**, where the two compounds differ in terms of the functionalization position and the extent of conjugation, highlighted in bold. The compound shown on the left is functionalized at the 3,5 positions and exhibits a greater extension of the π conjugated system, a smaller Stokes' shift, and a higher quantum fluorescence yield compared to the compound on the right, which is functionalized at the 2,6 positions.[8,9]

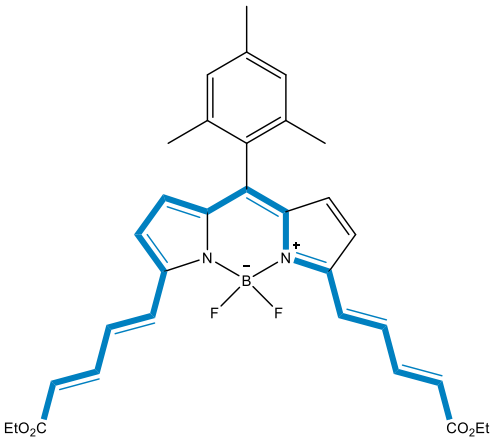

CH_2Cl_2

ϕ_F 0.53

λ_{abs} 641 nm

λ_{em} 651 nm

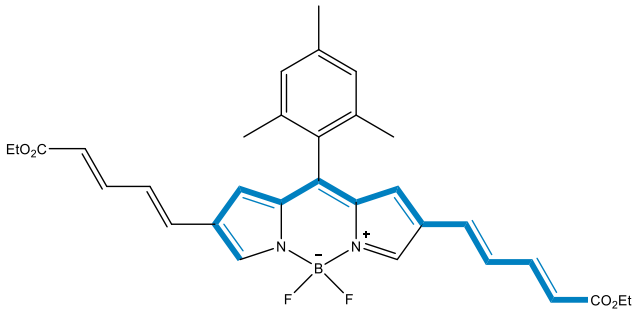

CH_2Cl_2

ϕ_F 0.054

λ_{abs} 633 nm

λ_{em} 662 nm

Figure 5. *Effect of the functionalization and the extent of conjugation on the photophysical properties of BODIPY derivatives. (Figure adapted from reference 9).*

Due to all the excellent physical and chemical properties of BODIPY derivatives, they are widely used as an analytical tool in several scientific areas, namely, as chemosensors for ions [14], probes for bioimaging [15], photosensitizers for photodynamic therapy for cancer treatment [16,17], inactivation of viruses and bacteria [18], components in the manufacture of solar cells sensitized by organic dyes [19], in organic light-emitting diodes (OLEDs) and photovoltaic cells [20,21], among many other applications.

1.2 BODIPY applications

1.2.1 Optical Chemosensors

The classic analytical methods, such as atomic absorption spectroscopy (AAS), mass spectroscopy coupled with inductive plasma (ICP-MS), ion chromatography, electrochemical methods, and capillary electrophoresis (CE), are evidenced by their selectivity and sensitivity in ionic detection, but they are time-consuming techniques that require expensive equipment, sample preparation, and experienced technicians. In this sense, optical chemosensors are a promising alternative concerning classic analytical techniques, as they present numerous advantages, mainly high sensitivity, reduced cost, non-destructive, technical simplicity, and rapid analysis.[22–24]

1.2.1.1 Types of optical chemosensors

An optical chemical sensor is, by definition, an abiotic molecule capable of generating an observable analytical signal after selective and reversible interaction with an analyte. Structurally, this type of sensor incorporates two complementary interconnected subunits. These are the binding subunit, which allows the interaction between the sensor and the analyte, and the signaling subunit, which functions as a transduction element capable of converting the chemical coordination phenomenon into a measurable analytical signal. The interaction of the analyte with the binding subunit causes changes in the photophysical characteristics of the signaling subunit, which allows studying the analyte qualitatively and quantitatively.[22,25]

In general, optical chemosensors allow to carry out analyzes on complex samples selectively, simply, quickly, and in real-time. Due to all these advantages, optical chemosensors have been widely explored and applied in areas such as environmental, medical, and biological. Depending on the nature of the observable optical response, optical chemosensors can be classified as colorimetric or fluorimetric sensors.[26]

Depending on how the two subunits are interconnected and how the binding subunit interacts with the analyte, three optical signaling approaches can be distinguished.

The most common method for developing optical chemosensors is the "bonding subunit - signaling subunit" approach, where the two subunits are connected by a covalent bond or a spacer. In this case, the chemical sensor reversibly interacts with the analyte through non-covalent intermolecular interactions, such as hydrogen bonds, Van der Waals forces, electrostatic interactions, etc. If the analyte is a cation or anion, its interaction with the binding subunit causes electronic changes at the level of the signaling subunit, and variations in color or fluorescence are observed (**Scheme 1**).[27–29]

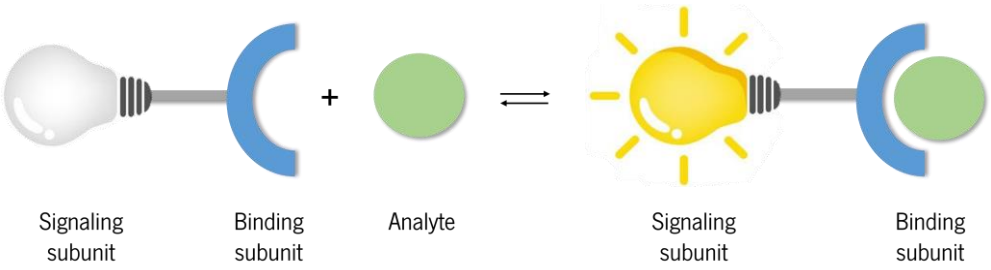

Scheme 1. *Representation of an optical chemosensor based on the "binding subunit - signaling subunit" approach and interaction of the sensor with an analyte. (Scheme adapted from reference 29).*

The "displacement" approach is similar to the previous approach in terms of reversible interaction with the analyte, but it is distinguished by the fact that the binding and signaling subunits are not covalently linked, but rather form a weak coordination complex. In this way, coordination of the analyte with the binding subunit results in the displacement of the signaling subunit accompanied by changes in its optical characteristics. However, for this process to take place, the stability constant of the new binding subunit - analyte complex must be greater than the stability constant of the initial binding subunit - signaling subunit complex (**Scheme 2**).[29–31]

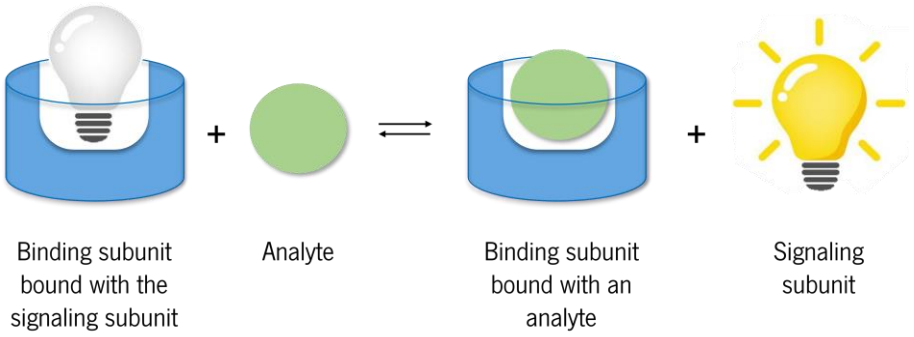

Scheme 2. *Representation of an optical chemosensor based on the "displacement" approach. (Scheme adapted from reference 29).*

Finally, there is the "chemodosimeter" approach, which differs from the two approaches mentioned above in the way that the sensor interacts with the analyte. In this situation, the presence of the analyte in solution causes irreversible chemical reactions, which result in the chemical transformation of the chemodosimeter, therefore forming a new product. For example, as can be seen schematically in **Scheme 3**, the analyte can be covalently linked to the chemodosimeter (**A**) or it can act as a catalyst for a chemical reaction (**B**), always forming a new product with spectroscopic characteristics distinct from the initial chemodosimeter. Therefore, it is designated as a single action sensor that gives rise to an optical response directly related to the concentration of the analyte.[25,28–31]

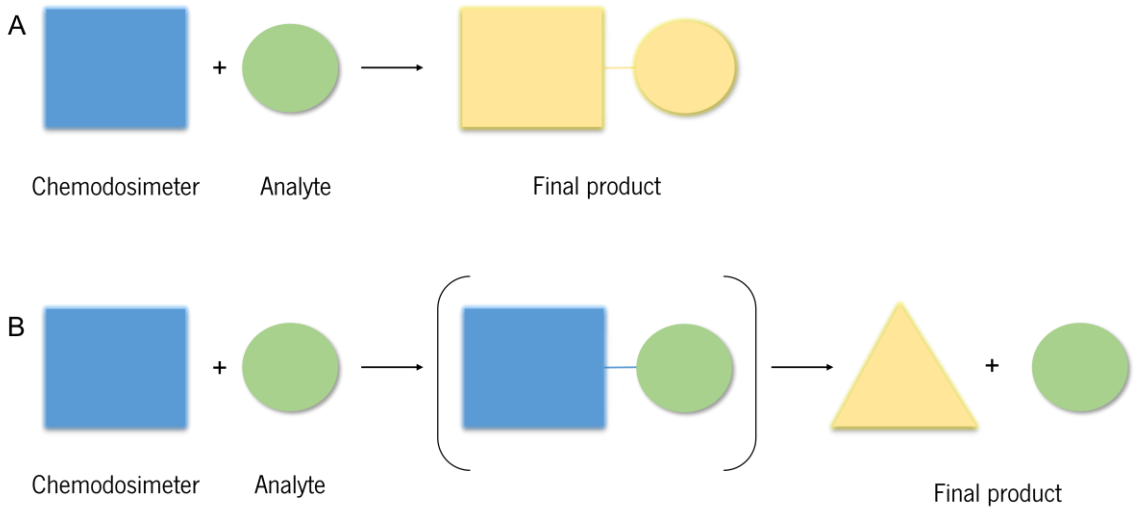

Scheme 3. *Representation of an optical chemosensor based on the "chemodosimeter" approach and possible reactions. (Scheme adapted from reference 29).*

Colorimetric chemosensors

Colorimetric chemosensors generally have, as a signaling subunit, an aromatic system with conjugated π bonds, which is called a chromophore, and a binding unit which is called an ionophore when the analyte in question is an ion. The chromophore, as the name implies, absorbs electromagnetic radiation in the visible region of the electromagnetic spectrum (400 - 700 nm) and is responsible for the color assigned to the compound. In the case of BODIPY derivatives as colorimetric metal ion sensors, the core of BODIPY is the chromophore. As an analytical tool, colorimetric chemosensors stand out for the fact that optical detection can be performed quickly by "naked eye", without the need for any type of auxiliary equipment.[29]

The initial color of the sensor is related to its chemical structure and depends on the energy difference between the LUMO and HOMO orbitals. More precisely, after the interaction with electromagnetic radiation, the compound absorbs energy equivalent to the energy difference of its orbitals and promotes the electronic transition from the fundamental state to the excited state of the molecule. The energy involved in this process corresponds to a specific wavelength of visible light, which gives the compound a characteristic color. Therefore, any variation in the energy difference between the HOMO and LUMO orbitals causes a change in the wavelength of the absorbed visible light and, consequently, in the color of the compound.[26,32]

Increasing the length of the conjugated π system increases the stability of the compound and, consequently, reduces the energy between the HOMO and LUMO molecular orbitals, causing a bathochromic deviation of the absorption band for longer wavelengths. On the other hand, functionalization of the π-bridge by electron donor groups, such as NR_2, NHR, NH_2, OH, OMe, O^-, increases the chromophore's electronic density and stability. In this way, a bathochromic deviation of the absorption band for the red region also occurs. The reverse is true for electron withdrawing groups, such as NO_2, SO_3H, SO_3^-, COOH, which decrease the chromophore's electronic density, its stability and increase the energy interval between the excited state and the ground state. This effect causes a deviation in the position of the chromophore absorption band for shorter wavelengths, that is, for the blue region of the electromagnetic spectrum, being described as a hypsochromic deviation.[26,30,32]

Likewise, the interaction of the analyte with the ionophore causes electronic changes in the chromophore, resulting in a color change in the solution due to the displacement of the absorption band to a different wavelength. If the chromophore has an electron donor group in its structure and there is interaction with an anion, the donor character of that group and the electronic density of the chromophore increase, which intensifies the conjugation and induces a red shift. In contrast, interaction with a cation causes a decrease in the electron donor character and, of course, a blue shift occurs (**Scheme 4**). In the case of functionalization of the chromophore with an electron-withdrawing group instead of a donor group, the opposite effects will occur.[26,29]

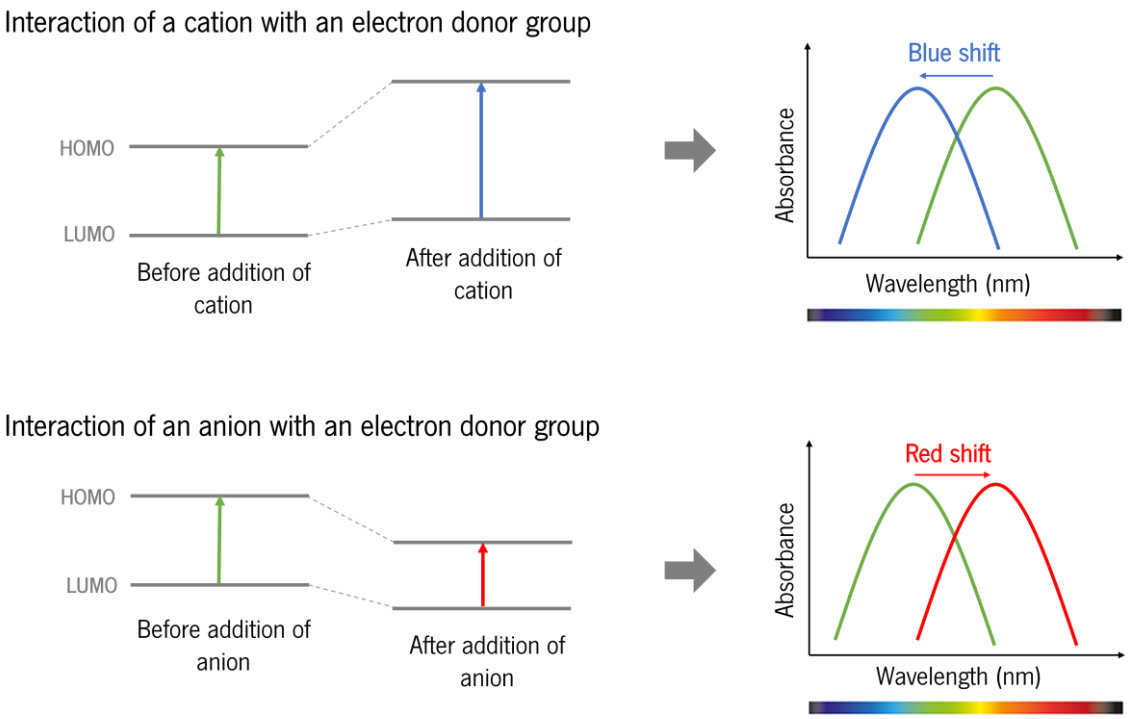

Scheme 4. *Effect of anion/cation interaction with an electron donor group on the chromophore absorption wavelength. (Scheme adapted from reference 26).*

Fluorimetric chemosensors

In terms of analytical technique, fluorometric detection methods stand out from colorimetric methods for their greater selectivity and sensitivity of detection. Optical detection is also achieved quickly and simply with the help of an ultraviolet-visible radiation chamber. Fluorimetric chemosensors have a fluorophore as a signaling subunit and can be characterized as photoluminescent compounds once they emit light after absorbing electromagnetic radiation. In the particular case of BODIPY derivatives, the fluorophore is, usually, the BODIPY core.[29,33]

The Perrin-Jablonski diagram (**Figure 6**) shows the possible electronic transitions in a molecule. Initially, the molecule absorbs a photon, consequently occurring the excitation of electrons from the fundamental state to a higher energy level, which in organic compounds normally consists of the electronic transition π-π^*. After this process, the electron tends to return to the ground state through a process called relaxation accompanied by energy dissipation. Therefore, the excited system can suffer collisions and rotations and cause non-radiative relaxation, as is the example of the internal conversion process, intersystem crossing, and vibrational relaxation, or, on the other hand, the electron can follow a radiative path and cause radiation emission in the form of fluorescence or phosphorescence.[30,32,33]

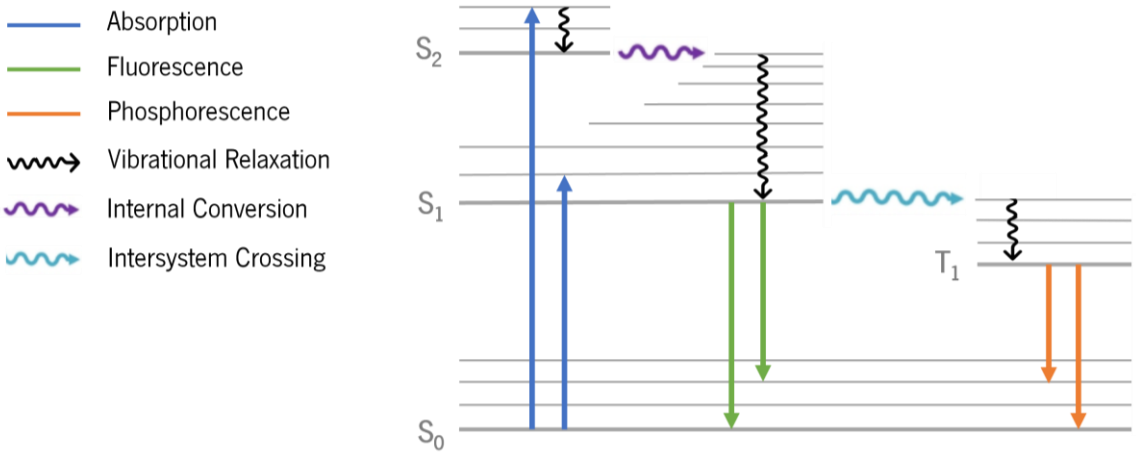

Figure 6. *Perrin-Jablonski diagram. (Figure adapted from reference 32).*

As the name implies, fluorimetric chemosensors are based on the emission of radiation in the form of fluorescence after interaction with the analyte. The concept of fluorescence is characterized by the release of energy between electronic states of the same spin multiplicity, specifically, between the first excited state singlet S_1 and the ground state S_0. Fluorescence emission always occurs at wavelengths greater than that of absorption, once there are energy losses involved in intermediate processes such as internal conversion and vibrational relaxation. The difference between the maximum absorption wavelength and the maximum emission wavelength is called Stokes' shift (**Figure 7**).

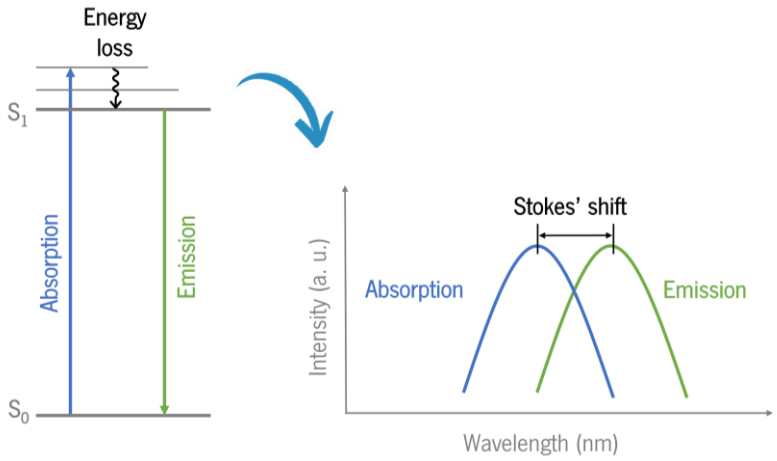

Figure 7. *Stokes' shift. (Figure adapted from reference 33).*

Fluorescence is also characterized by its emission intensity, which defines the emission efficiency of the fluorophore by the quantum fluorescence yield (ϕ_F). The quantum yield defines, more

concretely, the ratio between emitted photons and absorbed photons and, therefore, an ideal fluorescent compound has a quantum yield equal to 1 and a non-fluorescent compound has a quantum yield equal to 0.[32,33]

The interaction between the analyte and the binding subunit (ionophore) of the fluorimetric chemical sensor causes changes in the photophysical properties of the fluorophore and, consequently, produces a quantifiable optical signal. This optical signal can manifest itself through variations in the fluorescence intensity, maximum emission wavelength, and fluorescence lifetime.[34]

The development of fluorimetric sensors is based on different signal transduction mechanisms, such as intramolecular charge transfer (ICT), photoinduced electron transfer (PET), fluorescent resonance energy transfer (FRET), among others. However, PET and ICT are the main fluorescence mechanisms involved in the detection of metal ions by chemical fluorimetric sensors that incorporate BODIPYs. These two processes are differentiated by the type of fluorescent response they produce. In the case of the PET process, there is a change in the fluorescence intensity without pronounced spectral shifts after the analyte coordination, such as an increase in the fluorescence emission (Chelation-Enhanced Fluorescence, CHEF) or fluorescence extinction (Chelation-Enhanced Quenching, CHEQ). In the case of the ICT process, there are clear changes in the emission band of the sensor after the interaction between the sensor and the analyte, with bathochromic or hypsochromic deviations from the maximum emission wavelength.[9,35]

Photoinduced electronic transfer

Fluorimetric sensors based on the PET process normally incorporate a binding subunit and a fluorophore separated by a spacer. In general, the PET process involves the electronic transfer of an electron-rich species to an electron-poor species, caused by the absorption of light. The PET process can be classified as reductive PET or oxidative PET when the binding subunit is an electron donor or withdrawal group, respectively.[8,34]

In the case of the reductive PET process, the binding subunit is an electron donor group, that generally is a heteroatom (N, O, S, and P) with non-binding electron pairs. In electronic terms, reductive PET occurs from the full HOMO orbital of the binding subunit to the excited HOMO orbital of the fluorophore, causing the fluorophore reduction and the oxidation of the binding subunit. Then there is an additional electronic transition from the fluorophore LUMO orbital to the binding subunit orbital and

the stable ground state is thus recovered. Since the HOMO orbital of the binding subunit is located between the fluorophore HOMO and LUMO orbitals, it functions as a non-radiative alternative pathway that prevents normal electronic decay and, consequently, causes fluorescence quenching. Thus, the interaction of the metal ion with the sensor produces an energy decrease of the non-binding electron pair and reduces its HOMO orbital, preventing the PET process. Therefore, the emission from the LUMO orbital to the HOMO orbital of the fluorophore can occur normally and the sensor fluorescence is restored. This PET process is commonly called "turn on" fluorescence, once the analyte interaction with the sensor acts as a kind of switch that causes the fluorescence enhancement. (**Figure 8**).[23,29,30,35]

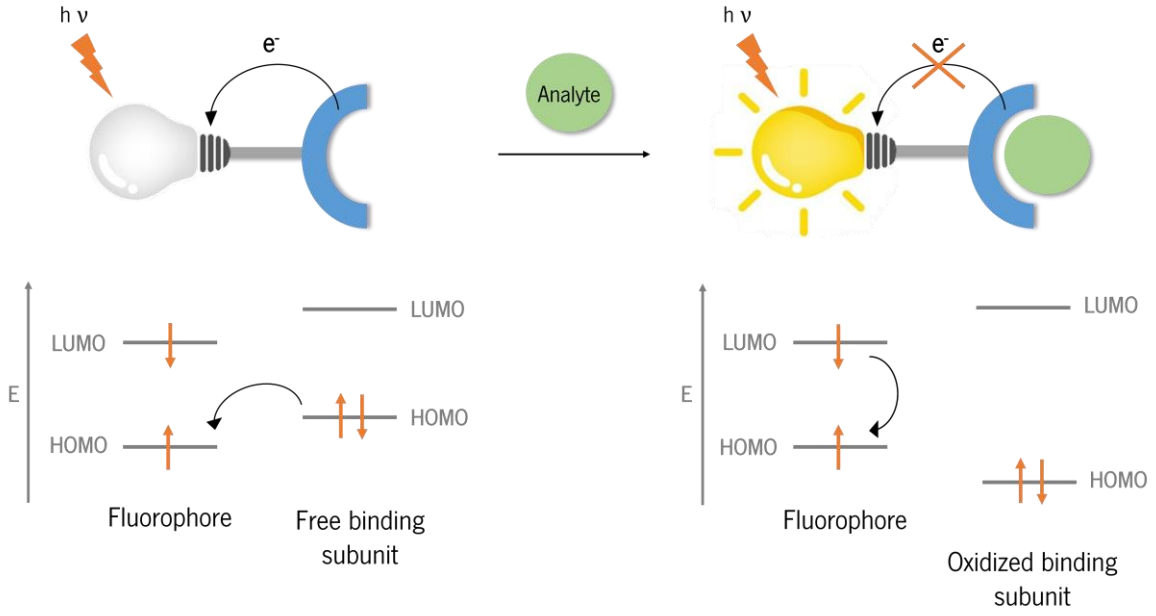

Figure 8. *Representation of fluorescence enhancement preventing the reductive PET process. (Figure adapted from reference 35).*

A practical case reported in the literature is the detection of cadmium ion (Cd^{2+}) mediated by the PET process. For this purpose, a fluorescent chemosensor composed of a BODIPY fluorophore functionalized with a pseudo-crown ether receptor dicarboxylate is used. Initially, the free fluorimetric sensor shows a very weak fluorescence (ϕ_F = 0.057) due to the PET process. This process involves the electronic transfer of the electron-donating amine group to the BODIPY core. After Cd^{2+} addition, there is a dramatic increase in the fluorescence intensity of the compound (ϕ_F = 0.43), which is due to the interaction of the probe with Cd^{2+} and the consequent formation of a complex capable of blocking the PET process. In terms of molecular orbitals, the ionophore HOMO is located between the HOMO and LUMO orbitals of the fluorophore, which leads to the occurrence of the PET process and, as a result, to

a low quantum fluorescence yield of the sensor. However, the coordination of Cd^{2+} with the sensor reduces the ionophore HOMO energy and thus the PET process is prevented. In this way, the probe becomes fluorescent after interaction with the analyte (**Figure 9**).[14]

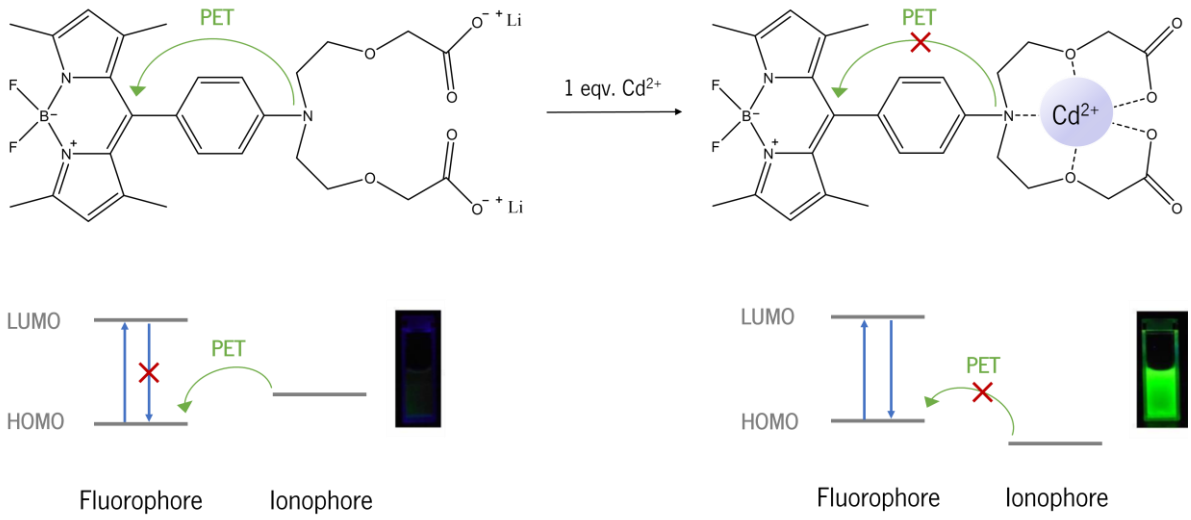

***Figure 9**. A practical example of "turn on" fluorescence in the analysis of Cd^{2+} with a BODIPY derivative through the hindrance of the "turn on" PET process. (Figure adapted from reference 14).*

Finally, the oxidative PET process involves an electron acceptor group as a binding subunit and occurs when the interaction between analyte and sensor reduces the LUMO orbital of the binding subunit. In this case, there is an electronic transfer from the excited fluorophore LUMO orbital to the empty LUMO orbital of the acceptor group and, consequently, the fluorophore oxidation and the binding subunit reduction. Likewise, this external orbital will block the normal emission pathway and form an alternative non-radiative pathway. In this sense, the analyte presence causes fluorescence quenching and the PET process can also be designated as "turn off" fluorescence (**Figure 10**).[8,23,30]

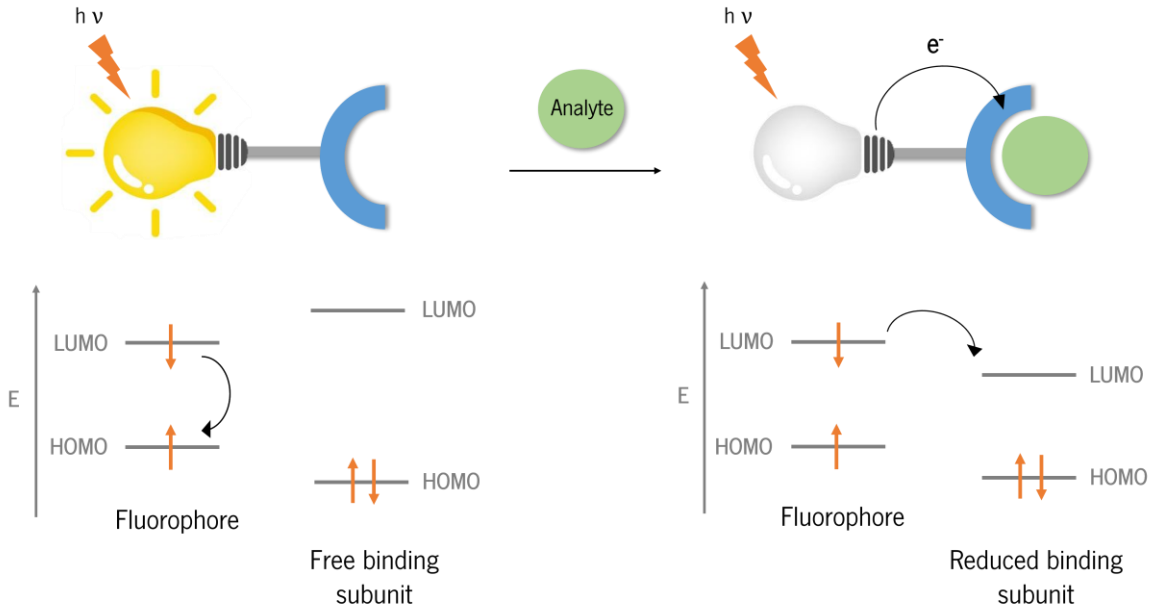

Figure 10. *Representation of the fluorescence enhancement preventing the oxidative PET process. (Figure adapted from reference 8).*

Intramolecular charge transfer

The intramolecular charge transfer process is observed in fluorophores with an electron donor group (D) conjugated to an electron acceptor group (A), through a π-bridge (π). When radiative excitation occurs in this type of molecule, a locally excited state (LE) is reached, and, from this, an additional state of intramolecular charge transfer (ICT) is formed due to the electron transfer from the donor group to the acceptor group. The ICT process produces a redistribution of the molecule's electronic density, leading to a separation of charges and an increase in the dipole moment. It should be noted that this process normally occurs in polar solvents that are in thermodynamic equilibrium with the dipolar fluorophore. In this way, two excited states are possible, allowing a double emission and the appearance of two emission bands in the molecule spectrum. The band assigned to the ICT status is a lower energy emission band and is shifted to the red region of the spectrum compared to the normal LE emission band (**Figure 11**).[8,36–39]

Owing to the increased dipole moment a change in the emission spectrum occurs, depending on the fluorophore microenvironment. For example, changes in temperature, viscosity, pressure, solvent, or even the presence of ions and biological systems, influence the ICT band.[40]

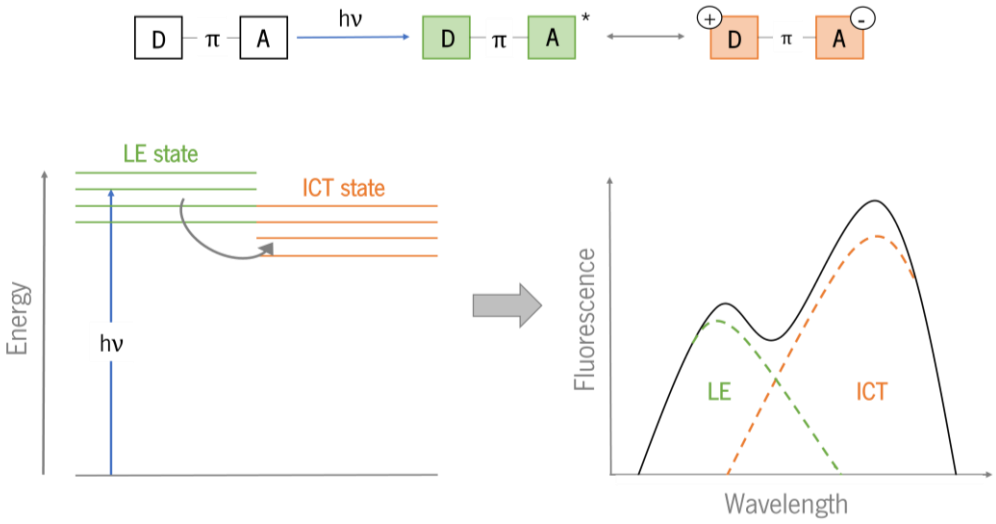

Figure 11. *Energy diagram associated with the ICT mechanisms and the emissions from a locally excited and an intramolecular charge transfer state. (Figure adapted from references 36 and 39).*

In the particular case of ion detection, the use of ICT fluorescent probes causes clear changes in the fluorescence band of the fluorophore after analyte binding. Therefore, it is possible to observe shifts in the fluorophore excitation/emission spectrum to higher or lower wavelengths, that is, a bathochromic or hypsochromic deviation, respectively.[8]

A practical case reported in the literature is the example of a fluorimetric sensor capable of detecting Cd^{2+} based on the ICT process. In this example, the Cd^{2+} binds to the sensor through the electron donor group, causing a decrease in its donor capacity and the extinction of the ICT transition. In terms of the emission spectrum, there is a blue shift in the sensor fluorescence (**Figure 12**).[41]

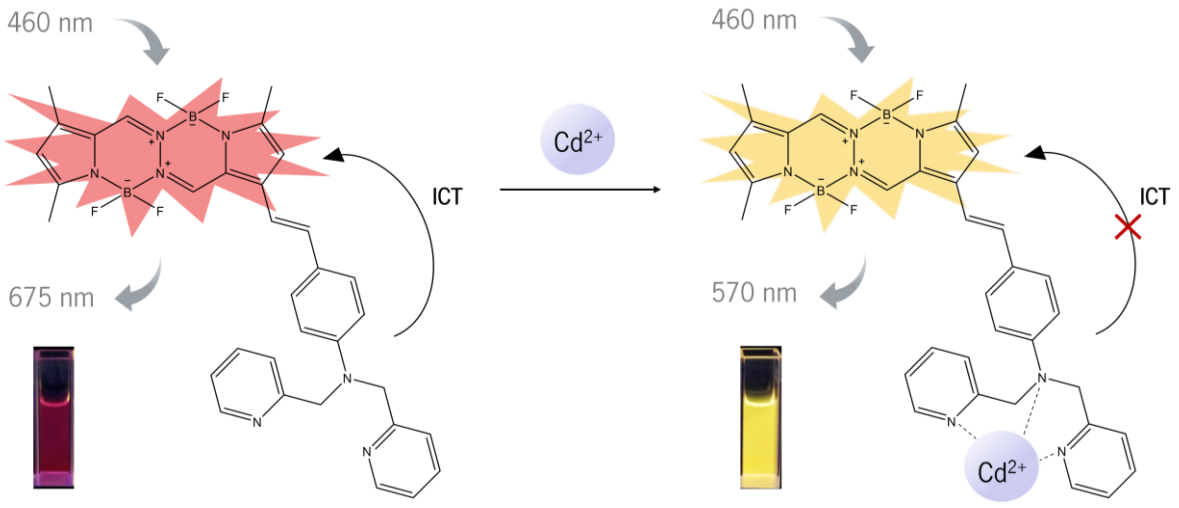

Figure 12. *Fluorometric Cd^{2+} chemosensor based on the ICT mechanism. (Figure adapted from reference 41).*

1.2.1.2 Examples of optical chemosensors

Ions exist widely in biological and environmental media and are one of the main analytes that can be studied with optical chemosensors. It is well known that any change in normal ion levels, both in terms of excess and scarcity, has adverse consequences for these media. In living organisms, some transition metals play an important role in a variety of chemical and biological processes, such as copper ion (Cu^{2+}), which is an example of a metallic cation essential for the proper functioning of the organism and metabolic processes. Consequently, changes in normal levels of this ion in the body can be harmful to human health. Indeed, excess Cu^{2+} in the human body causes cell toxicity, cancer, and several neurodegenerative diseases, including Alzheimer's, Parkinson's, Menkes and Wilson.[24,42,43]

An example of an optical (colorimetric and fluorimetric) chemical sensor sensitive to Cu^{2+} is the BODIPY derivative shown in **Figure 13**. The interaction of this BODIPY derivative with the Cu^{2+} occurs through the nitrogen atoms of ethynylpyridine moiety and BODIPY core, forming a complex with photophysical properties distinct from the initial BODIPY compound. Through the preliminary chemosensing study of this compound in the presence of several cations, it is possible to observe a selective response for the Cu^{2+} compared to other ions. After adding 10 equivalents of each ion to the CH_3CN solution of the compound, it is possible to observe from the images on the right a change in the color of the compound solution from pink to blue and, simultaneously, an evident fluorescence quenching in the presence of Cu^{2+}.[44]

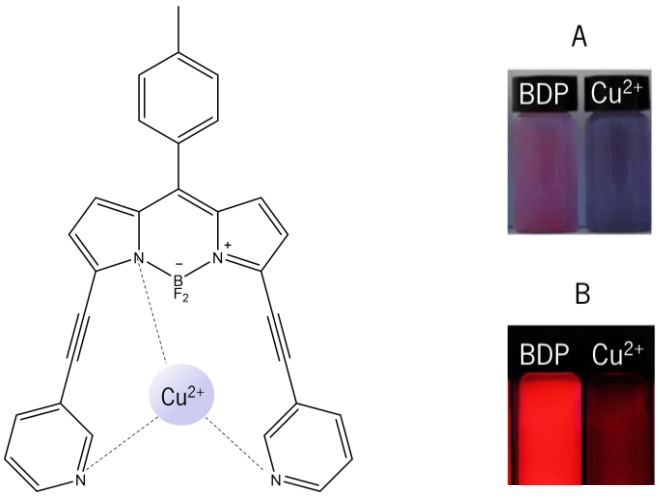

Figure 13. *Chemical structure of the BODIPY derivative and its interaction with Cu^{2+}. Visualization of the color change of the compound solution after interaction with Cu^{2+} under (A) ambient light and (B) fluorescence quenching after excitation at 365 nm. BDP = BODIPY derivative. (Figure adapted from reference 44).*

Currently, the industrial sector is one of the main sources of pollution that releases heavy metals into the environment, namely mercury (Hg^{2+}). This ion is known for the worst reasons since it is considered a toxic pollutant that is widely distributed in the ecosystem and the various food chains by bioaccumulation in living organisms. Mercury, even at low concentrations, is harmful to human health as it causes gastrointestinal, respiratory, and central nervous system problems, and is also at the center of the cause of diseases such as Alzheimer's, Minamata, and Hunter-Russell syndrome.[45–47]

The BODIPY derivative shown in **Figure 14** is an example of an optical chemical sensor for the selective detection of Hg^{2+} in aqueous environments since it contains an *N*-phenyl-1-aza-4,13-dithia-7,10-dioxacyclopentadecane macrocycle capable to interact with the analyte in question. The study was carried out for several ions and a selective response was obtained for Hg^{2+} in an acetonitrile/water solution (95:5), in which a change in the color of the compound solution from blue to pink and, simultaneously, a remarkable emission enhancement in the presence of 10 equivalents of Hg^{2+} was observed.[48]

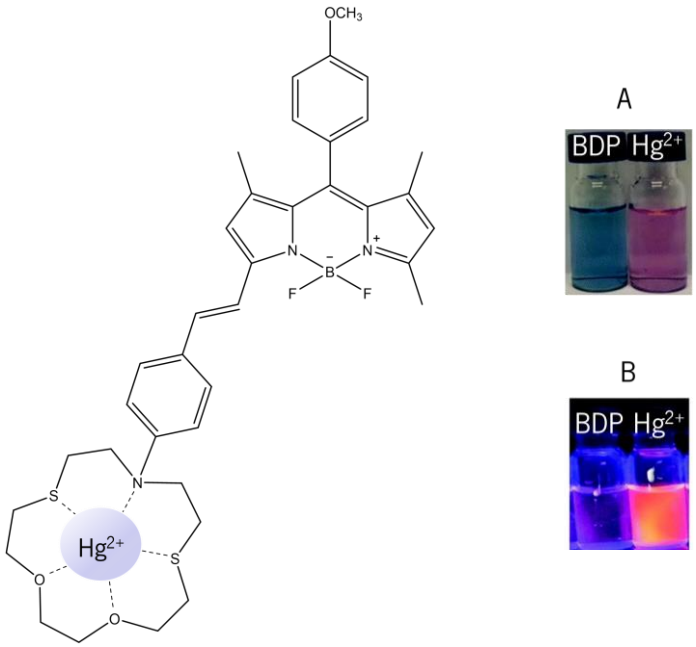

Figure 14. *Chemical structure of the BODIPY derivative and its interaction with Hg^{2+}. Visualization of the color change under (A) ambient light and (B) emission enhancement of the compound solution after interaction with Hg^{2+}. (Figure adapted from reference* 48*).*

Like cations, anions can also be detected in solution through interaction with appropriate optical chemosensors. Fluoride (F^-) is an example of anion that can be analyzed using optical probes and is

extremely important in terms of bone and dental resistance because its excess in the human body can cause dental fluorosis and bone diseases such as osteoporosis.[23,35,49]

The BODIPY derivative shown in **Figure 15** is an example of an optical chemosensor capable of detecting F^-. Through the preliminary chemosensory study of this compound, it is possible to observe a selective response to F^-. As for the colorimetric signal, a drastic color change from yellow to dark red was observed upon the addition of 20 fluoride equivalents to the compound's acetonitrile/water (7:3) solution (**Figure 15A**). As for the fluorometric signal, a change in the fluorescence color of the initial compound solution was observed (**Figure 15B**). The green fluorescent solution turned to deep blue after interacting with the F^- analyte.[50]

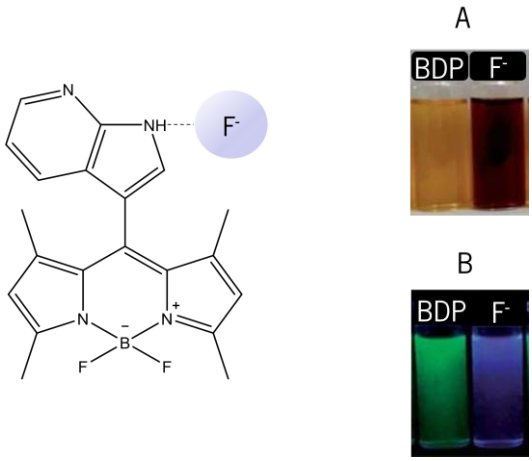

Figure 15. *Chemical structure of the BODIPY derivative and its interaction with F. Visualization of the color change of the compound solution after interaction with the F under (A) ambient light and (B) change of the fluorescence color after excitation at 366 nm under a portable UV lamp. (Figure adapted from reference* 50*).*

Due to the facts described above, the search for fast and effective analytical techniques for the detection and quantification of ions is of great importance. In this sense, optical chemosensors have proven to be a useful tool to minimize the risks of these ions to human health and the environment.

1.2.2 Bioimaging probes

The visualization of biological structures and phenomena inside living organisms in real-time has simplified the acquisition of dynamic information of molecules, elucidating cellular behavior, and obtaining diagnoses and treatment of various diseases. Techniques such as radioisotope labeling, X-ray radiography, and magnetic resonance imaging were previously used for this purpose, but they have disadvantages such as low sensitivity and selectivity, as well as the fact that they are time-consuming and invasive techniques. In this sense, the concept of fluorescence imaging has recently emerged, which has proved to be a very useful tool for the detection, visualization, and characterization of biological systems in animals and humans. Fluorescence imaging has the particularity of presenting low phototoxicity, high sensitivity, high selectivity, technical ease, and allowing fast and non-invasive monitoring in real time of cellular structures and phenomena.[51–55]

Several organic molecules are widely used as fluorophores, of which cyanines, coumarins, rhodamines, and fluoresceins stand out. However, BODIPY derivatives have achieved great notoriety in the field of the fluorescent image due to their excellent photophysical properties, especially large molar extinction coefficients, high quantum fluorescence yields, and chemical and photochemical stability.[56,57]

On the other hand, the BODIPY fluorophore is hydrophobic and insoluble in biological media and has absorption and emission wavelengths located at approximately 500 nm, which presents some disadvantages for its application in bioimaging. The truth is that the emission in the red and near-infrared region (650 to 900 nm) of the electromagnetic spectrum is one of the main characteristics that the fluorescence probes must have to be used as bioimaging probes. The fluorophores that absorb and emit in this spectral region have numerous advantages for the study of biological systems since they minimize the interference of the autofluorescence of biological samples, allow deeper and non-invasive penetration into tissues, increase the resolution of the image, and decrease the probability of damaging the cells, due to the lower radiation energy. In this sense, one of the advantages of the BODIPY core is the fact that it can be functionalized with suitable groups to improve its solubility in biological media and increase the absorption and emission wavelengths for the extreme red and NIR region.[58–61]

In practical terms, fluorescent bioimaging enables the location of subcellular organelles, such as mitochondria, lysosomes, and endoplasmic reticulum, through the selective marking of these structures with appropriate fluorescent probes. Recent studies have also shown that fluorescent probes can be applied to verify the physiological changes that can occur in the intracellular environment, such

as changes in viscosity, pH, temperature, and the presence of ions. Some examples concerning these applications are presented below.[15,54,62]

1.2.2.1 Example of organelle-targeted fluorescent probe

Mitochondrial tracking

One of the applications of fluorescent probes in bioimaging is the labeling of specific cellular components, such as mitochondria. Mitochondria is one of the main organelles in terms of cell structure and plays crucial roles such as energy generation and cellular respiration. Given its importance, the visualization of dysfunction or morphological alteration in the mitochondria can alert to a possible pathology. Currently, there are already commercial fluorescent probes specific for mitochondria, but, in general, they have weak fluorescence and low photostability. In this sense, new fluorescent probes specific to mitochondria have emerged, such as the example of a **TPPh-BODIPY** derivative shown in **Figure 16**.[51,56]

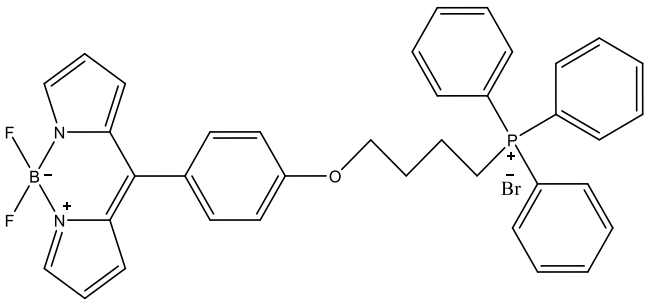

Figure 16. *Chemical structure of the* ***TPPh-BODIPY*** *probe. (Figure adapted from reference 63).*

This compound incorporates a cationic portion of triphenylphosphine (TPPh) that allows guiding the neutral core of BODIPY to the negatively charged mitochondrial membrane and increasing its solubility in the biological environment. On the other hand, it presents low cytotoxicity in cells and good photostability. Fluorescence images of HeLa cells obtained by confocal microscopy (**Figure 17**) show a green fluorescence of these cells in the presence of **TPPh-BODIPY** (**Figure 17A**) and red fluorescence in the presence of the specific MitoTracker® Deep Red FM (MTR) probe for mitochondria localization (**Figure 17B**). In **Figure 17C**, it can be seen that there is a perfect overlap between the two

fluorescences, which allows us to conclude that the fluorescent probe **TPPh-BODIPY** can be applied to mitochondrial-tracking in living cells.[63]

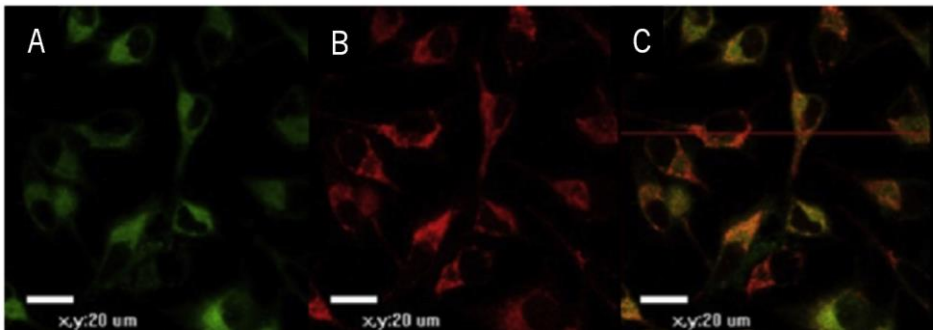

Figure 17. *Fluorescent images of HeLa cells in the presence of (A) 0.5 mM* ***TPPh-BODIPY*** *for 4 hours, (B) 0.5 mM MTR for 15 minutes, and (C) overlapping of both. (Figure adapted from reference 63).*

1.2.2.2 Examples of probes sensitive to the cellular environment

Lysosomal viscosity

Another application of fluorescence bioimaging is to monitor changes in the cellular environment. Lysosomes are an example of important cellular organelles that participate in several cellular processes, such as tissue remodeling and protein degradation. Thus, changes in the viscosity of lysosomes have implications for the transport and interaction of biomolecules. So, abnormal changes in this sense may be indicative of some type of disease, such as diabetes and Parkinson's disease. Therefore, monitoring the lysosome viscosity is of great importance.[64,65]

An example of a fluorescent probe for this type of application is the **Lyso-B** derivative presented by Li and co-workers depicted in **Figure 18**. This compound incorporates two morpholine groups that provide a selective binding to lysosomes. An increase in viscosity in this type of organelle prevents the rotation of the morpholine groups with the rest of the BODIPY molecule and leads to an increase in the fluorescence intensity and fluorescence lifetime, making this BODIPY derivative as a probe sensitive to lysosomal viscosity.[66]

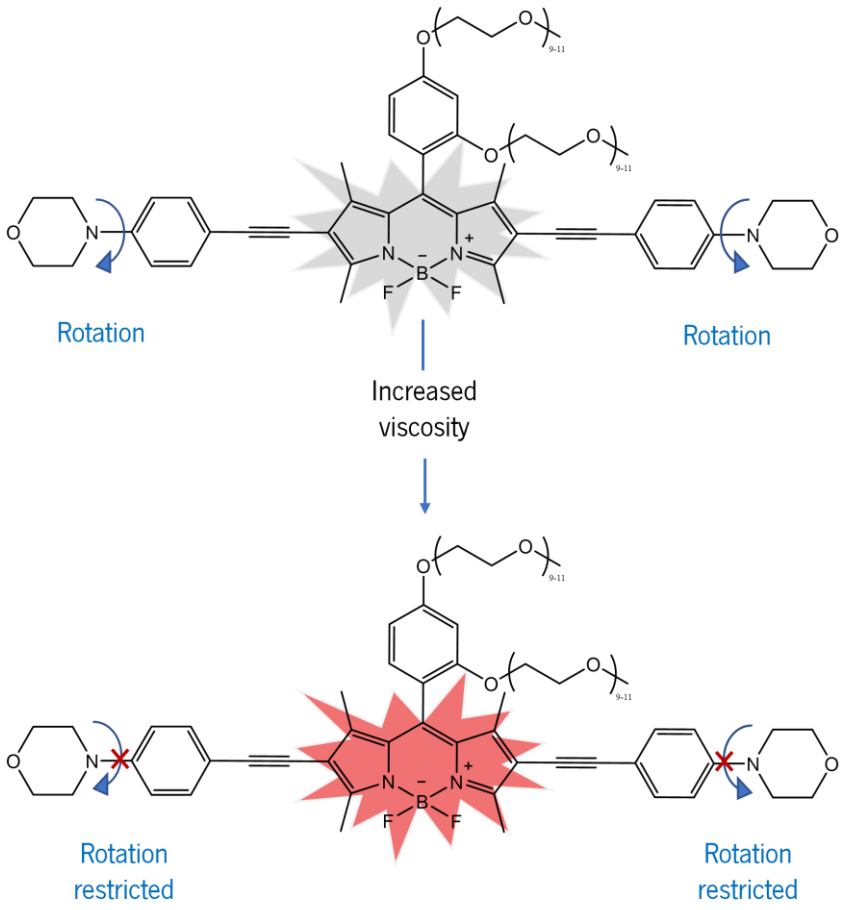

Figure 18. *Chemical structure of the* ***Lyso-B*** *probe and changes in fluorescence with increased viscosity. (Figure adapted from reference 66).*

In practical terms, the emission spectrum of this compound was obtained in H_2O/glycerol solutions, varying the viscosity of the solution. As can be seen, the increase in solution viscosity provides an increase in the fluorescence of **Lyso-B**. The usual clinical drug known as dexamethasone was used to increase the viscosity of lysosomes and fluorescence-lifetime imaging microscopy (FLIM) was used to obtain fluorescent bioimages. For this purpose, a color scale has been assigned to the fluorescence lifetimes of the probe, and fluorescence lifetimes close to 0.8 ns are shown in blue, and lifetimes close to 2.4 ns are shown in red. Therefore, the study of HeLa cells stained with **Lyso-B** with (**Figure 19A**) or without (**Figure 19B**) dexamethasone co-incubation, enables to observe noticeable changes from blue to red, indicating an increase in fluorescence lifetime and lysosome viscosity.[66]

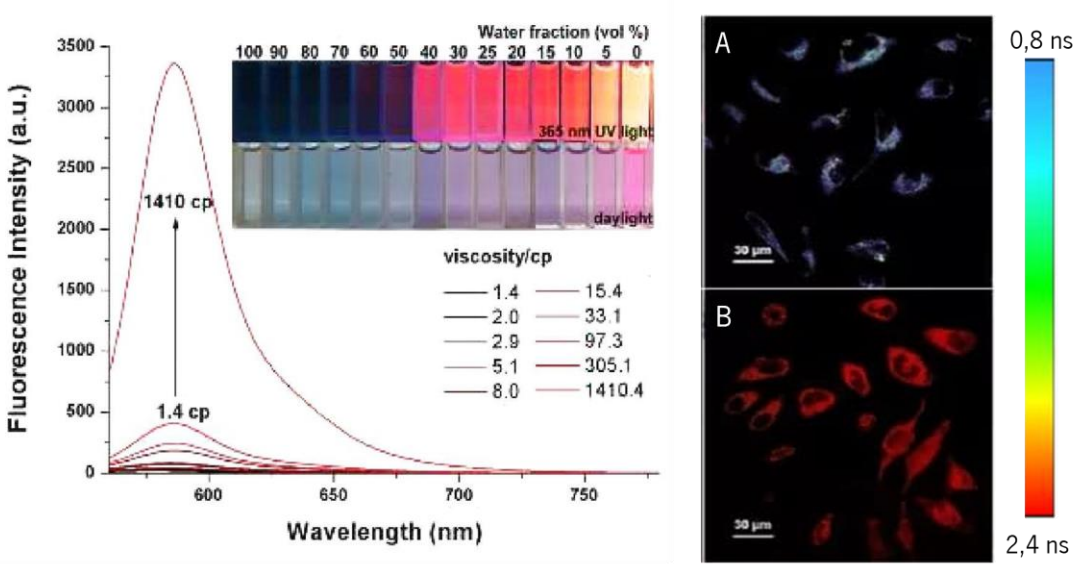

Figure 19. *(Left) Photos taken under 365 nm UV light and daylight and fluorescent spectrum of* ***Lyso-Bin*** *solutions with different viscosities. (Right) FLIM images of HeLa cells with* ***Lyso-B*** *(B) with and (A) without the presence of dexamethasone. (Figure adapted from reference 66).*

Detection of ions in the intracellular environment

As an example, the detection of zinc ion (Zn^{2+}) in cells is presented. Zn^{2+} is a very important species in biological systems, so a change in the normal levels of this ion in the body can cause the appearance of several diseases and pathologies, such as kidney dysfunction, Parkinson's disease, and epilepsy. Given these circumstances, the detection of this ion in cells is extremely important.[67,68]

Studies carried out in this regard have allowed the creation of selective fluorescent probes for Zn^{2+} for application in the cellular environment. The **1-OH** BODIPY derivative shown in **Figure 20** was reported by Zhu and co-workers as a fluorescent NIR probe for the selective detection of Zn^{2+}. The coordination of the zinc ion occurs through the nitrogen and oxygen atoms present in the molecule and causes an increase in structural rigidity, resulting in the CHEF effect.[68]

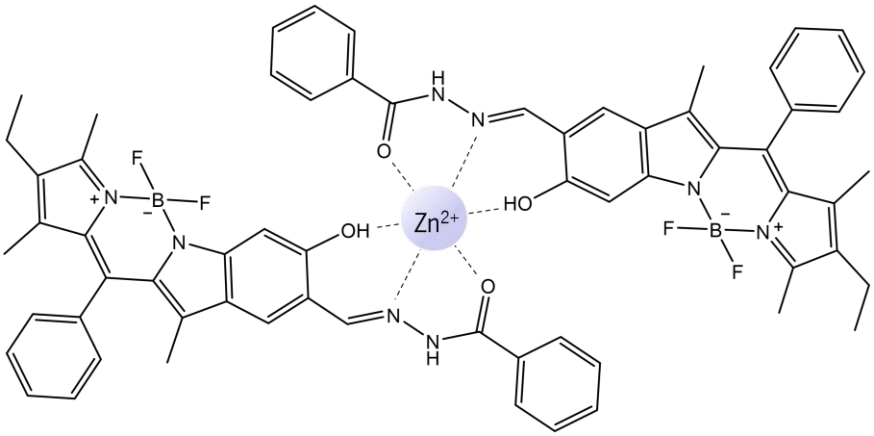

Figure 20. *Coordination between Zn^{2+} and* ***1-OH*** *BODIPY. (Figure adapted from reference 68).*

In experimental terms, the free **1-OH** probe has a maximum absorption wavelength of 548 nm and, after its coordination with Zn^{2+}, a new band appears with a maximum absorption wavelength of 617 nm, and an increase in fluorescence occurs. The application of this fluorescence probe to live breast cancer cells MCF-7 did not cause any significant visible changes, however, after treatment with Zn^{2+} an image of bright red fluorescence was obtained. Thus, it can be concluded that this fluorescent probe is promising for monitoring Zn^{2+} in living cells (**Figure 21**).[68]

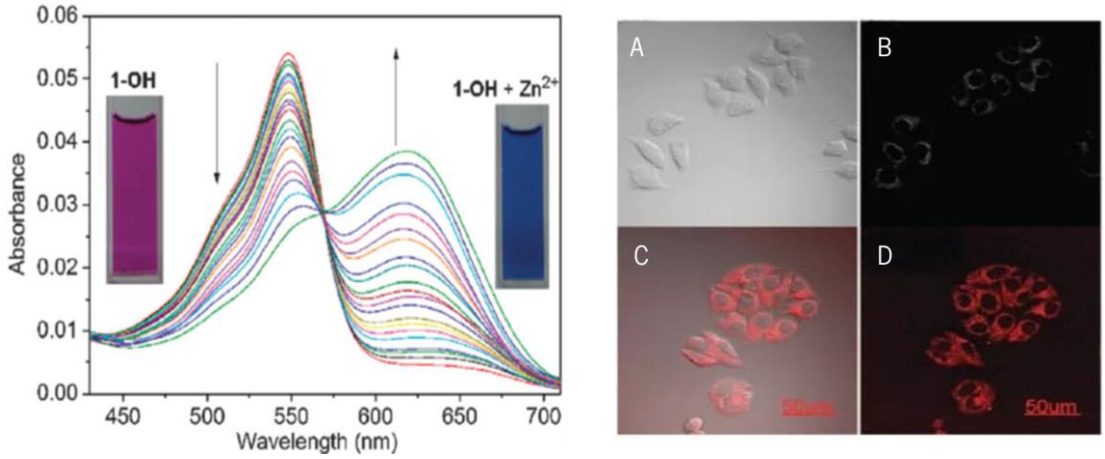

Figure 21. *(Left) Absorption spectra of the* ***1-OH*** *in the presence of different concentrations of Zn^{2+} (0 - 3 eqv.), in CH_3CN, and the respective color change of* ***1-OH*** *solution in the absence and presence of Zn^{2+}. (Right) Confocal fluorescence images of MCF-7 breast cancer cells: (A and B) cells incubated with 5.0 mM* ***1-OH*** *for 30 min; (C and D) cells incubated with 5.0 mM* ***1-OH*** *for 30 min, then treated with Zn^{2+} for another 30 min. (A, C) Overlapping field and (B, D) fluorescence image. (Figure adapted from reference 68).*

1.2.3 Aggregation-induced emission fluorophores

Fluorescent chemosensors have advantageous properties such as high sensitivity and quick operation, making their application accessible to several areas. However, fluorophores such as fluorescein, rhodamine, and cyanine emit only in diluted solutions, which shows an applicability disadvantage. When subjected to high concentrations, they extinguish their fluorescence emission and photostability. This phenomenon was observed by Foërster and Kasper in the particular case of pyrene. The increase in pyrene concentration caused a decrease in the solution fluorescence. However, this phenomenon has been experienced by other aromatic compounds.[69,70]

As the concentration increases, the sensor's aromatic molecules are closer to each other in solution and, consequently, undergo strong π - π stacking interactions through the aromatic rings. In planar luminogens, such as the pyrene case, these π - π stacking interactions promote the formation of non-emissive aggregates owing to the aggregation-caused quenching (ACQ) effect, as depicted in **Figure 22**.[70]

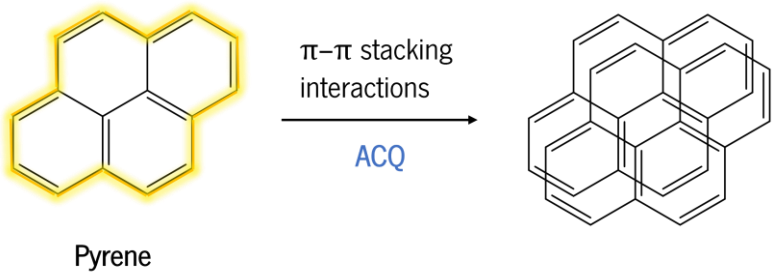

***Figure 22**. Example of the ACQ effect on the pyrene molecule. This planar luminogen becomes non emissive due to the strong π - π stacking interactions that lead to the formation of aggregates. (Figure adapted from reference 70).*

At first sight, the simplest way to prevent fluorescence extinction of these compounds is to introduce bulky groups or branched-chains in the ACQ molecules so that the formation of aggregates is prevented. However, in 2001, Tang and co-workers discovered a new class of compounds that exhibit an effect contrary to the ACQ effect, that is, they exhibit low fluorescence in diluted solutions and high fluorescence in a high concentration or aggregation state. This new concept was named by Tang as aggregation-induced emission (AIE) and was discovered in studies with silole molecules, more precisely, hexaphenylsilole (HPS).[71–74]

The HPS molecule is extensively conjugated and insoluble in water, so it would be expected to obtain high fluorescence when dissolved in good solvents, as acetonitrile, tetrahydrofuran, and chloroform. However, this did not occur, and the expected response was only obtained when large amounts of water were added to the HPS solution (**Figure 23**). By increasing the amount of water and solution polarity, the solvency power of the solution decreases, no longer being able to efficiently absorb the HPS molecules. Thus, the insoluble HPS molecules come together to form aggregates with high emission efficiency, as seen in **Figure 23**.[70]

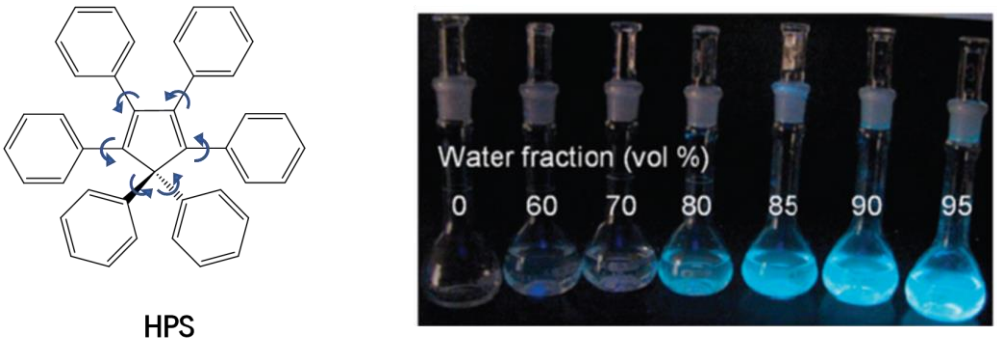

Figure 23. *(Left) Chemical structure of the HPS molecule. (Right) The study carried out on HPS solutions in acetonitrile-water mixtures revealing a fluorescence enhancement with an increase in the amount of water in the solution. Photographs were taken under an ultraviolet lamp. (Figure adapted from reference 70).*

The AIE effect is seen in non-planar luminogens with a highly twisted propeller-shaped, as in the case of the HPS molecule. It is believed that the main explanation for this phenomenon is the restriction of intramolecular movement that comes from the formation of molecular aggregates. In the solution, the HPS molecules are spaced from each other so that the six phenyl rings connected to the central silol ring can rotate freely. These intramolecular rotations consume the energy of photoexcitation and act as a radiationless pathway for energetic relaxation, leading to the extinction of the solution's photoluminescence. However, with the increase in concentration of the chromophore in solution and the formation of aggregates, the previous rotations in the HPS molecules are limited due to physical impediment and there is a restriction of intramolecular movement (RIM), which includes restriction of intramolecular rotation (RIR) and restriction of intramolecular vibration (RIV). The restriction of the molecule movement blocks the above-mentioned non-emissive pathway and allows radiative decay, leading to an increase in the quantum emission yield (**Figure 24**).[70,71,74–77]

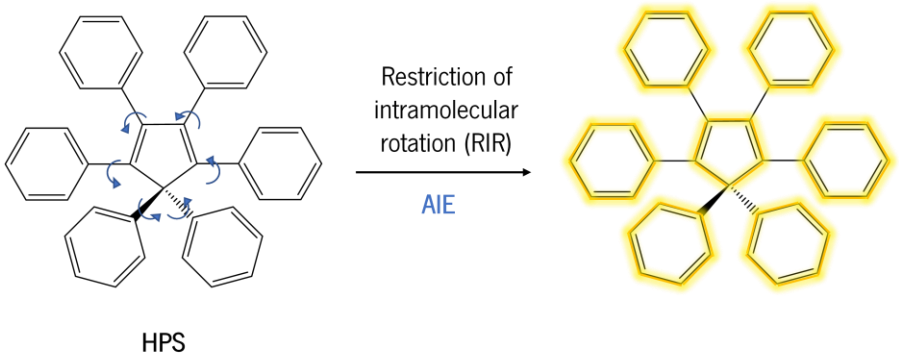

Figure 24. *Example of the AIE effect on the HPS molecule. This non-planar luminogen in the form of a twisted helix becomes emissive after the formation of aggregates, which restrict the intramolecular rotation of the molecule. (Figure adapted from reference 70).*

The viscosity increase and temperature decrease of the solutions are other complementary ways to minimize intramolecular movement. Studies carried out in this area supported experimentally this statement. The increase in viscosity makes the intramolecular rotation slower and, consequently, improves emission. On the other hand, cooling the solution suppresses intramolecular rotations and fortifies the RIR process, which increases the solution fluorescence intensity.[70,74,75]

Tang's discovery was a benefit for the scientific community and boosted the discovery of new propeller-shaped luminogens with AIE activity, such as tetraphenylpyrazine (TPPy), triphenylamine (TPA), 2,3,3-triphenylacrylonitrile (TPAN), and tetraphenylethylene (TPE), which is one of the most famous AIE luminogens (**Figure 25**). The incorporation of this variety of luminogens into ACQ-active molecules has been one of the strategies implemented to develop several AIE-active compounds, as in the case of the BODIPY core.[69,78,79]

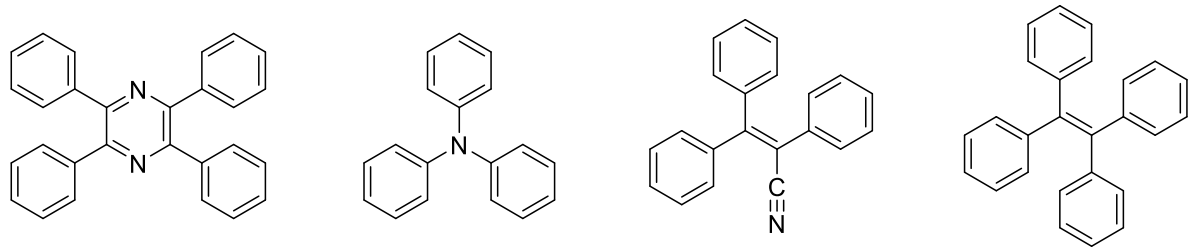

TPPy **TPA** **TPAN** **TPE**

Figure 25. *Several propeller-shaped luminogens with AIE activity.*

The BODIPY fluorophore is hydrophobic and insoluble in water, so increasing the solution polarity promotes the formation of ACQ-aggregate. As the BODIPY nucleus is a planar π-conjugated system, it suffers strong π - π stacking interactions in the aggregate state, which consequently causes fluorescence extinction. To prevent this event, BODIPY derivatives have been synthesized with AIE effect through the direct incorporation of AIE molecules in the BODIPY core. This fact has been observed experimentally in several studies carried out in this area.[51,80]

For example, the study carried out by Hu and collaborators involves the incorporation of a TPA unit in the BODIPY core. This compound shows a fluorescence increase when the percentage of water included in the compound's THF solution is greater than 70%. The introduction of the active-AIE unit in the BODIPY core allows to transform it into a compound with an AIE effect (**Figure 26**).[81]

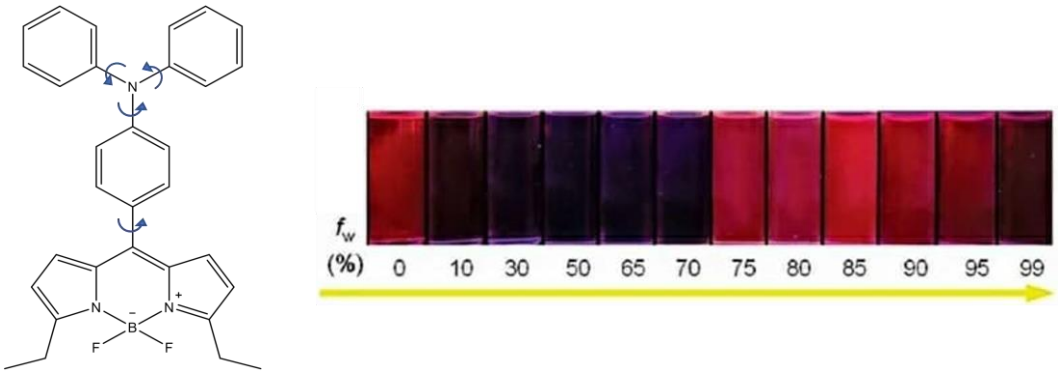

Figure 26. *(Left) Chemical structure of BODIPY derivative. (Right) BODIPY derivative in THF/water solutions with different fractions of water (fw) under UV illumination. (Figure adapted from reference 81).*

After discovering and understanding the AIE phenomenon, it was possible to take advantage of its benefits and apply AIE-active luminogens in several important areas, such as optical chemosensors, bioimaging, and OLEDs.[82,83]

1.2.4 Photodynamic therapy photosensitizers

Photodynamic therapy (PDT) can be described as a treatment of target lesions through a photochemical reaction generated by the combination of light, oxygen, and a photosensitizer, which is a chemical sensitive to light. These three components essential to PDT do not present toxicity individually, but when combined they promote the formation of highly cytotoxic species. This therapeutic concept was discovered by serendipity in Germany when a medical student accidentally noticed the death of microorganisms incubated with dyes caused by exposure to light. This randomly discovered photodynamic action has led to the current PDT which has been widely explored and applied in the treatment of various diseases.[84]

In practical terms, the PDT process begins with intravenous or topical administration of photosensitizer (PS), which after some time accumulates ideally in the lesion area. Then the lesion area is irradiated with an appropriate wavelength light. This causes the PS activation (PS*) and the transfer of energy to the surrounding oxygen molecules, carrying out a photochemical reaction and the formation of reactive oxygen species (ROS) that lead to cell death and tissue damage (**Figure 27**).[85,86]

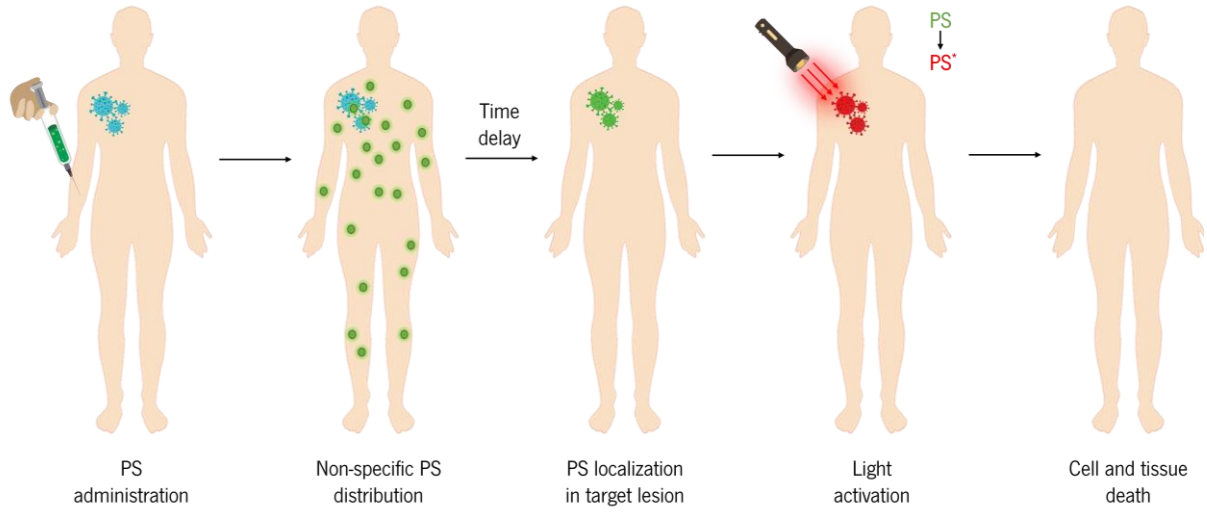

Figure 27. *The general procedure of PDT treatment. (Figure adapted from reference 85).*

The photochemical mechanism involved in the PDT process is represented in detail in **Figure 28**. Initially, the PS molecule is in the singlet fundamental state and, after absorbing light of an appropriate wavelength, one of its electrons is excited to a highest energy singlet state. Soon afterward, the excited electron tends to return to the most stable ground state by radiation emission (fluorescence)

or heat release during the internal conversion (IC) process. In contrast, the PS molecule in the singlet excited state can also undergo intersystem crossing (ISC) and form the most stable excited triplet state. The triplet state has a longer lifetime (≈ μs) compared to the singlet state (≈ ns) and, for this reason, it is possible to occur two types of photochemical reactions. In the type I reaction, the excited triplet state reacts directly with an organic substrate, such as the cell membrane, and ROS is formed in the presence of oxygen, such as hydroxyl radical ($OH^{\bullet}$), hydrogen peroxide (H_2O_2), and radical superoxide anion ($O_2^{\bullet-}$). Alternatively, the type II reaction involves the energy transfer from the excited triplet state to the surrounding oxygen molecules, leading to the singlet oxygen ($^1O_2$) formation. These reactive species have cytotoxic properties that lead to cell death.[87–89]

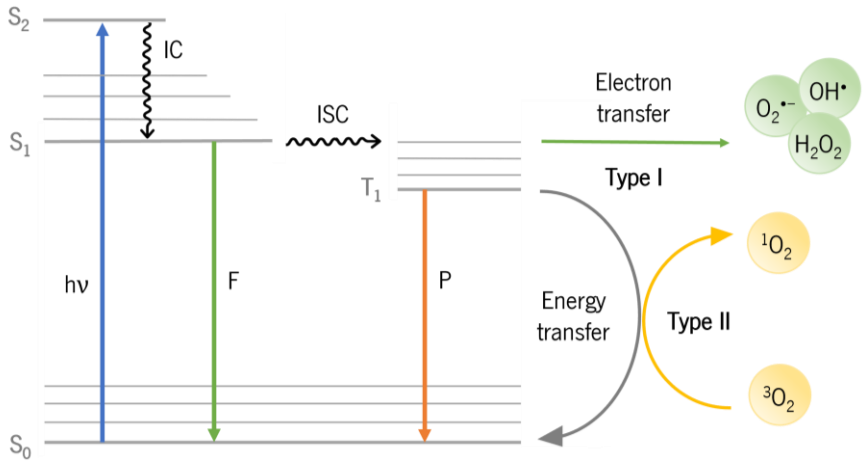

Figure 28. *Photochemical mechanism involved in the PDT process (Figure adapted from reference 89).*

After realizing the capabilities of the PDT, this process was accepted as a promising alternative for the treatment of cancer. The first PS approved and used in this sense was Photofrin®. Although this PS is still used today, it has some disadvantages such as the long duration of skin photosensitivity and a relatively short absorption wavelength that does not allow penetration into deeper tumors. Since the PS is a central component in the PDT process, it is of great importance to produce an efficient PS for the proper application in this therapy. In this sense, several important characteristics have been pointed out to reach new PSs effective in the treatment of cancer, infections, and other diseases. The ideal PS should be a pure compound with a high triplet quantum yield, a significant ROS production, and, consequently, high phototoxicity. It must have good water solubility, high photostability, no toxicity in the dark due to possible side effects and be selectively located in damaged tissues. Finally, the PS must

show strong absorption in the therapeutic window, that is, in the red and NIR region (between 600 and 800 nm), because this spectral region allows deeper penetration into the tissues.[90–93]

BODIPY derivatives have been explored in the PDT area due to their excellent photophysical properties and their disadvantages can be overcome by the strategic chemical modification of their core. One of the disadvantages associated with this type of application is the fact that BODIPY suffers from low triplet quantum yields. To overcome this obstacle, several strategies have been chosen to facilitate intersystem crossing and to promote the singlet oxygen yield. One of them is the introduction of heavy atoms (I, Br, Pt, etc.) and/or the introduction of electron withdrawing or donating groups in the BODIPY core, the use of aza-BODIPYs and metal complexes, etc.[17,94–96]

The **SBDPiR690** derivative is a practical example of BODIPY with antitumor effects used as PS in the PDT treatment (**Figure 29**).[97]

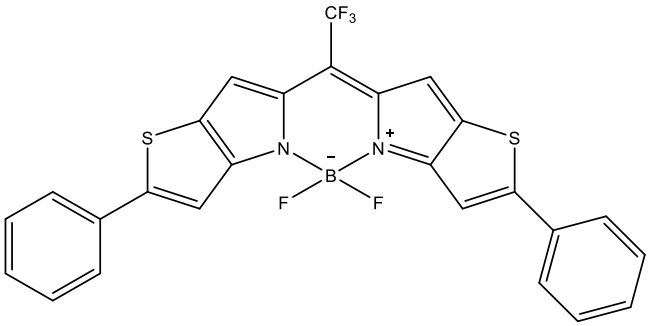

Figure 29. *Chemical structure of* ***SBDPiR690****. (Figure adapted from reference 97).*

Watley and colleagues found that this BODIPY derivative free of heavy atoms can generate singlet oxygen (ϕ_Δ = 0.42) and fluorescence (ϕ_F = 0.22) in the NIR region. This PS was injected intravenously into live mice, and the effect of the **SBDPiR690** on subcutaneous tumor growth was studied. This *in vivo* study was carried out with 4 groups of rats in different study conditions and only the group that used the PS **SBDPiR690** and light obtained positive results regarding the decrease in tumor volume. This result can also be seen in the images of the rats after post-treatment PDT (**Figure 30**).[97]

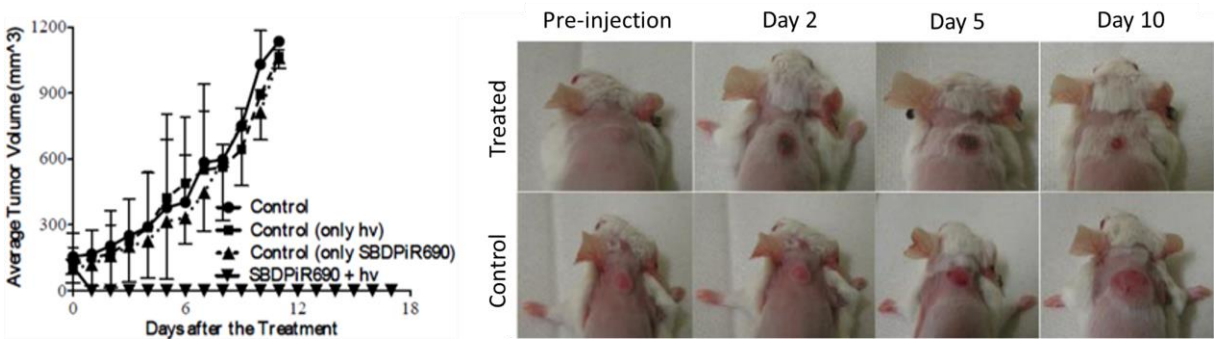

Figure 30. *(Left) Tumor growth over time with 200 µL of* ***SBDPiR690*** *compound and (Right) mouse post-treatment PDT images. (Figure adapted from reference 97).*

In addition to the application in cancer treatments, the photodynamic action of PS has also been explored for antimicrobial treatments and this technique is called photodynamic inactivation (PDI). This is a recent area of research that emerges as an alternative to antibiotics that cause antimicrobial resistance and has been applied to inactivate viruses, fungi, and Gram-positive and Gram-negative bacteria. The production of ROS by combining PS with light and oxygen causes oxidative stress that compromises the integrity of cells, leading to cell death (**Figure 31**). In this sense, BODIPY derivatives with pronounced charges have been one of the options for selective electrostatic interaction with microbial cells.[18,98–101]

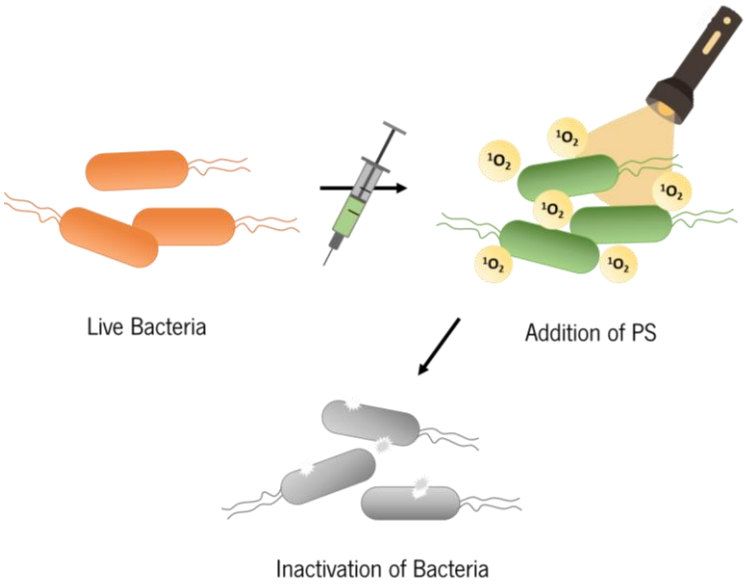

Figure 31*. Representation of PDI treatment. (Figure adapted from references 101).*

Chapter 2

Experimental section

2. Experimental section

2.1 General

All reagents were purchased from Sigma-Aldrich, Acros, and Fluka and used as received.

Thin-layer chromatography (TLC) analysis was performed on 0.25 mm thick precoated silica plates (Merck Fertigplatten Kieselgel 60F254) and the spots were visualized under UV light. Dry flash and column chromatography were carried out using silica gel 60 of diameter between 230-400 mesh (Merck).

The UV-Vis absorption spectra were obtained on a UV/2501PC spectrophotometer (Shimadzu) and fluorescence emission spectra were obtained on a FluoroMax-4 (Horiba). The singlet oxygen phosphorescence was collected in a Horiba-Jobin-Ivon Fluorolog 322 spectrometer using an Hamamatsu R5509-42 photomultiplier cooled to 193 K in a liquid nitrogen chamber (Products for Research model PC176TSCE-005).

The ^{1}H and ^{13}C nuclear magnetic resonance spectra were recorded on a Bruker Avance III apparatus at an operating frequency of 400 MHz for ^{1}H and 100.6 MHz for ^{13}C, at 25 °C using the solvent peak as an internal reference. The assignment of ^{1}H and ^{13}C signals was performed using two-dimensional heteronuclear correlation techniques. The deuterated solvent used in nuclear magnetic resonance spectroscopy was $CDCl_3$ with 99.8% deuteration degree, containing 0.03% v/v of tetramethylsilane (Sigma Aldrich). The melting point was measured on a Stuart Scientific Melting Point SMP1 apparatus.

Low and high resolution mass spectra were performed by "C.A.C.T.I. – Unidad de Espectrometria de Masas", at the University of Vigo, Spain.

Fluorescence images in cell media were acquired using a confocal microscope LSM 780 (Zeiss).

The uptake results were acquired using the Novocyte 3000 cytometer (ACEA).

BODIPY **1**[102] and **2**[103] were previously synthesized in the research group.

2.2 Synthesis of BODIPY derivatives

2.2.1 Synthesis of precursor 3' by Suzuki coupling

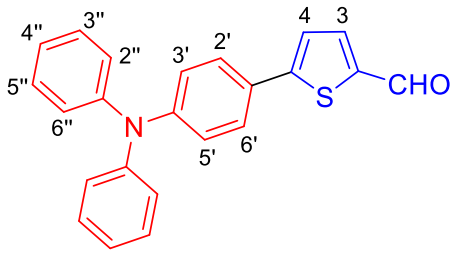

3'

In a glass vial, 5-bromo-2-thiophenecarboxaldehyde (108 mg, 0.56 mmol) dissolved in dry DME (10 mL) and $Pd(PPh_3)_4$ (0.032 g, 0.028 mmol) were added. It was left stirring in an IKA® magnetic stirrer plate for 10 minutes at 80 °C under a nitrogen atmosphere. Next, 4-(diphenylamino)phenylboronic acid (212 mg, 0.73 mmol), dissolved in the smallest possible volume of ethanol and Na_2CO_3 2 M aqueous solution (0,56 mL, 1.1 mmol), was added. The reaction mixture was left stirring at 80 °C under a nitrogen atmosphere and was monitored by TLC (reaction time = 32 hours). The reaction mixture was cooled to room temperature and a saturated NaCl solution (30 mL) and DCM (30 mL) were added. After the separation of the two phases, the organic phase was washed with distilled water (3 x 20 mL) and a solution of 10% NaOH (1 x 20 mL). Then the organic phase obtained was dried with anhydrous $MgSO_4$, filtered and the solvent removed under vacuum to give the crude product, which was submitted to column chromatography on silica gel with hexane/DCM (1:2) as eluent to obtaining the pure precursor **3'**[104] as a yellow solid (171 mg, 86%).

^{1}H NMR (400 MHz, $CDCl_3$): δ = 7.07–7.17 (m, 8H, H-3', H-5', 2 × H-2'', 2 × H-4'' and 2 × H-6''), 7.29–7.33 (m, 5H, H-4, 2 × H-3'' and 2 × H-5''), 7.53 (d, J = 8.8 Hz, 2H, H-2' and H-6'), 7.70 (d, J = 4.0 Hz, 1H, H-3), 9.86 (s, 1H, CHO) ppm.

2.2.2 Synthesis of BODIPY **3**

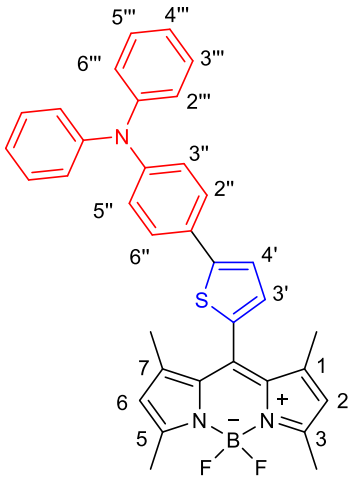

3

In a three-neck round-bottom flask, 5-(4-(diphenylamino)phenyl)thiophene-2-carbaldehyde (100 mg, 0.28 mmol) and 2,4-dimethylpyrrole (54 mg, 0.56 mmol) were added and dissolved in dry DCM (14 mL) under nitrogen atmosphere. Four drops of trifluoroacetic acid (TFA) were added to the reaction mixture, and the resulting mixture was stirred in the dark for 50 minutes under a nitrogen atmosphere at room temperature. Then, DDQ (2,3-dichloro-5,6-dicyano-*p*-benzoquinone) (127 mg, 0.56 mmol) was added to the reaction mixture. After stirring for more 50 minutes, triethylamine (TEA) (0.64 mL, 4.6 mmol) and $BF_3{\cdot}OEt_2$ (0.95 mL, 7.7 mmol) were subsequently added to the mixture and left stirring 15 minutes and 30 minutes, respectively. The crude product was purified by column chromatography on silica gel using hexane/DCM (1:1) as eluent to obtain the pure BODIPY **3** as a red solid (4.5 mg, 2.8%).

^{1}H NMR (400 MHz, $CDCl_3$): δ =1.75 (s, 6H, CH_3-1 and CH_3-7), 2.56 (s, 6H, CH_3-3 and CH_3-5), 6.02 (s, 2H, H-2 and H-6), 6.92 (d, J= 4 Hz, 1H, H-4'), 7.06 – 7.14 (m, 8H, H-3'', H-5'', 2 × H-2''', 2 × H-4''' and 2 × H-6'''), 7.26 – 7.30 (m, 5H, H-3', 2 × H-3''' and 2 × H-5'''), 7.50 (d, J = 8.4 Hz, 2H, H-2'' and H-6'') ppm.

2.2.3 Synthesis of BODIPY **4**

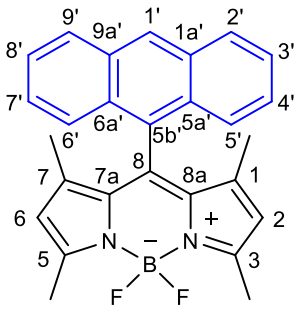

4

2,4-Dimethylpyrrole (181 mg, 1.9 mmol) and anthracene-9-carbaldehyde (200 mg, 0.97 mmol) were dissolved in dry DCM (100 mL) and this reaction mixture was stirred for 50 min after adding a drop of TFA. Subsequently, a solution of DDQ (440 mg, 1.9 mmol) dissolved in dry DCM (100 mL) was added and the stirring time was extended for another 50 min. Then, TEA (2.2 mL, 16 mmol) was added and, after 15 min, $BF_3.OEt_2$ (3.3 mL, 26.8 mmol) was added to the reaction mixture, which was stirred for 30 min. The crude product obtained after evaporation of the solvent under reduced pressure was purified by dry flash chromatography using a petroleum ether/AcOEt (4:1) mixture as eluent. The pure BODIPY derivative **4**[105] was obtained as a dark red solid (108 mg, 26%). Melting point: 238 – 240 °C.

^{1}H NMR (400 MHz, $CDCl_3$): δ = 0.64 (s, 6H, CH_3-1 e CH_3-7), 2.63 (s, 6H, CH_3-3 and CH_3-5), 5.89 (s, 2H, H-2 and H-6), 7.41 (dt, J = 1.2 and 8.2 Hz, 2H, H-3' and H-8'), 7.48 (dt, J = 1.2 and 8 Hz, 2H, H-4' and H-7'), 7.91 (dd, J = 0.8 and 8.8 Hz, 2H, H-2' and H-9'), 8.04 (d, J = 8.8 Hz, 2H, H-5' and H-6'), 8.57 (s, 1H, H-1') ppm.

^{13}C NMR (100.6 MHz, $CDCl_3$): δ = 13.29 (C1-CH_3 and C7-CH_3), 14.67 (C3-CH_3 and C5-CH_3), 121.15 (C2 and C6), 125.07 (C2' and C9'), 125.72 (C4' and C7'), 126.93 (C3' and C8'), 128.25 (C5' and C6'), 128.32 (C1'), 129.66 (C5b'), 131.28 (C5a' and C6a'), 132.35 (C7a and C8a), 138.94 (C8), 142.87 (C1 and C7), 155.74 (C3 and C5) ppm.

MS (ESI) *m/z* (%): 426 ($[M + 2]^{+\cdot}$, 29), 425 ($[M + 1]^{+\cdot}$, 92), 424 ($[M]^{+\cdot}$, 26), 405 (100), 291 (31), 209 (7), 147 (8), 102 (29). **HRMS** (ESI) *m/z*: $[M + 1]^{+\cdot}$ calcd for $C_{27}H_{24}BF_2N_2$, 425.1995; found 425.1989.

2.3 Photophysical characterization of BODIPY derivatives **1**-**4**

The photophysical characterization of BODIPY derivatives was studied in different solvents considering the application of each compound. The BODIPY **1** derivative was studied in acetonitrile solution, the BODIPY **2** and **3** derivatives were studied in toluene and THF solutions, and BODIPY **4** was studied in a THF solution.

The fluorescence quantum yields were obtained by the comparative method using appropriate reference compounds with known spectroscopic properties, namely, Rhodamine 6G in ethanol, ϕ_F = 0.95, as reference compound for BODIPY **1** and rubrene in chloroform, ϕ_F = 0.54, as reference compound for BODIPY derivatives **2**, **3** and **4**.

In this sense, diluted solutions of the different BODIPY derivatives and the respective reference compounds were prepared and the spectroscopic studies were carried out in quartz cells. The sample solutions were optically matched with those of the reference compound at the excitation wavelength at absorbance around 0.1. Hence, the compound and the reference were excited at the same wavelengths. The emission spectra were corrected for the wavelength response of the system. After plotting the respective emission spectrum of each compound and the reference, the area under the curve was determined and the quantum fluorescence yield of the BODIPY derivatives was calculated using **Equation 1**:

$$\phi_{F\,cp} = \frac{F_{cp} \times n_{ref}^2}{F_{ref} \times n_{cp}^2} \times \phi_{F\,ref} \qquad \textbf{Equation 1}$$

where F is the integrated area under the emission curve and n is the refractive index value of the solvents used. $\phi_{F_{ref}}$ represents the fluorescence quantum yields value of the respective reference. subscript ref and cp refer to the reference and compound under study, respectively.

Additionally, the singlet oxygen sensitization quantum yield of BODIPY **4** was determined using tetraphenylporphyrin (TPPo) as reference compound in the same solvent as the compound solution, in THF (ϕ_Δ = 0.60). The BODIPY solution was optically matched with the reference compound solution at the excitation wavelength at absorbance less than 0.3. The singlet oxygen phosphorescence was detected at 1276 nm, which is the characteristic wavelength of the $^1O_2$ emission band. To avoid the

overlap of the fluorescence emission second harmonic signal with the singlet oxygen phosphorescence emission band centered at 1276 nm a Newport longpass dielectric filter with 1000 nm cut-on was used. The singlet oxygen sensitization quantum yield value is then determined by comparing the integrated area under the emission spectra of the sample solutions and the reference solution, applying **Equation 2**:

$$\phi_{\Delta_{cp}} = \frac{F_{cp}}{F_{ref}} \times \phi_{\Delta_{ref}} \qquad \textbf{Equation 2}$$

where F is the integrated area under the singlet oxygen emission curve and $\phi_{\Delta_{ref}}$ represents the singlet oxygen sensitization quantum yield of the reference compound. subscript ref and cp refer to the reference and compound under study, respectively.

2.4 Evaluation of BODIPY **1** as optical chemosensor

2.4.1 Preliminary study of the chemosensory capacity of BODIPY **1**

In a first step, a preliminary study of the chemosensory capacity of the BODIPY derivative was carried out. This procedure is a simple and quick approach to check the possible occurrence of the interaction of BODIPY with the chosen cations and anions. These ions were selected due to their biological and medicinal interest.

Therefore, a solution of BODIPY derivative **1** ($1x10^{-5}$ M) was prepared in acetonitrile. Then solutions of cations (Ag^{+}, K^{+}, Li^{+}, Hg^{2+}, Ca^{2+}, Co^{2+}, Pb^{2+}, Mn^{2+}, Fe^{2+}, Zn^{2+}, Ni^{2+}, Cd^{2+}, Cu^{2+}, Pd^{2+}, Fe^{3+}, and Al^{3+}) ($1x10^{-2}$ M) in the form of perchlorate salts, except Pd^{2+} and Li^{+} whose counter-ion was tetrafluoroborate, and of anions ($H_2PO_4^-$, HSO_4^-, CN^-, F^-, I^-, NO_3^-, AcO^-, Br^-, ClO_4^-, BzO^-) in the form of tetrabutylammonium salts, were prepared in acetonitrile with a concentration of $1x10^{-2}$ M.

Considering the results obtained in acetonitrile solutions, it was decided to perform a new test in an aqueous medium. For this purpose, the solution of compound **1** was prepared in an acetonitrile/water mixture (75:25) with a concentration of $1x10^{-5}$ M. The ionic solutions used were the same and, similarly, 50 equivalents of each ion were added to the solution of the compound.

In both tests, the color variation of the solutions was visualized under natural light, while the fluorescence variation was visualized with the aid of a UV-vis viewing cabinet, at the excitation wavelength of 365 nm.

2.4.2 Spectrophotometric and spectrofluorimetric titrations of BODIPY **1**

In a second step, spectrophotometric and spectrofluorimetric titrations were carried out to complete the preliminary study of the chemosensory capacity of BODIPY derivatives carried out previously.

The titrations were made at room temperature, using the solution of BODIPY **1** in a mixture of acetonitrile/water (75:25) ($1x10^{-5}$ M), and the solutions of Pd^{2+}, Hg^{2+}, Fe^{3+}, and Al^{3+}, in acetonitrile ($1x10^{-2}$ M). In this sense, 3 mL of BODIPY **1** solution was put into a 1 cm quartz cuvette, followed by successive addition of cations equivalents, and the absorption and emission graphs of the compound were obtained. For fluorescence spectra measurement, the excitation wavelength was set at 484 nm and a slit of 2 nm was chosen.

2.5 Evaluation of BODIPY **1** as fluorescent probe for bioimaging

This study was performed at the International Iberian Nanotechnology Laboratory (INL) as part of an existing collaboration between this institution and the research group in which this thesis was developed at the Centre of Chemistry at the University of Minho.

2.5.1 Cell culture

The live human cervical cancer cells (HeLa) were chosen for bioimaging studies due to its high proliferation and stability *in vitro*. This type of cell line comes from cervical cancer epithelial cells and was obtained from Henrietta Lacks in 1951. Since then, the HeLa cells have been used extensively in scientific research.

HeLa cells were cultured in RPMI 1640 medium (Roswell Park Memorial Institute), supplemented with 10% fetal bovine serum (FBS) and 1% Penicillin-Streptomycin, at 37 °C in a humidified environment with 95% air and 5% CO_2.

Before each experimental assay, it is necessary to count and divide the cells. For this purpose, the cells are previously washed with warm phosphate-buffered saline (PBS) and subjected to the trypsinization process for 5 minutes at 37 °C. Then RPMI is added to inhibit the trypsin activity and the cell suspension is transferred to a falcon with medium to centrifuge at 1200 rpm for 5 minutes. Finally, the cell pellet is resuspended in a new medium and the number of cells is counted in the Neubauer chamber to determine the appropriate cell concentration for the experimental assay.

2.5.2 Dark cytotoxicity assay

The cell viability was determined by the Resazurin assay, which allowed evaluation of the cytotoxicity of compound **1**, in HeLa cells, quickly and simply. This method is based on the use of a redox indicator, whose oxidized form is blue and non-fluorescent (Resazurin), and its reduced form is pink and fluorescent (Resorufin). In this way, healthy cells will provide an irreversible reduction of the indicator, showing a change in their coloration from blue to pink and, simultaneously, an increase in fluorescence. As a result, the fluorescence intensity of the solution is proportional to the number of healthy cells in the sample.

For this assay, approximately 3000 cells were plated per well in 96-well plates and kept in incubation for 24 hours. The BODIPY **1** was dissolved in DMSO to a stock solution of 1.24×10^4 µM and maintained in a refrigerator at 4 °C. To prepare a range of working solutions concentrations (6.25, 12.5, 25, 50, and 100 µM), BODIPY was diluted in RPMI 1640 medium. Then, 2 mg of Resazurin sodium salt was dissolved in 20 mL of PBS to prepare a stock solution of 0.4 mM and this was diluted 10 times to prepare the Resazurin working solution.

Concerning the procedure, the cells were first treated with different concentrations of BODIPY **1** and, after 24 hours of incubation, the Resazurin indicator was added, and the plates were stored for 2 hours in the dark. Then fluorescence was measured at an excitation wavelength of 528 nm and an emission wavelength of 590 nm. The fluorescence intensity was read in the Biotek Synergy H1 microplate reader and the cell viability values were calculated using **Equation 3** and expressed in percentage concerning the values obtained from the negative control (untreated cells). The blank

represents the fluorescence mean value of the RPMI 1640 medium. For each assay, three independent replicates were made and the respective mean ± standard deviation was determined. Statistical analysis of results was performed using GraphPad Prism 5.0 software. One-way ANOVA was conducted to study statistical significance between the treated and untreated groups and significance levels were established at $P < 0.05$.

$$Viability = \frac{Treated\ cells - blank}{Untreated\ cells - blank} \times 100 \qquad \text{Equation 3}$$

2.5.3 Fe^{3+} intracellular detection

For the Fe^{3+} intracellular detection assay, approximately 20000 cells per well were plated in µ-dish 35 mm (Ibidi cat. number 80466) and allowed to adhere for 24 hours. Afterward, the cells were treated with BODIPY **1** solution dispersed in RPMI (40 µM) and incubated at 37 °C for 20 minutes and were rinsed with PBS to remove the remaining **1**. Then, stock solutions of two different iron sources ($FeCl_3$ and $Fe(NO_3)_3 \cdot 9\ H_2O$) were prepared in PBS buffer (pH 7.4) with a concentration of 1 mM, and the cells were treated with $FeCl_3$ (50, 100, and 1000 µM) and $Fe(NO_3)_3 \cdot 9\ H_2O$ (100 µM) solutions dispersed in RPMI and incubated another 20 minutes. For the compound control experiment, only the BODIPY **1** solution in RPMI medium (40 µM) was used instead of the Fe^{3+} solution. The nucleus of the cells was stained with Hoechst 33342 (1:1000, cat. no. ab139481, Abcam), and the sample was incubated at 37 °C for 10 minutes. The commercial fluorescent probe solution was prepared according to the instructions of the suppliers. The fluorescence cell images were taken with a Zeiss LSM 780 confocal laser-scanning microscope under a 63X oil-immersion objective lens. The cells were excited with a 405 nm and 488 nm excitation laser, for the location of the cell nucleus in the blue channel (450–490 nm) and BODIPY **1** in the green channel (510–550 nm), respectively.

Additionally, the intracellular detection of Fe^{3+} with mSLN and SLN was studied, and, therefore, 15000 cells per well were plated in µ-dish 35 mm (Ibidi cat. number 80466) and allowed to adhere for 24 hours. Then, the cells were treated with a 1 mM solution of mSLN/SLN (7 mM stock) dispersed in RPMI and incubated overnight at 37 °C. After that, the cells were rinsed with PBS to remove the remaining nanoparticles and the cells were treated with BODIPY **1** solution (40 µM) dispersed in RPMI, incubating them at 37 °C for 20 minutes. For the compound control, only the BODIPY **1** solution (40

μM) in RPMI medium was used and for the mSLN control, only the 1 mM mSLN solution was used to treat the HeLa cells. In all experiments, the nucleus of the cells was stained with Hoechst 33342 (1:1000, cat. no. ab139481, Abcam), and the sample was incubated at 37 °C for 10 minutes. The commercial fluorescent probe solution was prepared according to the instructions of the suppliers. Finally, the fluorescence cell images were taken with a Zeiss LSM 780 confocal laser-scanning microscope under a 63X oil-immersion objective lens. The cells were excited with a 405 nm and 488 nm laser excitation, for the location of the cell nucleus in the blue channel and BODIPY **1** in the green channel, respectively.

2.5.4 Sub-cellular localization

The co-localization studies with different commercial fluorescent probes were carried out to assess the subcellular distribution of the BODIPY **1** derivative in the presence of mSLN. In this sense, 15000 HeLa cells were plated per well in μ-dish 35 mm (Ibidi cat. number 80466) and, after 24 hours of adhesions, were treated with a 1 mM solution of mSLN/SLN (7 mM stock) dispersed in RPMI and incubated overnight at 37 °C. Then, the cells were treated with commercial fluorescent probes for the study of subcellular localization, namely, with a solution of LysoTracker Deep Red (74 nM, cat. no. L12492, Invitrogen) for 1 hour to label lysosomes and with a solution of LipidSpot™ (1:1000, cat. no. 70069-T, Biotium) for 30 minutes to label lipid droplets in the cell cytoplasm. Then, cells were washed with PBS and incubated with a BODIPY **1** solution (40 μM) dispersed in RPMI at 37 °C for 20 minutes and, next, with Hoechst 33342 (1:1000, cat. no. ab139481, Abcam) for 10 minutes to stain the cell nucleus. The commercial fluorescent probes solutions were prepared according to the instructions of the suppliers. Finally, the fluorescence cell images were taken with a Zeiss LSM 780 confocal laser-scanning microscope under a 63X oil-immersion objective lens, using the 405 nm laser to visualize the cell nucleus, the 488 nm laser to visualize the BODIPY **1** derivative, and the 633 nm laser to visualize the lysosomes and lipid droplets. Additionally, different groups of cells incubated with a single fluorescent marker in the presence and absence of mSLN were used as control groups.

Moreover, it was used oleic acid complexed with BSA to induce lipid droplet formation in cultured cells as a positive control for LipidSpot™ staining. For this study, 15000 cells were incubated per well in μ-dish 35 mm (Ibidi cat. number 80466) for 24 hours, and oleic acid and defatted BSA solutions were prepared for further complex formation. Therefore, the oleic acid was heated to 37 °C

until it is completely liquefied, oleic acid 47 µL was mixed with 50% ethanol 953 µL to prepare a 150 mM solution, and the mixture was Vortexed and stored at 4 °C. Moreover, a 100 mg/ml BSA solution was prepared by dissolving the defatted BSA in dH_2O and stored at -20 °C. Finally, on the day of cells treatment, the oleic acid/BSA complex was prepared. Thus, the oleic acid solution was resuspended by heating to 37 °C and vortexing, and then equal volumes (20 µL) of 150 mM oleic acid and 100 mg/mL defatted BSA in dH_2O were combined. The mixture was incubated at 37 °C for 1 hour. Then, this oleic acid/BSA complex was diluted 1:150 in complete RPMI medium for a final concentration of 500 µM oleic acid, and the cells were incubated with this solution overnight at 37 °C. Then, cells were washed with PBS and incubated at 37 °C with a solution of LipidSpot™ (1:1000, cat. no. 70069-T, Biotium) for 30 minutes to label lipid droplets in the cell cytoplasm, with a BODIPY **1** solution (40 µM) dispersed in RPMI for 20 minutes and, finally, with Hoechst 33342 (1:1000, cat. no. ab139481, Abcam) for 10 minutes to stain the cell nucleus. The commercial fluorescent probes solutions were prepared according to the instructions of the suppliers. Finally, the fluorescence cell images were taken with a Zeiss LSM 780 confocal laser-scanning microscope under a 63X oil-immersion objective lens, using the 405 nm laser to visualize the cell nucleus, the 488 nm laser to visualize the BODIPY **1** derivative, and the 633 nm laser to visualize the lipid droplets.

2.6 Evaluation of BODIPY **2** and **3** as aggregation-induced emission fluorophores

This study was performed at the Chemistry Department at the University of Coimbra as part of an existing collaboration between this institution and the research group in which this thesis was developed at the Centre of Chemistry at the University of Minho.

This study is based on the preparation of mixtures of two miscible solvents in which the compound to be analyzed is soluble in only one of the solvents. In this sense, THF:water mixtures were prepared and THF was used as a good solvent and water as a bad solvent. The volumetric fractions of water were controlled to induce the formation of aggregates in these mixtures.

Therefore, THF stock solutions of BODIPY derivatives **2** and **3** were prepared at absorbance around 0.8. Then 200 µL of these solutions were transferred to a volumetric cell and appropriate

amounts of THF and water were added to prepare a 2 ml final solution with a specific water fraction. The water content ranged from 0-90 vol %.

After sample preparation, the absorption and emission spectra of the resulting BODIPY solutions were measured immediately. For fluorescence spectra measurement of BODIPY **2** and **3**, the excitation wavelength was set at 470 nm and 490 nm, and a slit of 2 nm and 4 nm was chosen, respectively.

2.7 Evaluation of BODIPY **4** as photosensitizer for photodynamic therapy

This study was performed at the Chemistry Department at the University of Coimbra as part of an existing collaboration between this institution and the research group in which this thesis was developed at the Centre of Chemistry at the University of Minho.

2.7.1 Cell culture

4T1 is a breast carcinoma cell line originally derived from a mammary gland tissue of BALB/c mice. These cells have been used to study breast cancer metastasis as they closely mimic human breast cancer. This cell line was chosen for PDT studies due to its high proliferation and stability *in vitro*.

4T1 cells were cultured in DMEM medium (Dulbecco's modified eagle medium), supplemented with 10% FBS and 1% Penicillin-Streptomycin, at 37 °C in a humidified environment with 95% air and 5% CO_2.

Before each experimental assay, it is necessary to count and divide the cells. For this purpose, the cells are previously washed with PBS and subjected to the trypsinization process for 5 minutes at 37 °C. Then DMEM is added to inhibit the trypsin activity and the cell suspension is transferred to a falcon with medium to centrifuge at 1200 rpm for 5 minutes. Finally, the cell pellet is resuspended in a new medium and the number of cells is counted in the Neubauer chamber to determine the appropriate cell concentration for the experimental assay.

2.7.2 Dark cytotoxicity assay

The cell viability was determined by the Resazurin assay, which allowed evaluation of the cytotoxicity of compound **4**, in 4T1 cells, quickly and simply. For this assay, approximately 6000 cells were plated per well in 96-well plates and kept in incubation for 24 hours to allow the attachment of the cells. The BODIPY **4** was dissolved in DMSO to a stock solution of 10 mM and maintained in a refrigerator at 4 °C. To prepare a range of working solutions concentrations (3.125, 6.25, 12.5, 25, 50, and 100 µM), BODIPY was diluted in DMEM medium. Then, 2 mg of Resazurin sodium salt was dissolved in 20 mL of PBS to prepare a stock solution of 0.4 mM and this was dilute 10x to prepare the Resazurin working solution. Dark cytotoxicity studies were performed in triplicates and repeated in two sets of tests and proceeded as described above. Statistical analysis of results was performed using GraphPad Prism 5.0 software. One-way ANOVA was conducted to study statistical significance between the treated and untreated groups and significance levels were established at $P < 0.05$.

2.7.3 Uptake assay

The uptake study was performed by flow cytometry and therefore 40,000 cells were seeded in 24-well plates in a final volume of 1 mL of DMEM at 37 °C in a comfortable humidified incubator with 5% CO2. The BODIPY **4** stock solution (10 mM) was diluted to a final concentration of 2.5 µM. After 24 h of culturing, 500 µl of compound **4** was added to the cells considering different time points of compound incubation (0.5, 1, 3, and 6 hours). Then the cells were washed and detached with 250 µl of trypsin, transferred to a 96-well U-shaped plate, and centrifuged at 1200 rpm for 5 min. The supernatant was discarded, and the pellet was resuspended in 200 µl PBS. Finally, the analysis was performed by flow cytometry using the Novocyte 3000 cytometer (ACEA) with 488 nm laser excitation and filter 530/30. This experiment was performed in duplicate and repeated in two sets of tests. Statistical analysis of results was performed using GraphPad Prism 5.0 software. One-way ANOVA was conducted to study the statistical significance of the short incubation times for the 6h of incubation and significance levels were established at $P < 0.05$.

2.7.4 Photocytotoxicity assay

For this assay, approximately 6000 cells were seeded per well in 96-well plates and kept in incubation overnight at 37 °C in a humidified environment with 5% CO_2. To prepare a range of working solutions concentrations (0.16, 0.3, 0.6, 1.3, 2.5, and 5 μM), BODIPY **4** stock solution was diluted in DMEM medium. To prepare Resazurin working solution, the stock solution of 0.4 mM was diluted 10 times. After 30 minutes of incubation with compound **4**, the cells were washed with PBS and 200 μl of RPMI without Phenol Red was added. Controls of the untreated cell were included on every plate. Afterward, the cells were irradiated with a fluence rate of 3 mW/cm^2 until a total of 1 J was reached using a green laser light source (505 nm). Finally, cell viability was performed using the Resazurin method after 24 hours of photodynamic treatment. This experiment was performed in triplicate and repeated in three sets of tests and proceeded as described above.

Chapter 3

Results and Discussion

3. Results and Discussion

The aim of this work was the synthesis and photophysical characterization of BODIPY derivatives, and the study of these compounds for different applications, namely as optical chemosensors, fluorescent probes for bioimaging, AIE fluorophores, and photosensitizers for PDT. **Figure 32** shows the BODIPY derivatives studied throughout this dissertation, highlighting the group of compounds studied for each application. BODIPY derivatives **1**[102] and **2**[103] were previously synthesized by investigators from the research group in which this project was developed. On the other hand, BODIPY derivatives **3** and **4**[105] were synthesized during this dissertation.

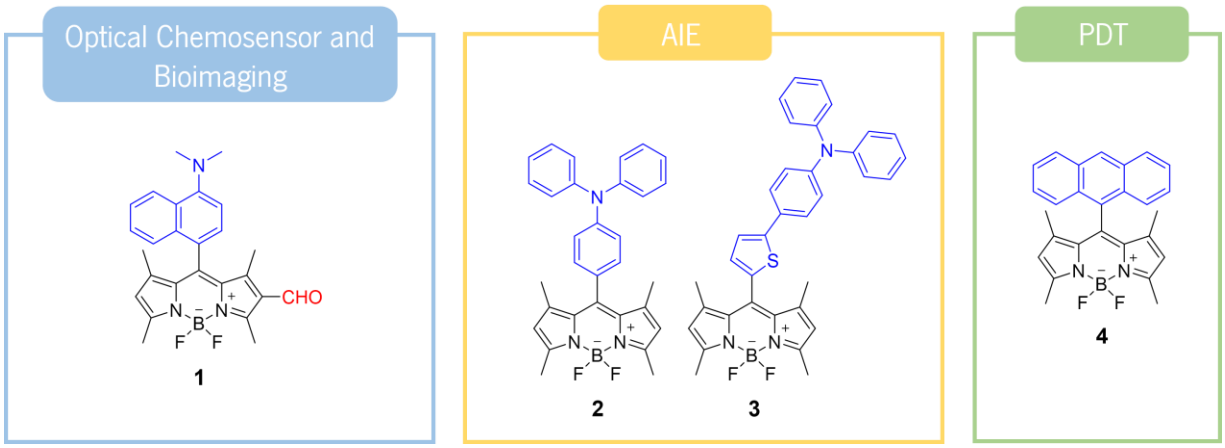

Figure 32. *BODIPY derivatives (**1-4**) and their applications.*

3.1 Synthesis of BODIPY 3

BODIPY **3** was designed and synthesized having in mind its application as AIE fluorophore, and it was decided to functionalize the BODIPY core at the *meso* position with a functional group that presents a greater possibility of rotation compared to BODIPY **2**.

In this sense, the aldehyde precursor **3'**[104] was synthesized through a Suzuki coupling reaction between boronic acid **1'** and hetero(aromatic) bromide **2'** derivative (**Scheme 5**) in order to be used as a precursor for the synthesis of BODIPY **3**.

Suzuki-Miyaura cross-coupling is one of the most used reactions for the formation of carbon-carbon bonds between hetero(aromatic) compounds and consists of the reaction between a boronic acid group and a halogenated compound, such as a bromide, in the presence of a palladium catalyst.[106]

The aldehyde **3'** synthesized was purified by column chromatography on silica gel with hexane/DCM (1:2) as eluent and the pure aldehyde precursor **3'**[104] was obtained as a yellow solid in 86% yield.

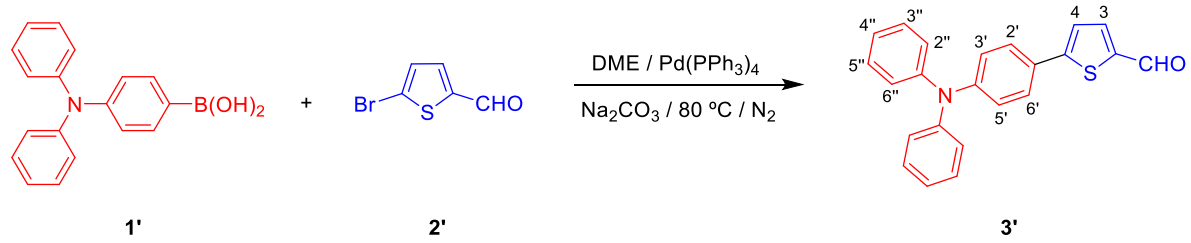

1' **2'** **3'**

Scheme 5. *Synthesis of aldehyde precursor **3'**.*

The aldehyde **3'** was characterized by ^{1}H NMR spectroscopy, which confirmed its structure and purity. Signals corresponding to aromatic and heteroaromatic protons appeared as doublets and multiplets while the formyl group appeared as a singlet with a chemical shift of 9.86 ppm. Of the two doublets that appear in the spectrum, the most deprotected (7.70 ppm) was assigned to proton H-3 of the thiophene ring due to the electron-acceptor character of the formyl group. Additionally, this proton exhibited a coupling constant of J = 4 Hz, characteristic of the coupling constants of adjacent protons in di-substituted thiophene derivatives. The other doublet that appears at lower chemical shift (7.53 ppm) was assigned to triphenylamine aromatic protons H-2' and H-6', showing a coupling constant of 8.8 Hz. The remaining two spectrum signals appear as multiplets that were assigned to the remaining aromatic protons of this compound. At higher chemical shifts (7.29 – 7.33 ppm), the multiplet appears with integration of 5 H corresponding to the H-4 proton of the thiophene ring and twice the H-3'' and H-5'' protons due to the symmetry of the triphenylamine group. At smaller chemical shifts (7.07 – 7.17 ppm) the last multiplet appears with integration of 8 H corresponding to the H-3', H-5' protons and twice the H-2'', H-4'' and H- 6'' protons. These aromatic protons are the most protected due to the electron-donating effect of the amino group.

After the synthesis of the aldehyde precursor **3'**, the respective BODIPY **3** was synthesized in two reactional steps at room temperature. The first step consisted in the condensation reaction of 2,4-

dimethylpyrrole (**4'**) and 5-(4-(diphenylamino)phenyl)thiophene-2-carbaldehyde (**3'**) in the presence of a catalytic amount of TFA in order to obtain the dipyrromethane core (**5'**). The second reactional step involved the oxidation of the dipyrromethane to dipyrromethene, through the addition of a solution of DDQ followed by the complexation reaction with BF_3OEt_2 in the presence of triethylamine (**Scheme 6**). The crude product was purified by column chromatography on silica gel using hexane/DCM (1:1) as eluent to obtain the pure BODIPY **3** as a red solid in 2.8% yield.

The very low yield could be due to the stereochemical constraint that exists in the precursor aldehyde (**3'**), which hinders the first reaction step of condensation with 2,4-dimethylpyrrole (**4'**) due to its bulky structure.

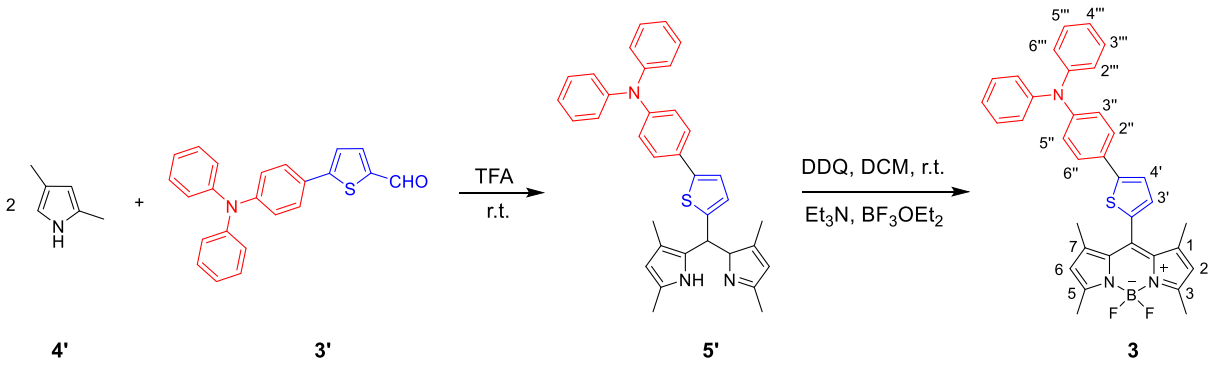

Scheme 6. *Synthesis of BODIPY **3**.*

Likewise, the BODIPY **3** derivative was characterized by ^{1}H NMR spectroscopy. By analyzing the ^{1}H NMR spectrum, it was possible to distinguish the signals associated with the BODIPY core and the *meso* substituent group. The presence of the protons of the substituent group in *meso* position was confirmed by the doublet and multiplet signals located in the aromatic region of the spectrum, which is in agreement with the signals obtained in the ^{1}H spectrum of the respective aldehyde precursor **3'**. At lower chemical shifts, the signals from the protons of the BODIPY **3** core appear as singlets. The signal corresponding to protons H-2 and H-6 appeared at 6.02 ppm. The signal from the protons of the methyl groups at positions 1 and 7 appeared at 1.75 ppm, while those at positions 3 and 5 appeared at 2.56 ppm.

3.2 Synthesis of BODIPY **4**

Compound **4** is a BODIPY derivative functionalized at *meso* position with the anthracene group, and it was synthesized in two reaction steps at room temperature. The first step consisted of the condensation reaction of 2,4-dimethylpyrrole (**4'**) and anthracene-9-carbaldehyde (**6'**), in the presence of a catalytic amount of TFA to form the dipyrromethane core (**7'**). The second reaction step consisted of the oxidation of dipyrromethane to dipyrromethene, through the addition of a solution of DDQ, followed by a complexation reaction with $BF_3.OEt_2$ in the presence of triethylamine (**Scheme 7**). Finally, after purifying the product by dry flash chromatography, the pure BODIPY derivative **4** was obtained as a dark red solid in 26% yield.

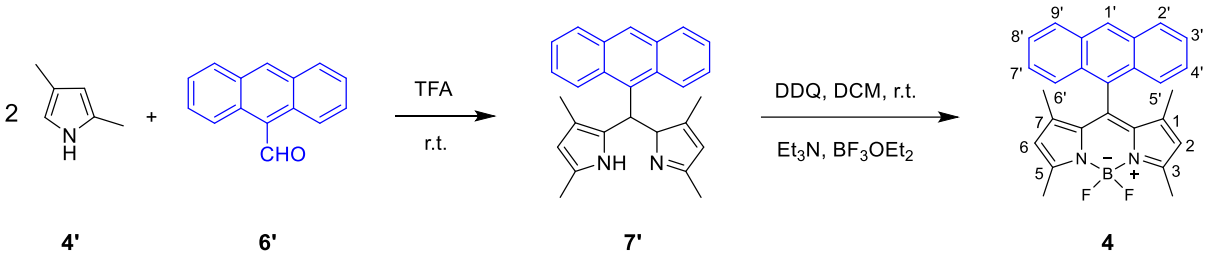

Scheme 7. *Synthesis of BODIPY **4**.*

The structure and purity of BODIPY **4** were confirmed by ^{1}H and ^{13}C NMR spectroscopy. The interpretation of the ^{1}H NMR spectrum allowed us to confirm the presence of the anthracene group at the *meso* position of the BODIPY core, with the characteristic signals of protons appearing in the aromatic zone of the spectrum. Most signals have an integration of 2 H because this molecule has vertical symmetry. In this sense, the aromatic protons H-3' and H-8' appear at 7.41 ppm and the H-4' and H-7' at 7.48 ppm, both as a double triplet signal with J = 1.2 and 8.2 Hz and J= 1.2 and 8.0 Hz, respectively. The protons H-2' and H-9' appear at 7.91 ppm as a double doublet signal with J= 0.8 and 8.8 Hz, the H-5' and H-6' appear at 8.04 ppm as a doublet signal with J = 8.8 Hz and finally, the H-1' appears as a singlet at 8.57 ppm. Additionally, the ^{1}H spectrum also allows confirming the presence of the BODIPY core through the singlet signals at lower chemical shifts due to the methyl groups. The signal from the protons of the methyl groups at positions 1 and 7 appeared with a chemical shift of 0.64 ppm, while those at positions 3 and 5 appeared at 2.63 ppm. The H-2 and H-6 protons appear at 5.86 ppm.

The ^{13}C NMR spectrum was also obtained, and the assignment of its signals agreed with the expected structure. The assignment of the signals in the ^{1}H and ^{13}C NMR spectra was confirmed by the two-dimensional HMQC and HMBC spectra. These allowed to correlate the proton signals with the carbon signals and thus obtain a more accurate and detailed characterization.

The identity of compound **4** was also confirmed by high resolution mass spectrometry. Additionally, the melting point of BODIPY **4** was determined (238 – 240 °C).

3.3 Evaluation of BODIPY 1 as optical chemosensor

Concerning the group of compounds mentioned initially, BODIPY **1**[102] was evaluated as an optical chemosensor and as a fluorescent probe for bioimaging (**Figure 33**).

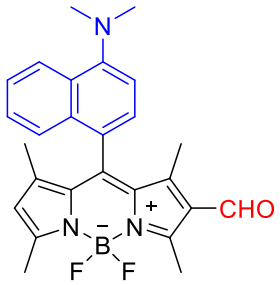

1

Figure 33. *Chemical structure of BODIPY derivative* ***1.***

3.3.1 Photophysical characterization of BODIPY 1

Photophysical characterization of the BODIPY **1** derivative was carried out in acetonitrile solution. The fluorescence quantum yield was obtained by the comparative method using Rhodamine 6G (ϕ_F = 0.95) in ethanol, as fluorescence reference compound.[107]

Table 1 presents the absorption and emission data of BODIPY **1** in acetonitrile solution.

*Table 1. Room temperature spectroscopic and photophysical data for BODIPY derivatives **1** in ACN solution.*

λ_{abs} (nm)	λ_{em} (nm)	ϕ_F	Δ_{SS} (cm^{-1})
494	509	0.148	596

This compound presents an intense absorption band at 494 nm and an emission band at 509 nm (**Figure 34**). The Stokes' shift (Δ_{ss}) obtained was relatively low, however, it is characteristic of this class of compounds.[13] On the other hand, this factor did not limit the application of derivative **1** in bioimaging, as will be demonstrated later. Finally, a relatively good value of fluorescence quantum yield was obtained (ϕ_F = 0.148) which is associated with the combination of the planarity of the naphthalen-1-yl π-conjugate group with the strong donor effect of the *N,N*-dimethylamino moiety present in this compound.

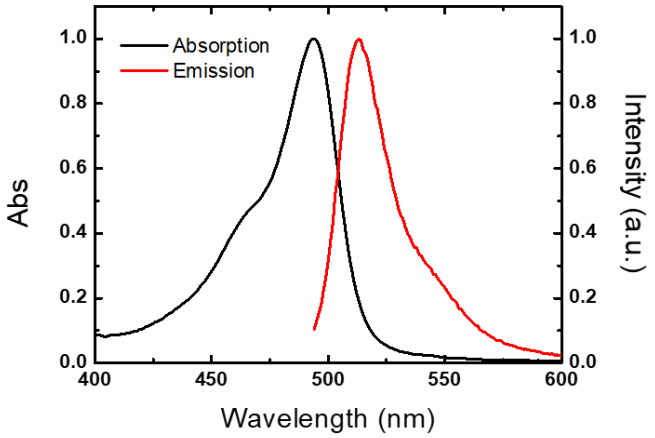

*Figure 34. Normalized absorption and emission spectra of the BODIPY **1** in acetonitrile.*

3.3.2 Preliminary study of the chemosensory capacity of BODIPY 1

To evaluate the chemosensory capacity of the BODIPY derivative **1** to ions with biological and environmental interest, a preliminary study of the interaction between the compound and different cations and anions was carried out. To this end, a $1x10^{-5}$ M BODIPY **1** solution and $1x10^{-2}$ M solutions of cations (Ag^{+}, K^{+}, Li^{+}, Hg^{2+}, Ca^{2+}, Co^{2+}, Pb^{2+}, Mn^{2+}, Fe^{2+}, Zn^{2+}, Ni^{2+}, Cd^{2+}, Cu^{2+}, Pd^{2+}, Fe^{3+} e Al^{3+}) and anions ($H_2PO_4^{-}$, HSO_4^{-}, CN^{-}, F^{-}, I^{-}, NO_3^{-}, AcO^{-}, Br^{-}, ClO_4^{-}, BzO^{-}) were prepared in acetonitrile. The study was carried

out in acetonitrile because it is an aprotic solvent, which cannot establish hydrogen bonds and interfere with the recognition system of these analytes.

The study consisted of adding 50 equivalents of each cation solution to the BODIPY **1** solution and observing the effect of these ions on the optical properties of the compound.

For anions study, there was no colorimetric or fluorometric signal after interaction with the compound, however, BODIPY **1** was able to detect some of the cations under study.

Regarding the colorimetric behavior, it was observed by "naked eye" the detection of Pd^{2+}, Hg^{2+}, Fe^{2+}, Fe^{3+}, and Al^{3+} through an obvious color change of the compound solution from orange to yellow for Pd^{2+}, Hg^{2+}, and Fe^{2+}, and from yellow to green for Al^{3+}. On the other hand, the addition of Fe^{3+} to the BODIPY **1** solution results in a colorless solution (**Figure 35A**).

Simultaneously, a fluorescent enhancement was observed under a UV lamp at 365 nm for compound **1** in the presence of the ions mentioned above, Pd^{2+}, Hg^{2+}, Fe^{2+}, Al^{3+} and, additionally, for Cu^{2+} and Pb^{2+} (**Figure 35B**).

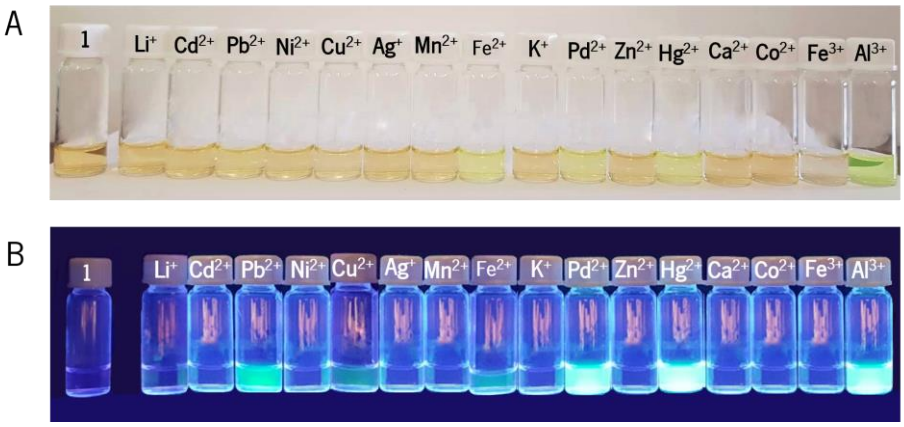

Figure 35. *Solutions of compound **1** in ACN under (A) natural light and (B) UV radiation at λ_{max} = 365 nm upon addition of various cations.*

Considering these results, the chemosensory capacity of the BODIPY derivative **1** to metal ions was investigated in an aqueous medium, to evaluate its potential application for the detection of ions in real samples. For this purpose, solutions of ions ($1x10^{-2}$ M) and compound ($1x10^{-5}$ M) were similarly prepared in a mixture of acetonitrile/water (75:25).

After adding 50 equivalents of each ion to the BODIPY **1** solution it was found that it became more selective in the aqueous medium. Regarding the colorimetric behavior, there was a small increase

of intensity in the orange color of the compound solution in the presence of Fe^{3+} (**Figure 36A**) and, concerning fluorimetric behavior, it was observed an increase in the fluorescence intensity of the compound solution after interaction with Pd^{2+}, Al^{3+}, Hg^{2+} and Fe^{3+} (**Figure 36B**).

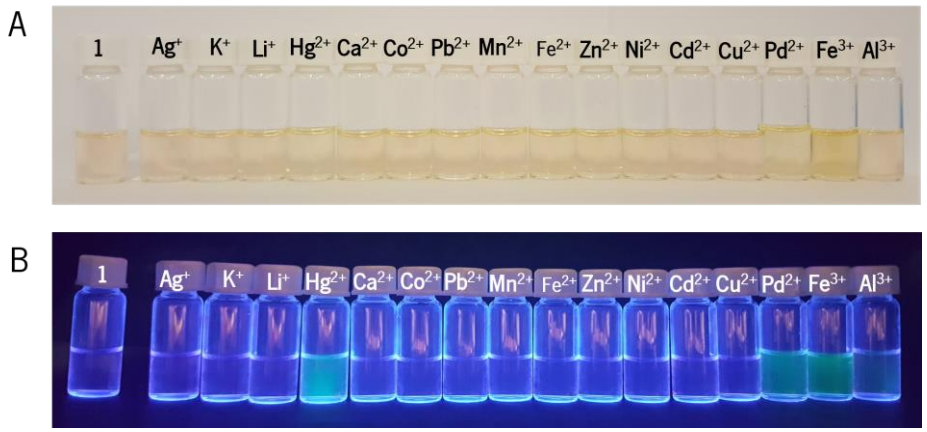

Figure 36. *Solutions of compound **1** in ACN/water (75:25) under (A) natural light and (B) UV radiation at λ_{max} = 365 nm upon addition of various cations.*

Thus, the intensity of the response obtained in the chemosensory study in aqueous media proved to be lower than in the study in organic solvent. This fact is probably due to the effect of solvation of the cations by the solvent's water molecules, which hinders the interaction between the ion and the compound. Moreover, the results showed that there is an increase in the selectivity of BODIPY **1** in an aqueous solution since it detects only four cations. As a result, the BODIPY **1** showed to be very promising for further application as a fluorescent probe in biological samples since this compound could detect analytes fluorimetrically in aqueous media.

3.3.3 Spectrophotometric and spectrofluorimetric titrations of BODIPY **1**

According to the results obtained in the preliminary evaluation of the chemosensory capacity of the BODIPY **1** and considering their application in biological samples, spectrophotometric and spectrofluorimetric titrations were carried out to investigate the efficiency of BODIPY **1** towards Pd^{2+}, Al^{3+}, Hg^{2+} and Fe^{3+} detection in an aqueous medium. For this purpose, solutions of ions ($1x10^{-2}$ M) and compound **1** ($1x10^{-5}$ M) were similarly prepared in a mixture of acetonitrile/water (75:25). Thus, the addition of increasing amounts of cation to the compound solution was made, and, simultaneously, the

corresponding absorption/emission spectrum was obtained. These titration graphs allowed to follow the changes in the compound absorption/emission bands concerning the number of equivalents of each cation added. The cation solutions were prepared with a higher concentration than the compound solution (around 10^3 times) so that the successive additions of cations did not change the final volume of the solution and consequently the final concentration of the compound.

Regarding the colorimetric behavior, BODIPY **1** seemed to show an intensification of its orange color in the presence of Fe^{3+}, however, when the corresponding spectrophotometric titration was carried out, there was a successive overlap of the absorption bands, and no shift of the absorption band occurred upon addition of increasing amounts of this cation. As a result, it was concluded that BODIPY **1** is not a colorimetric sensor for Fe^{3+} and the intensification of solution color was due to the orange coloration of the Fe^{3+} solution.

Subsequently, spectrofluorimetric titrations of BODIPY **1** with Pd^{2+}, Al^{3+}, Hg^{2+}, and Fe^{3+} ions were carried out in an aqueous medium. As could be seen, in all cases, the progressive addition of ion to compound solution induced a gradual enhancement of the BODIPY **1** emission band at around 514 nm (**Figure 37**), without displacement of the emission band.

On the other hand, it was obtained the relationship between the fluorescence intensity of BODIPY **1** and the equivalents number of cations. In the case of Fe^{3+}, 143 equivalents were needed to reach the maximum increase of fluorescence intensity (**Figure 37A**). Regarding the other cations, Hg^{2+}, Pd^{2+}, and Al^{3+}, 280, 204, and 225 equivalents were used, respectively, and the end of the titration was not reached due to depletion of the cell capacity (**Figure 37B, 37C, and 37D**).

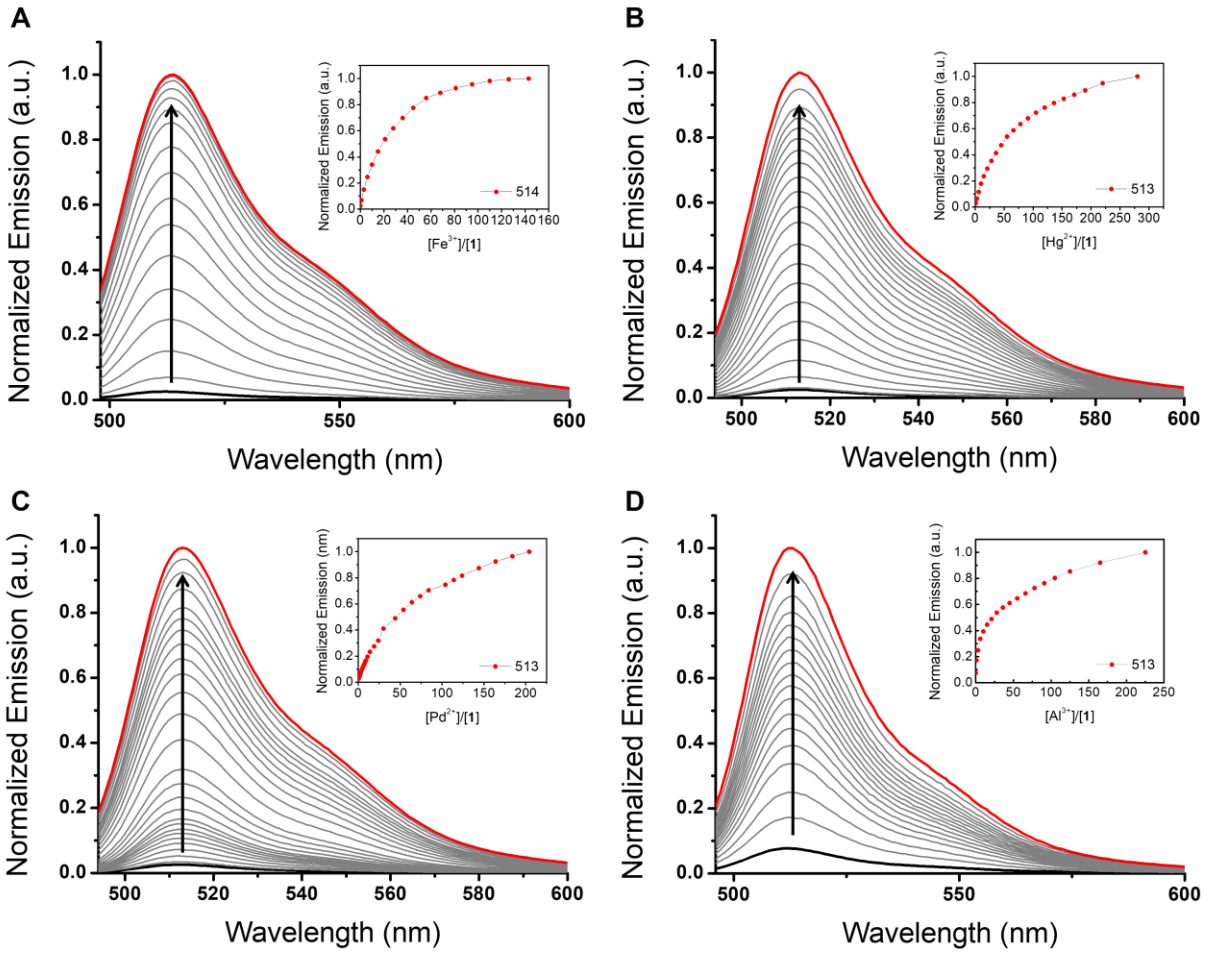

Figure 37. Spectrofluorimetric titrations of compound **1** *with addition of increasing amounts of (A) Fe^{3+}, (B) Hg^{2+}, (C) Pd^{2+} and (D) Al^{3+}, in acetonitrile/water (75:25). The inset represents the normalized emission at 514 nm as a function of $[Fe^{3+}]$ / [**1**] and at 513 nm as a function of $[Hg^{2+}]$ / [**1**], $[Pd^{2+}]$ / [**1**] and $[Al^{3+}]$ / [**1**]. ([**1**] =1x10^{-5} mol·dm^{-3}, $[Hg^{2+}]$ =$[Fe^{3+}]$ =$[Al^{3+}]$ =$[Pd^{2+}]$ =1x10^{-2} mol.dm^{-3}, λ_{exc} = 494 nm, T = 298 K).*

Compared to the other cations studied, BODIPY **1** showed the most efficient response to Fe^{3+}. However, in all cases, a high number of ion equivalents was necessary to achieve the maximum increase in the fluorescence intensity of the compound, since the aqueous medium is a competitive medium that hinders the interaction between the compound and the analyte.

Furthermore, these spectrofluorimetric results agree with the previous preliminary studies since it was verified in all cases the increase in fluorescence intensity after the addition of cations to the compound solution. This increase in the fluorescence intensity of BODIPY **1** is known as the CHEF effect and suggests that the signaling mechanism involved in the coordination process with cations is the PET process. The interaction of the cation with the compound's receptor subunit blocks the PET process, which allows the reestablishment of the fluorophore's fluorescence emission. This is reflected in the increase of fluorescence intensity of BODIPY **1**, without changing the emission band.

Finally, **Table 2** summarizes the results obtained in the sensing capacity studies of the BODIPY derivative **1** to metal ions in acetonitrile and acetonitrile/water (75:25), which were confirmed by spectrophotometric and spectrofluorimetric titrations.

Table 2. *Results of the chemosensory ability studies of BODIPY **1** with various cations, in ACN and ACN/water (75:25).*

Acetonitrile		**Acetonitrile/Water (75:25)**	
Colorimetric Signal	Fluorimetric Signal	Colorimetric Signal	Fluorimetric Signal
Pd^{2+}, Al^{3+}, Hg^{2+}, Fe^{3+}, Fe^{2+}	Pd^{2+}, Al^{3+}, Hg^{2+}, Fe^{2+}, Pb^{2+}, Cu^{2+}	—	Pd^{2+}, Al^{3+}, Hg^{2+}, Fe^{3+}

3.4 Evaluation of BODIPY 1 as fluorescent probe for bioimaging

According to the results obtained previously in the preliminary test of the chemosensory capacity, BODIPY **1** showed to be fluorescent in aqueous medium. So, it was decided to test its potential application as a bioimaging probe in live cells. The preliminary study of BODIPY **1** as a fluorimetric probe for bioimaging was carried out in collaboration with International Iberian Nanotechnology Laboratory (INL), on the ambit of the FCT financed project "*Self-reporting immunostimulating formulation for on-demand cancer therapy with realtime treatment response monitoring",* (PTDC/QUI-COL/28052/2017), using HeLa cancer cells and fluorescence and confocal microscopy techniques.

3.4.1 Dark cytotoxicity assay

Before carrying out any cellular imaging assay, it was decided to investigate the biocompatibility of BODIPY derivative **1** concerning HeLa cells, using the simple method of Resazurin. HeLa cells were treated with different concentrations of BODIPY (6.25, 12.5, 25, 50, and 100 μM) and, after 24 hours of incubation, the respective fluorescence intensity was analyzed, and the percentage of live cells was obtained. Compared to the negative control values (untreated cells), it was concluded that the compound does not induce significant cytotoxic effects within the range of concentrations tested, since

there is a high percentage of living cells (**Figure 38**). Statistical analysis of the results also proves the non-toxicity of the compound to HeLa cells since there is no statistically significant difference in cell viability between the groups of cells treated with different concentrations of compound and the control of untreated cells. Thus, BODIPY **1** proved to be biocompatible with this cell line and appropriate for further bioimaging experiments.

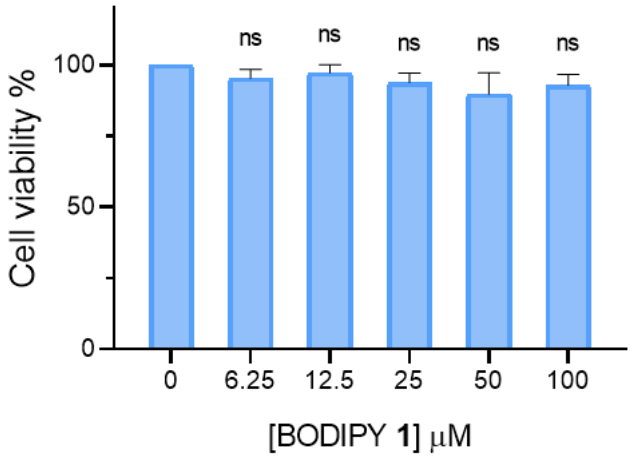

Figure 38. *Evaluation of the HeLa cells viability after 24 hours of incubation with different concentrations of BODPY **1**. Cell viability was determined using the Resazurin method. Data are presented as mean ± standard deviation and ns indicates the statistical significance between the cell viability of treated and untreated groups.*

3.4.2 Fe^{3+} intracellular detection

The toxicity of metal ions and their wide distribution in the environment have raised serious concerns about their impact on human health. In this sense, fluorescent probes have been presented as useful tools for the detection and quantification of metal ions in the body. Iron is an essential element in our body since it plays a crucial role in a variety of biological processes, from cell metabolism to enzymatic reactions. Iron detection in the cellular environment is important because its deregulation in the body causes the appearance of serious diseases, such as Alzheimer's, Parkinson's, organ dysfunction, etc.[108,109]

Given this, there is interest in investigating the possible use of BODIPY derivatives as fluorescent probes for ion intracellular detection. According to the preliminary tests of sensing capacity and spectrofluorimetric titrations in aqueous media presented above, compound **1** showed potential to be used as a fluorescent probe for the intracellular detection of Fe^{3+}. Furthermore, the previous cell

viability study confirmed its good biocompatibility with HeLa cells. Taking all these aspects into account, cell imaging experiments were conducted to investigate the Fe^{3+} sensing ability of BODIPY **1** in HeLa cells. For this type of study, confocal microscopy was used, which makes possible to monitor in real time the influence of the presence of the cation on the fluorescence intensity of the compound. Therefore, the cells were excited with a 405 nm and 488 nm excitation laser, for the location of the cell nucleus in the blue channel and BODIPY **1** in the green channel, respectively.

First, it was compared in terms of fluorescence the controls of untreated cells and cells treated only with a 40 μM solution of BODIPY **1**. As shown in **Figure 39A**, only the fluorescence of the cell nucleus marker is observable in the absence of the compound, whereas cells in the presence of BODIPY **1** show greenish fluorescence in the cytoplasmic region surrounding the cell nucleus (**Figure 39B**). This indicates that BODIPY **1** is able to rapidly diffuse across the cell membrane and accumulate inside cells. Furthermore, cell morphology remains in good condition after the entry of this compound into HeLa cells, indicating the low toxicity and the good cytocompatibility of this compound.

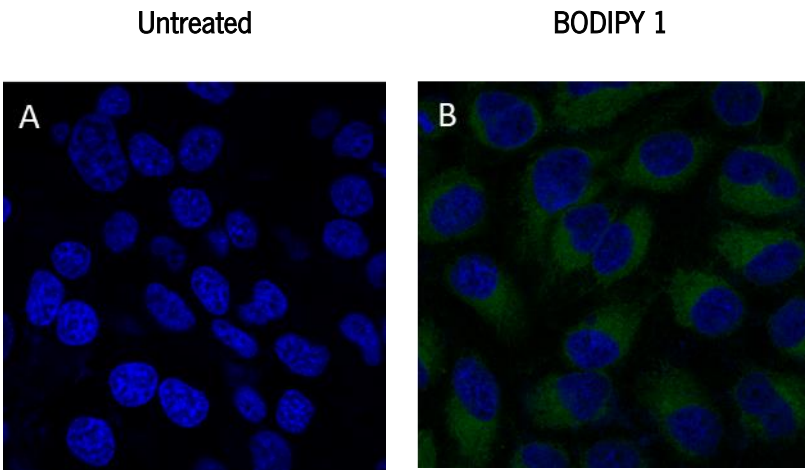

Figure 39. *Fluorescence confocal microscopic images of living HeLa cells stained with Hoechst 33342, (A) in the absence and (B) presence of BODIPY **1** (40 μM).*

Then, the study of the intracellular detection of Fe^{3+} was carried out and, therefore, HeLa cells were incubated with 40 μM solution of BODIPY **1** followed by the addition of different concentrations of $FeCl_3$ solution (50, 100 μM, and 1 mM). As shown in **Figure 40**, there was no change in compound fluorescence intensity in the presence of the different concentrations of Fe^{3+} compared to the BODIPY **1** control shown above (**Figure 39**).

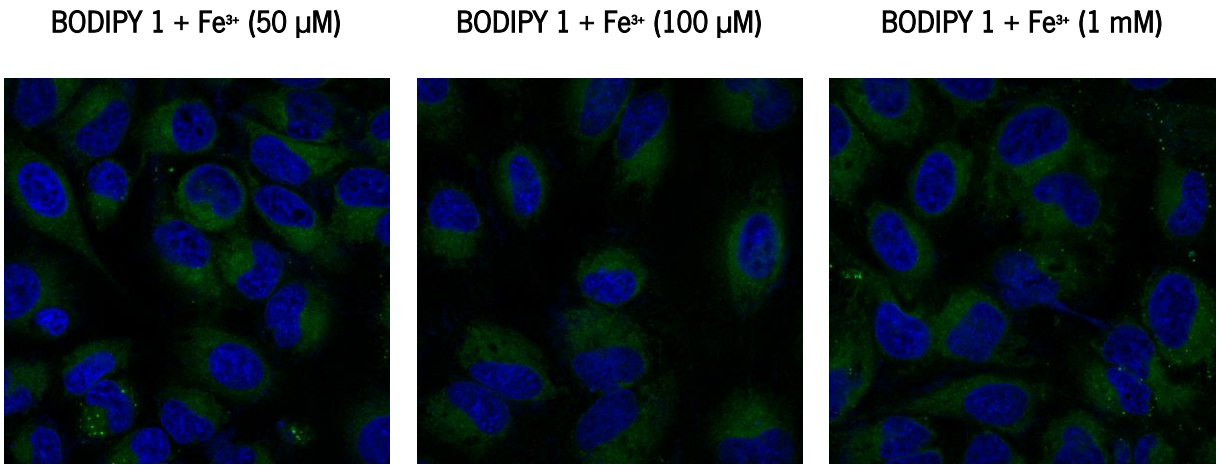

Figure 40. *Fluorescence confocal microscopic images of living HeLa cells treated with BODIPY* ***1*** *(40 µM) and $FeCl_3$ solutions of different concentrations (50 µM, 100 µM, and 1 mM).*

Given these results, it was decided to change the iron source and instead of using iron chloride, a solution of iron nitrate was used. Therefore, the cells were treated equally with a 40 µM solution of BODIPY **1** and then with 100 µM solution of $Fe(NO_3)_3 \bullet 9\ H_2O$. However, it was again found that there was no change in the fluorescence of BODIPY after the addition of the iron nitrate solution (**Figure 41**).

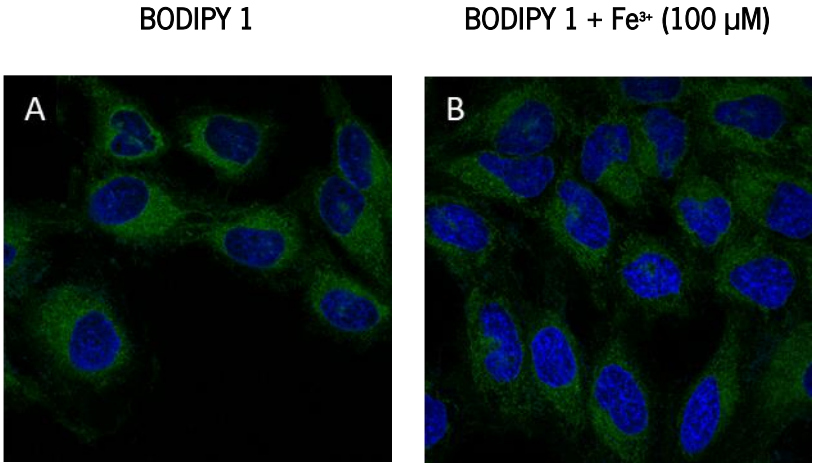

Figure 41. *Fluorescence confocal microscopic images of living HeLa cells treated with BODIPY* ***1*** *(40 µM) (A) in the absence and (B) presence of $FeCl_3$ (100 µM).*

Finally, it was decided to change some of the experimental conditions, such as the incubation time of the cells with the Fe^{3+} solution and the order of treatment of the cells with BODIPY and the iron solutions, to see if they had any influence on the results. Concerning the incubation time of the cells with the iron solutions, incubation times shorter (10 minutes) and longer (1 h and 24 h) than the usual

20 minutes were tested, but even so, no increase in the fluorescence intensity of the compound was observed. Next, the order of treatment of the cells was reversed, that is, the cells were incubated first with the iron solution and then with BODIPY **1**, but even so there was no change in the results. Thus, it could be concluded that it is not possible to detect changes in the fluorescence intensity of BODIPY **1** in cells treated with iron salts, however, the compound can rapidly diffuse through the cell membrane and stain cell cytoplasm.

As no results were obtained with Fe^{3+} salts, it was decided to evaluate an alternative source of iron based on nanoparticles. Having this in mind, studies with magnetic solid lipid nanoparticles (mSLN), which consist in a solid lipid core that incorporates iron oxide (Fe_3O_4) and is stabilized by a surfactant (**Figure 42**), were performed. These nanoparticles have Fe^{3+} in their constitution, and additionally, they also present important characteristics for cell studies, such as low toxicity due to the lipid matrix and an easy internalization by different physiological barriers.[110]

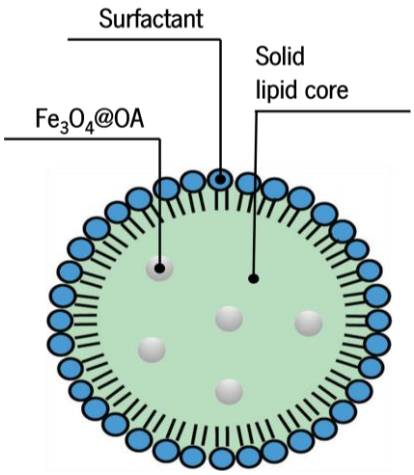

Figure 42. *Structure of magnetic Solid Lipid Nanoparticle. OA = Oleic acid. (Figure adapted from reference 106).*

This study resembles the previous one in which control from cells treated with BODIPY **1** (40 μM) and cells treated only with mSLN (1 mM) were first analyzed for fluorescence. Thus, it was again observed that there is cell internalization of BODIPY **1** through the greenish labeling of the cytoplasm (**Figure 43A**) and that the mSLN does not show fluorescence in the cells (**Figure 43B**). At last, cells treated with both BODIPY **1** and mSLN were analyzed and the fluorescence intensity was compared with the compound control. In this case, it was observed that the presence of mSLN causes an increase

in the fluorescence intensity of compound **1** in the form of green dots located in the cell cytoplasm (**Figure 43C**).

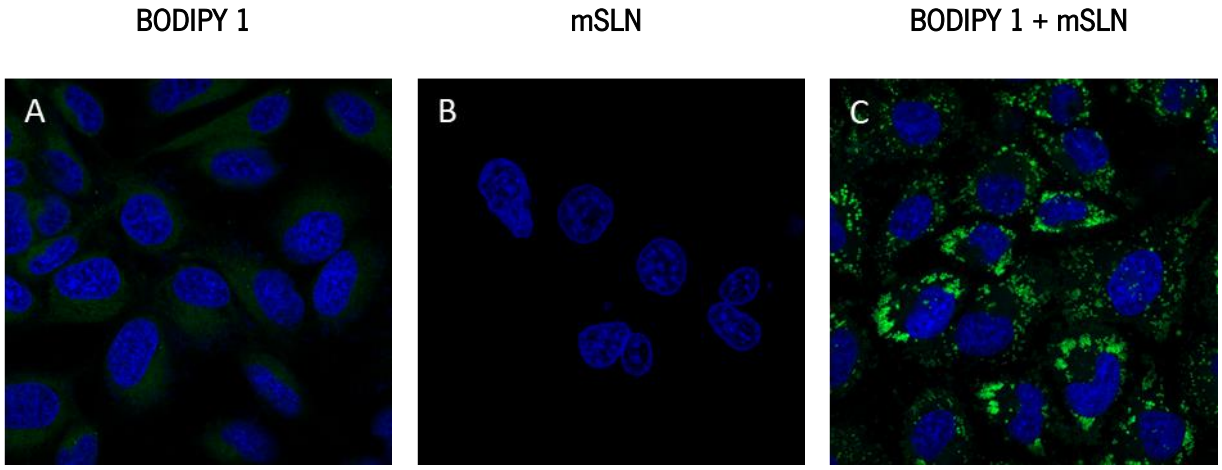

Figure 43. *Fluorescence confocal microscopic images of living HeLa cells treated with (A) BODIPY **1** (40 µM), (B) mSLN (1 mM) and (C) both BODIPY **1** (40 µM) and mSLN (1 mM).*

Regarding this result, to understand if the increase in fluorescence intensity could be due to the signaling of mSLN iron oxide by the compound, an additional study was carried out with two groups of HeLa cells in which both were treated with BODIPY **1**, but one group of cells was incubated with mSLN and the other with simple SLN, that is, the same type of nanoparticles, but without iron oxide in its constitution. From this assay, it was observed an increase in compound fluorescence in the form of small green dots in both experiments (**Figure 44**).

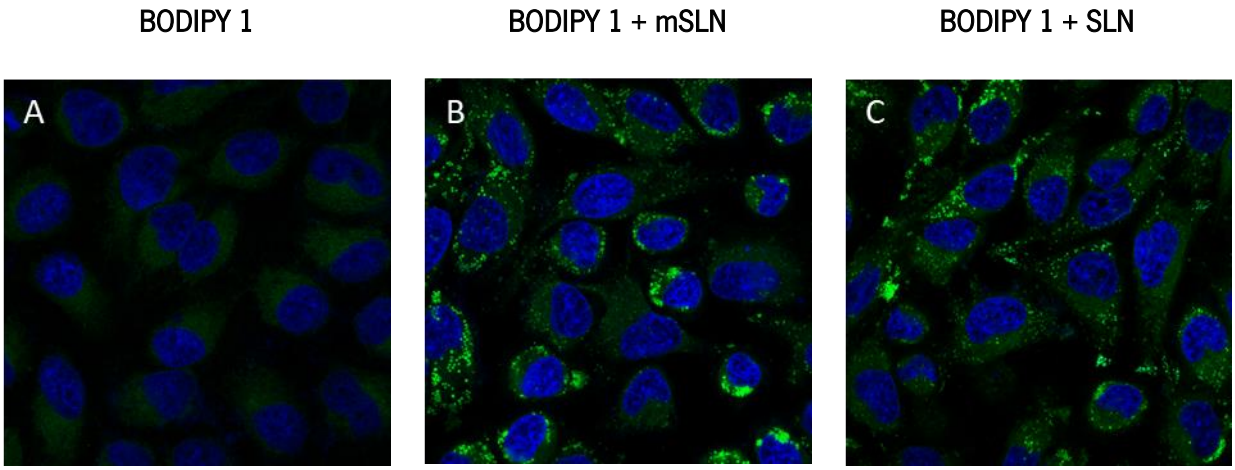

Figure 44. *Fluorescence confocal microscopic images of living HeLa cells treated (A) only with BODIPY **1** (40 µM) and (B) with BODIPY **1** in the presence of SLN (1 mM) with iron oxide and (C) without iron oxide.*

Therefore, it was concluded that this signaling was not related to the presence of iron oxide in the nanoparticles. This result is in agreement with the results obtained with iron salts and allowed to completely rule out the possibility that BODIPY **1** is a fluorescent probe for the intracellular detection of Fe^{3+}.

3.4.3 Sub-cellular localization

Since the possibility of intracellular Fe^{3+} signaling by BODIPY **1** was ruled out, co-localization studies with different commercial fluorescent probes were carried out in order to assess the subcellular distribution of the BODIPY **1** derivative in the presence of mSLN.

In a first step, the fluorescence pattern of BODIPY in the presence of this type of nanoparticles was considered, suggesting its accumulation in specific places in the cytoplasm of cells. Therefore, the possible affinity of BODIPY **1** to lysosomes was studied, since these are cell organelles located in the cytoplasm of eukaryotic cells, whose main function is cell digestion. Lysosomes incorporate a variety of digestive enzymes in their interior capable of degrading both particles coming from the external environment and structures of the cell itself.[111–113]

Thus, HeLa cells were treated with mSLN (1 mM) and then incubated with BODIPY derivative **1** (40 μM), and the commercial LysoTracker™ Deep Red probe, which is a selective fluorescent marker for lysosomes. The fluorescence of BODIPY **1** is observed through the green channel with the 488 nm excitation laser (**Figure 45A**), while the fluorescent labeling by the commercial probe is detected through the red channel with the 633 nm excitation laser (**Figure 45B**). Given this, it was possible to verify that these fluorescence patterns are not similar, as evidenced after the overlapping of the two images. (**Figure 45C**). If this were observed, the resulting color from the red and green fluorescence overlap would be yellow. So, this result suggests that the BODIPY **1** derivative is not located in lysosomes after mSLN internalization into HeLa cells.

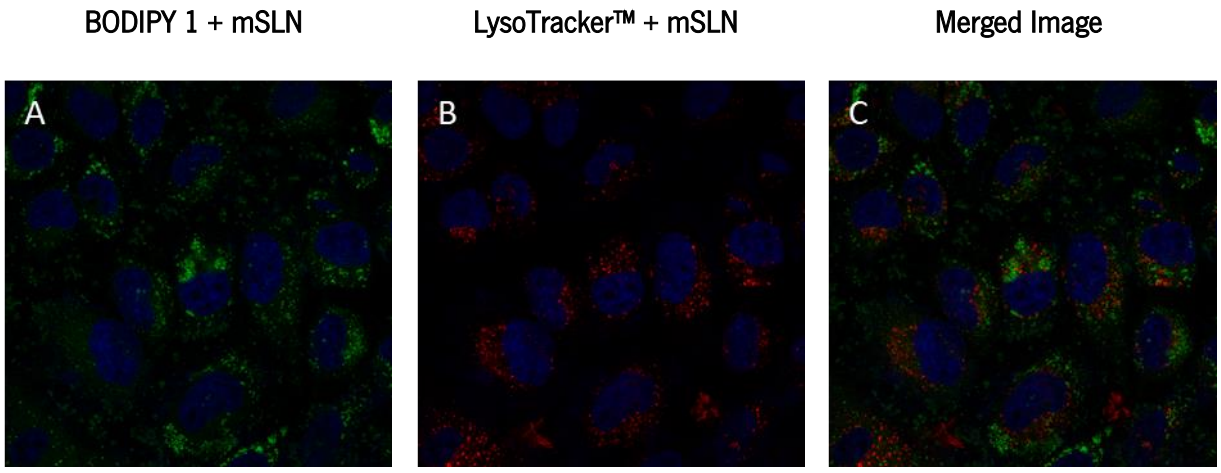

Figure 45. *Fluorescence confocal microscopic images of living HeLa cells treated with mSLN (1 mM) and incubated with BODIPY* ***1*** *(40 µM) and LysoTracker™ Deep Red probe. (A) Image of BODIPY* ***1;*** *(B) image of LysoTracker™ Deep Red probe. (C) Overlapped image of (A) and (B).*

In a second step, the structure of the mSLN was considered and, once the intracellular detection of Fe^{3+} was discarded, it was decided to investigate whether BODIPY **1** is able to signal the presence of lipids in cells, since, as mentioned above, these nanoparticles are constituted by lipids. Therefore, the commercial probe LipidSpot ™ was used for rapid and specific labeling of lipid droplets in the cells, to see if there was an overlap between the fluorescence of the commercial probe and BODIPY **1**, indicating the affinity of compound **1** for lipid clusters.

Thus, the cells were first treated with mSLN (1 mM) and then incubated with the BODIPY **1** (40 µM) and the LipidSpot™ probe to be further analyzed by confocal microscopy. Through this essay, it was seen that the fluorescent labeling of BODIPY **1** (**Figure 46A**) shows a pattern similar to the fluorescent labeling of the commercial lipid droplet probe (**Figure 46B**). After the overlap of these images, there is a perfect co-localization between the green channel and the red channel, which results in a yellow signal (**Figure 46C**).

Based on these results, it can be seen that BODIPY **1** behaves similarly to the commercial probe, which suggests that this compound has an affinity for lipid clusters. Thus, it was concluded that BODIPY **1** can detect lipid clusters induced by mSLN internalization inside cells through an increase in their fluorescence intensity.

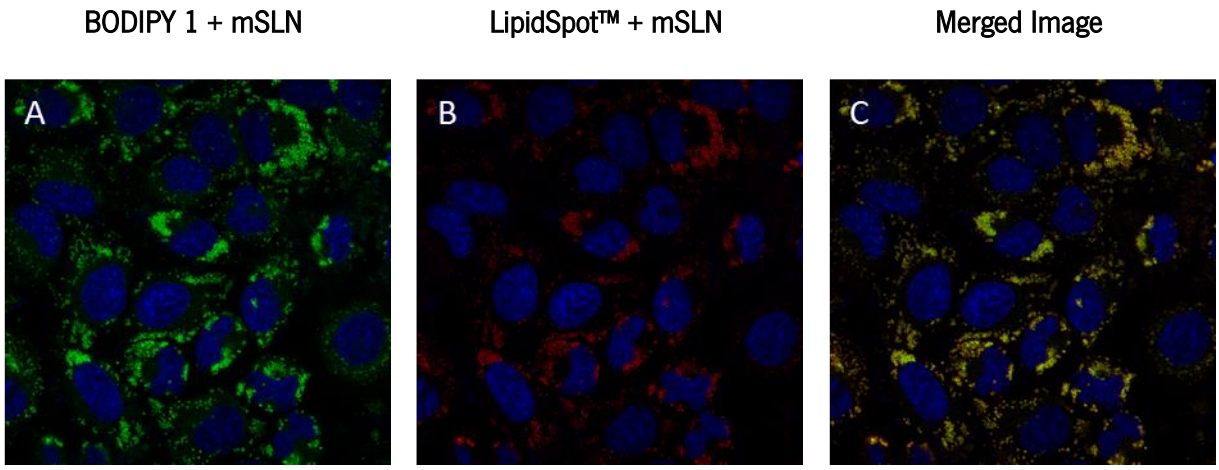

Figure 46. *Fluorescence confocal microscopic images of living HeLa cells treated with mSLN (1 mM) and incubated with BODIPY* ***1*** *(40 µM) and LipidSpot™ probe. (A) Image of BODIPY* ***1****; (B) image of LipidSpot™ probe. (C) Overlapped image of (A) and (B).*

To complete the results obtained above, it was followed a specific protocol to induce the formation of lipid droplets in HeLa cells and, at the same time, to prove that BODIPY **1** is capable of labeling lipid clusters even in the absence of mSLN.

It is important to note that lipid droplets are currently seen as important cytoplasmic structures that are involved in the storage and regulation of neutral lipids in most cells. Furthermore, lipid droplets are associated with the synthesis and repair of the cell membrane and with metabolic disorders such as diabetes and obesity. In this sense, fluorescent dyes specific for this type of structure are important to visualize and monitor the active and morphological relationships of lipid droplets with other cell organelles.[114–116]

Therefore, this study consisted of treating HeLa cells overnight with 500 µM oleic acid to form vesicle-like lipid droplets in the cytoplasm. Then, the cells were incubated with the commercial probe LipidSpot™ to label the lipid droplets and, finally, they were incubated with BODIPY **1** (40 µM) to check if the overlap between the fluorescence of the commercial probe and BODIPY **1** occurred again, confirming its affinity for lipid droplets.

Through the images obtained by confocal microscopy, it is possible to observe again a similar fluorescence pattern between the labeling of BODIPY **1** (**Figure 47A**) and the LipidSpot™ probe (**Figure 47B**). As can be seen in the merged image (**Figure 47C**), the overlap of these two images resulted in a yellow fluorescent signal indicative of the existence of a perfect co-localization between compound **1** and the commercial lipid droplet probe.

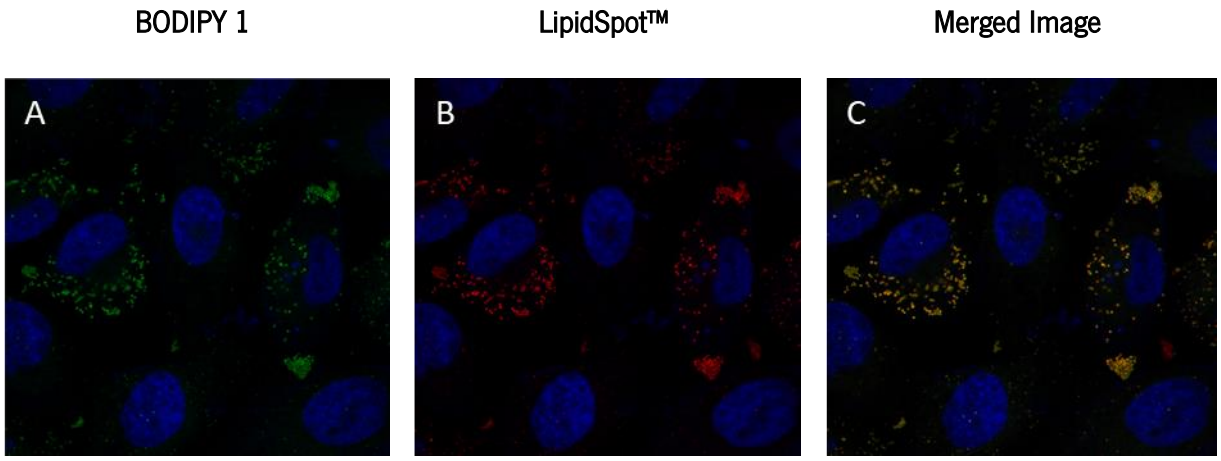

Figure 47. *Fluorescence confocal microscopic images of living HeLa cells treated overnight with oleic acid (500 μM) and incubated with BODIPY* ***1*** *(40 μM) and LipidSpot™ probe. (A) Image of BODIPY* ***1;*** *(B) image of LipidSpot™ probe. (C) Overlapped image of (A) and (B).*

With this study, it was demonstrated that BODIPY **1** has a high affinity for lipid clusters and leads to fast and efficient staining of lipid droplets in HeLa cells cytoplasm. Therefore, BODIPY **1** can be used as a fluorescent probe for intracellular detection of lipid droplets.

3.5 Evaluation of BODIPY **2** and **3** as aggregation-induced emission fluorophores

To explore the application of BODIPY derivatives as fluorescence sensors in biological media, the BODIPY derivative **3** bearing the non-planar TPA group was synthesized in order to try to observe the phenomenon of AIE. The literature describes many π-conjugate donor-acceptor systems containing the TPA group where the AIE effect is observed when aggregation is promoted in mixtures of "good and bad solvent" or in solid state.[80,117,118]

Overall, planar molecules such as BODIPY in the solid state tend to aggregate which, due to intermolecular interactions (π - π stacking interactions), results in the suppression of fluorescence emission when compared to samples in solution. With the introduction of bulky groups such as TPA, without any steric hindrance in different chromophores, there is the possibility that, in solution, the molecules are poorly fluorescent due to the intramolecular rotation of the TPA group, which favors the non-radiative deactivation of the excited state. However, when moving to solid state, an increase in

fluorescence intensity (AIE) is observed, since π - π stacking interactions and intramolecular rotation are hindered.

The spectroscopic and photophysical properties of the BODIPY **3**, bearing donor-π-conjugated spacer-acceptor, were investigated in solution and compared with the model compound BODIPY **2** (**Figure 48**).

This study was performed in solvents of different polarities (toluene and THF) and in THF:water mixtures (mixture of good and bad solvents) in order to induce aggregation and investigate the occurrence of AIE in these derivatives The study of BODIPYs **2** and **3** as AIE fluorophores was carried out at the Chemistry Department at the University of Coimbra.

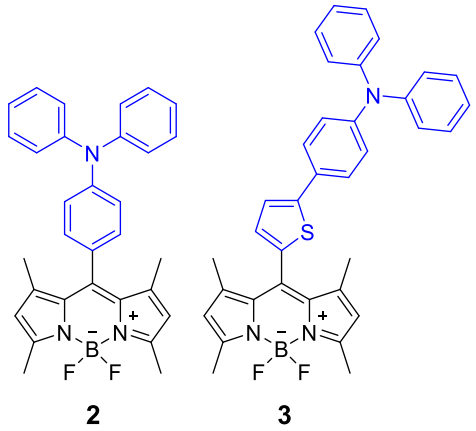

Figure 48. *Chemical structure of BODIPY derivatives **2** and **3**.*

3.5.1 Photophysical characterization of BODIPY **2** and **3**

Before proceeding with the aggregation studies, the influence of the solvent polarity on the spectroscopic and photophysical properties of BODIPY derivatives **2** and **3** was studied. In this sense, toluene was chosen as the non-polar solvent and THF as the polar solvent. The fluorescence quantum yield was obtained by the comparative method using rubrene in chloroform (ϕ_F = 0.54), as reference compound.[119]

All the results obtained for absorption and fluorescence of BODIPY derivatives **2** and **3** in the two solvents are gathered in **Table 3**.

*Table 3. Room temperature spectroscopic and photophysical data for BODIPY derivatives **2** and **3** in toluene and THF solution. (* charge transfer band)*

	λ_{abs} (nm)		λ_{em} (nm)		ϕ_F		Δ_{SS} (cm^{-1})	
	Toluene	THF	Toluene	THF	Toluene	THF	Toluene	THF
BDP 2	504	500	515	512 * 650	0.44	0.12	423	468 * 4615
BDP 3	518	514	530 * 610	525 * 690	0.02	0.006	437 * 2911	407 * 4962

Regarding the absorption spectra (**Figure 47**), both BODIPY derivatives showed intense absorption bands in the spectral region between 500 - 518 nm, assigned to the π - π* transition of the BODIPY unit. For both compounds with the increase in solvent polarity a small blue-shift 4 nm was observed in the absorption maximum. Comparison between BODIPYs **2** and **3** shows that in both solvents the absorption and emission spectra of BODIPY **3** are shifted to longer wavelengths than BODIPY **2**, which indicates that the introduction of the thiophene unit increases the conjugation for all π-conjugated molecule (**Table 3**).

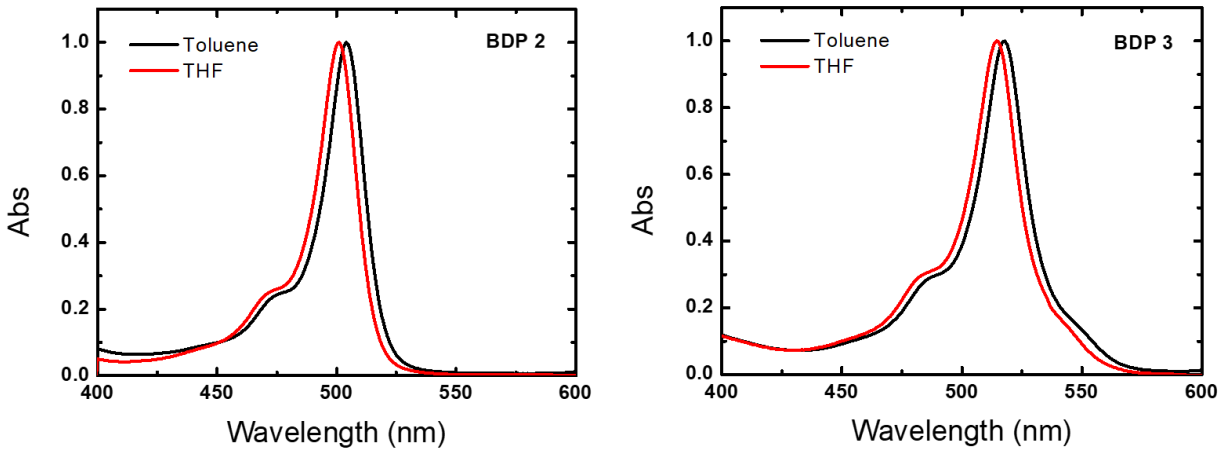

*Figure 49. Normalized absorption spectra of the BODIPY derivatives **2** and **3** in toluene and THF.*

Regarding the emission spectra (**Figure 50**), it was possible to observe large differences in the emissive behavior of these compounds with the polarity of the solvent. The maximum emission wavelength of BODIPY **2** (515 nm) and BODIPY **3** (530 nm) also exhibits a slight blue shift with

increasing solvent polarity (3 and 5 nm respectively). The fluorescence intensity decreases drastically with the increase of the solvent polarity, changing from a fluorescence quantum yield of 0.44 to 0.12 in the case of BODIPY **2** and from 0.02 to 0.006 in the case of BODIPY **3** (**Table 3**). It should be noted that the quantum fluorescence yields of BODIPY **2** are higher than those of BODIPY **3**. This may be due to the greater stereo effect caused by the methyl groups in the rotational movement of the TPA group, which makes BODIPY **2** structurally more rigid, decreasing the efficiency of the non-radiative excited state decay process. As a result of the restriction in intramolecular rotations, the BODIPY **2** derivative becomes more emissive than the BODIPY **3**.

In addition to the decrease in fluorescence intensity of the characteristic BODIPY fluorescence emission band (which in this case is associated with the emission of a locally excited state), with increasing solvent polarity, a largely red-shifted emission band appear with maximum emission at 650 nm for BODIPY **2** and 690 nm for BODIPY **3** (**Figure 50**). According to the literature, this new band is attributed to the occurrence of intramolecular charge transfer in the excited state between the electron donor units TPA and TPA-thiophene and the BODIPY core (electron acceptor).[120] This phenomenon is generally stabilized by the effect of polar solvent solvation and is responsible for the decrease in the quantum yield of fluorescence with increasing solvent polarity (ϕ_F = 0.44 vs. 0.12 for BODIPY **2** and ϕ_F = 0.02 vs. 0.006 for BODIPY **3** in toluene and THF, respectively (**Table 3**)), as it promotes the non-radiative deactivation of the excited of these BODIPY derivatives.

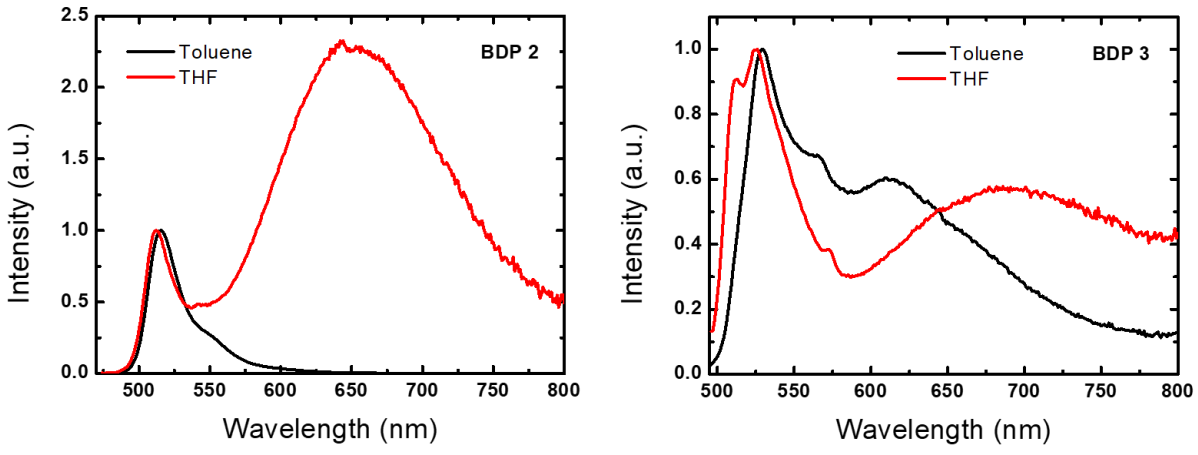

Figure 50. *Normalized emission spectra of the BODIPY derivatives **2** and **3** in toluene and THF.*

It should be noted that contrary to what is observed for BODIPY derivative **2** where in toluene only the characteristic emission band of BODIPY is observed, for the BODIPY derivative **3** the charge

transfer band is observed both in toluene (λ_{max} = 610 nm) as in THF (λ_{max} = 690 nm). This effect has been reported in the literature for other BODIPY derivatives in moderately polar solvents, thus showing that the emission properties of the BODIPY derivatives do not follow the classical solvatochromic behavior but also depend on the nature of the substituent groups.[81,121,122]

Finally, the Stokes' shifts obtained for the emission band at higher energies characteristic of the BODIPY chromophore are relatively low (Δ_{ss}= 407 – 468 cm^{-1}) which is usual for this class of compounds[13], while the Δ_{ss} values associated with lower energy bands had high values (2911 – 4962 cm^{-1}), which supports the assignment of these bands to a CT band (**Table 3**).

3.5.2 Aggregation-induced emission study

After studying the emission behavior of BODIPY derivatives **2** and **3** in toluene and THF, their optical properties were investigated in a medium with higher polarity through THF/water mixtures. Since BODIPY derivatives are not soluble in water, it is expected that they aggregate in an aqueous medium with a high percentage of water. Successive addition of water to the THF solution results in an increase in solvent polarity and complete quenching of the CT band fluorescence. However, red fluorescence is usually recovered by the AIE process. The formation of aggregates in an aqueous medium restricts the intramolecular rotations of the molecule, which leads to an increase in the emission intensity.[121,123]

In this sense, a spectroscopic study (fluorescence absorption and emission) of BODIPY **2** and **3** derivatives was carried out in different THF:water mixtures.

The emission spectra of both compounds present a band relative to the LE state of BODIPY and a lower energy CT band. Concerning the emission of BODIPY **2** and **3**, the addition of 50% of water to the THF solution causes a total extinction of the fluorescence intensity of the CT band. It is noteworthy that for the water fractions of 80 and 90%, an increase in the emission intensity of the CT band was observed (**Figures 51**). However, in general, solutions of BODIPY derivatives **2** and **3** exhibit low fluorescence quantum yields (ϕ_F = 0.070 and 0.0069 respectively (**Table 4**)).

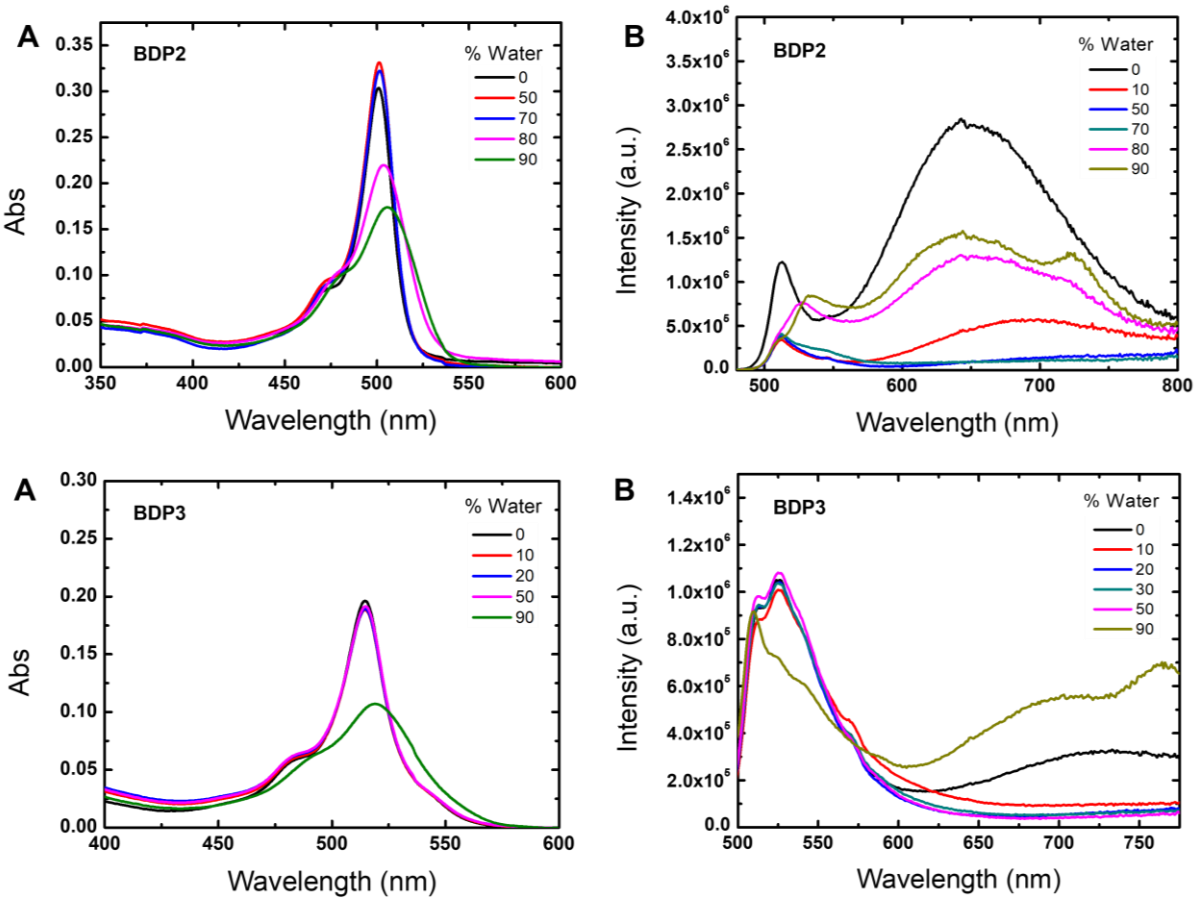

Figure 51. *(A) Absorption and (B) emission spectra of BODIPY derivative **2** (top) and **3** (bottom) in THF/water mixtures with different fractions of water. Excitation wavelength: 470 nm and 490 nm, respectively.*

Table 4. *Quantum fluorescence yield of BODIPY derivatives **2** and **3** in THF/water mixture.*

BODIPY 2		BODIPY 3	
% Water	ϕ_F	% Water	ϕ_F
0	0.12	0	0.0055
10	0.027	10	0.0041
50	0.010	20	0.0036
70	0.010	30	0.0036
80	0.062	50	0.0035
90	0.070	90	0.0069

The red-shift in the absorption spectra of derivatives BODIPY **2** and **3** (**Figure 51**) with the increase in the water fraction suggests the formation of J-aggregates (head-to-tail type aggregates),

which is in agreement with the observation of fluorescence emission for these aggregates. Indeed, H-type aggregates are in general non-fluorescent.[124]

Therefore, with this study, it was concluded that for BODIPY **2** and **3** derivatives the AIE effect is not observed since, after promoting aggregation, a significant increase in fluorescence emission was not seen.

3.6 Evaluation of BODIPY **4** as photosensitizer for photodynamic therapy

Finally, BODIPY derivative **4** was the last compound studied in this dissertation (**Figure 52**). The evaluation of this compound as photosensitizer in photodynamic therapy was carried out at the Chemistry Department at the University of Coimbra.

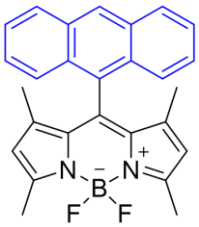

4

Figure 52. *Chemical structure of BODIPY derivative* ***4****.*

3.6.1 Photophysical characterization of BODIPY **4**

The photophysical characterization of the BODIPY derivative **4** was investigated in THF as polar solvent. The fluorescence quantum yield was obtained by the comparative method using rubrene in chloroform (ϕ_F = 0.54), as fluorescence reference compound, and the singlet oxygen sensitization quantum yield was obtained using TPPo in THF (ϕ_Δ = 0.60) as singlet oxygen sensitizer reference compound.[119,125]

Table 5 shows the absorption and emission features of BODIPY **4** as well as its oxygen sensitization quantum yield (ϕ_Δ).

*Table 5. Room temperature spectroscopic and photophysical data for the BODIPY derivative **4** in THF solution.*

λ_{abs} (nm)	λ_{em} (nm)	ϕ_F	Δ_{SS} (cm^{-1})	ϕ_Δ
505	515	0.43	384	0.27

The compound showed an intense absorption band with maximum at 505 nm and an emission band centered at 515 nm (**Figure 53**). The bands observed in the region with λ < 400 nm are characteristic of the anthracene group present at the *meso* position of the BODIPY core.[126]

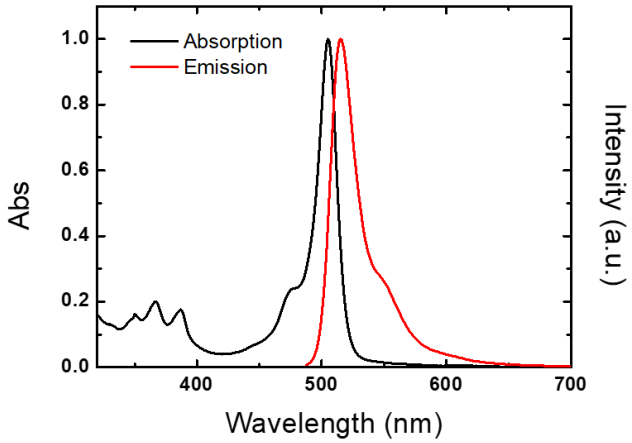

***Figure 53.** Normalized absorption and emission spectra of the BODIPY derivative **4** in THF.*

The Stokes' shift obtained was relatively low, however, it is characteristic of this class of compounds.[13] Additionally, BODIPY **4** exhibited an efficient fluorescence emission, showing a fluorescence quantum yield value of 0.43 in polar solvent. Moreover, to evaluate the ability of the BODIPY derivative as PDT agent, singlet oxygen sensitization quantum yield was determined, and it was found to be 0.27 (**Table 5**). The satisfactory singlet oxygen sensitization efficiency of this compound in THF solution suggested its potential as a photosensitizer for *in vitro* studies.

3.6.2 Dark cytotoxicity assay

The cytotoxicity of the BODIPY derivative **4** was evaluated in 4T1 cells in the absence of radiation, using the Resazurin standard method. 4T1 cells were treated with different concentrations of BODIPY **4** (3.125, 6.25, 12.5, 25, 50, and 100 μM) and, after 24 hours of incubation, the percentage

of viable cells were analyzed. Compared to the control (untreated cells), it was found that the cell viability remained high even at higher concentrations of BODIPY **4**, which means that the compound does not induce any cytotoxic effect in 4T1 cells (**Figure 54).** Statistical analysis of the results also proves the non-toxicity of the compound to 4T1 cells since there is no statistically significant difference in cell viability between the groups of cells treated with different concentrations of compound and the control of untreated cells. Hence, BODIPY **4** demonstrated to be biocompatible and suitable for further experiments.

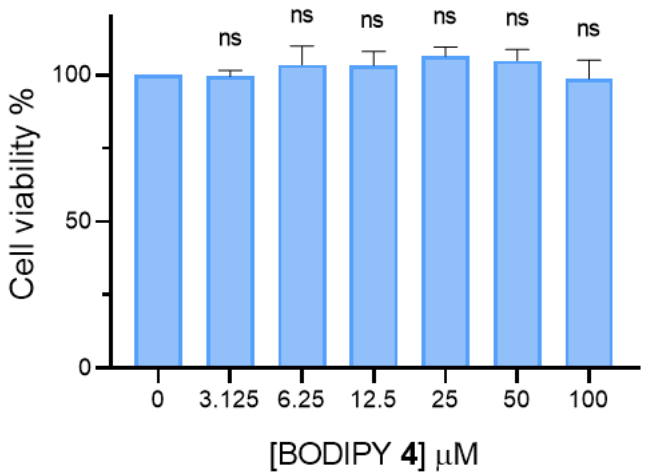

Figure 54. *Evaluation of the 4T1 cells viability after 24 hours of incubation with different concentrations of BODPIY* ***4.*** *Cell viability was determined using the Resazurin method. Data are presented as mean ± standard deviation and ns indicates the statistical significance between the cell viability of treated and untreated groups.*

3.6.3 Uptake assay

To investigate the cellular internalization of BODIPY **4**, uptake studies were performed in 4T1 cell line. The cells were treated with compound **4** (2.5 μM) and analyzed after different incubation times (0.5, 1, 3, and 6 hours) by flow cytometry.

Flow cytometry is an analytical technique widely used in biological studies which allows a rapid analysis of several parameters in a complex sample. This system analyzes each cell or particle suspended in a liquid flow that moves through a beam of light. Cell light scattering and fluorescence are measured using various detectors and filters and, after the computational analysis, different types of information about the physiological and chemical properties of each individual particle are acquired. The main cell properties characterized by this technique are size, shape, and fluorescence intensity.[127,128]

This study aimed to detect the presence of BODIPY **4** within 4T1 cells and understand the influence of the incubation time on the internalization of the compound. In this sense, the mean fluorescence intensity of the cells was measured for each incubation time (**Figure 55**).

According to these results, it was possible to verify a good internalization of compound **4** by the cells, even for short incubation times. These results were further confirmed by a confocal microscopy assay which proved that BODIPY **4** could stain the cells and be internalized. Additionally, it was observed that the incubation time influences the internalization of the compound since it was observed a gradual increase in the mean fluorescence intensity inside the cells with the increase of the incubation time. Statistical analysis of the results also proves that there is a statistically significant difference in compound internalization between shorter incubation times and 6 hours of incubation, even though it was observed an efficient uptake for shorter incubation times (**Figure 55**).

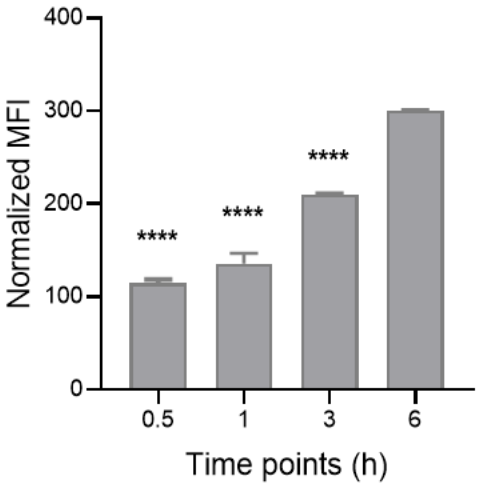

Figure 55. *Flow cytometry analysis of cellular uptake of the BODIPY **4** (2.5 μM) in 4T1 cells after 0.5, 1, 3 and 6 hours of incubation. Data are presented as mean ± standard deviation and **** indicates the statistical significance between shorter incubation times and 6 hours of incubation.*

Therefore, it was concluded that compound **4** is able to cross the cellular membrane and the uptake process was time-dependent, showing a greater internalization for longer incubation times.

3.6.4 Photocytotoxicity assay

Once the biocompatibility in the dark and the good internalization of the BODIPY **4** in 4T1 cells were confirmed, its photocytotoxicity was investigated. In this study the cells were incubated with different concentrations of compound **4** for 30 minutes, followed by irradiation of the cells with an appropriate LED (505 nm, 3 mW/cm^2) for 6 minutes. After 24 hours of incubation, cell viability was determined by the Resazurin method.

According to the results shown in **Figure 56**, after irradiation at concentrations below 5 μM of the compound it was not observed a cytotoxic effect, showing a percentage of live cells greater than 78%. However, after irradiation at a concentration of 5 μM of the compound, it was observed a clear decrease of cell viability to 28%. Additionally, the half-maximal inhibitory concentration (IC_{50}) value of BODIPY **4** against 4T1 cells was calculated to be 2.7 μM, which means that only 2.7 μM leads to 50% of cell death after irradiation under the conditions mentioned above. Thus, BODIPY **4** showed a significant phototherapy effect upon laser irradiation, inducing a significant cellular death with only 5 μM of the compound.

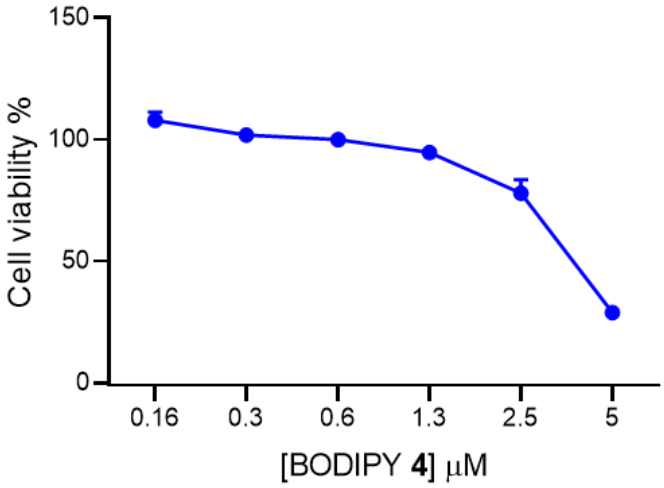

Figure 56. *Photocytotoxicity of BODIPY **4** against 4T1 cells at different concentrations (0.16, 0.3, 0.6, 1.3, 2.5 and 5 μM).*

Overall, these results demonstrated the strong potential of BODIPY **4** as photosensitizer for PDT due to its good uptake by 4T1 cells, high phototoxicity after green light irradiation, and non-cytotoxicity in the absence of light. Furthermore, BODIPY **4** may be considered promising for application in

theragnostic as it combines an efficient fluorescence emission for bioimaging diagnosis and a notable photosensitization performance for PDT treatment.

Finally, it is important to mention that although BODIPY **4** is activated within the green region of the electromagnetic spectrum and not in the NIR therapeutic range, it could be applied in the treatment of superficial cancers such as skin or oral cancers.

Chapter 4

Conclusions and Perspectives

4. Conclusions and Perspectives

The new BODIPY **3** derivative functionalized with the thiophene-TPA group at the *meso* position of the BODIPY core was synthesized through two reaction steps. The precursor aldehyde **3'** was first synthesized by a Suzuki reaction between 5-bromo-2-thiophenecarboxaldehyde and 4-(diphenylamino)phenylboronic acid with a yield of 86%, followed by a condensation reaction between 2,4-dimethylpyrrole and 5-(4-(diphenylamino)phenyl)thiophene-2- carbaldehyde (**3'**) to obtain pure BODIPY **3** in 2.8% yield. BODIPY derivative **4** functionalized at the *meso* position with the anthracene group was prepared by condensation reaction between 2,4-dimethylpyrrole and the commercial anthracene-9-carbaldehyde, giving the pure compound with a yield of 26%. The synthesized BODIPY derivatives were characterized using mass spectrometry and ^{1}H and ^{13}C NMR spectroscopy techniques, from which it was possible to verify the chemical structures and the purity of the compounds.

The photophysical characterization of BODIPY derivative **1** was evaluated in acetonitrile and demonstrated a relatively good value of fluorescence quantum yield (ϕ_F = 0.148) which could be probably explained due to the combination of the planarity of the naphthalen-1-yl π-conjugate group with the strong donor effect of the *N,N*-dimethylamino moiety. Due to their photophysical properties, studies concerning its application as optical chemosensor and fluorescent probe for bioimaging were also performed.

The evaluation of the BODIPY **1** derivative as an optical chemosensor was carried out in solutions of acetonitrile and acetonitrile/water (75:25). The results of this study showed an increase in the selectivity of the compound in aqueous media, with a fluorimetric response to Pd^{2+}, Hg^{2+}, Fe^{3+}, and Al^{3+}. Regarding the respective spectrofluorimetric titrations in an aqueous medium, a more efficient response was obtained for Fe^{3+} compared to the other ions, however, in all cases, a high number of ion equivalents was necessary to achieve the maximum increase in the fluorescence intensity of the compound. The fluorescent behavior suggests that the signaling mechanism involved in cation coordination is the PET process, since the increasing addition of ions to the compound solution causes an increase in the fluorescence intensity of the compound, without changing the emission band.

Contrary to expected, studies carried out with BODIPY derivative **1** in HeLa cancer cells demonstrated that the compound is not a Fe^{3+} fluorescent probe in an intracellular medium. On the other hand, it was found that the derivative is biocompatible with this cell line, and, through the

fluorescence images acquired by confocal microscopy, it was possible to verify that it can permeate the cell membrane, accumulating inside the cells. Furthermore, subcellular localization studies revealed that BODIPY derivative **1** has a high affinity for lipid droplets and can be used as a fluorescent probe for intracellular detection of lipid droplets in the cytoplasm of HeLa cells.

The photophysical characterization of BODIPY **2** and **3** derivatives in THF and toluene allowed to evaluate the influence of the polarity and chemical structure of the solvent on the spectroscopic and photophysical properties of these compounds. The introduction of the thiophene spacer allowed to increase the possibility of intramolecular rotation of the TPA group and BODIPY **3** conjugation, observing lower quantum yields of fluorescence and bathochromic shifts in the absorption and emission bands when compared to model compound **2**. Furthermore, it was found that the fluorescence intensity of both compounds drastically decreases with increasing solvent polarity, and a widely shifted red-shifted emission band appears due to the occurrence of intramolecular charge transfer in the excited state between the TPA and TPA-thiophene electron donor units and the BODIPY chromophore.

The spectroscopic study of BODIPY **2** and **3** derivatives, carried out in different mixtures of THF:water, allowed to conclude that there is the formation of J aggregates but the AIE effect is not observed for these compounds since, after promoting the aggregation, a significant increase in the fluorescence emission was not seen.

The photophysical characterization of the BODIPY **4** derivative in THF demonstrated a high value of fluorescence quantum yield (ϕ_F = 0.43) and singlet oxygen sensitization quantum yield (ϕ_Δ = 0.27) for this compound, which allowed its evaluation as a photosensitizer for *in vitro* studies.

The evaluation of BODIPY derivative **4** as a photosensitizer for photodynamic therapy was analyzed in 4T1 cancer cells performing uptake and viability studies in the absence and presence of radiation. The dark viability study of this compound demonstrated its biocompatibility with this cell line and the uptake study showed good internalization of the compound by the cells, even for short incubation times. Additionally, the phototoxicity study revealed that BODIPY **4** showed a significant phototherapy effect, inducing a significant cellular death upon laser irradiation. The combination of these results translates into a strong potential of BODIPY **4** as a photosensitizer for PDT and, considering its high quantum fluorescence yield, BODIPY **4** can be considered a promising compound for application in theragnostic as it combines an efficient fluorescence emission for bioimaging diagnosis and a notable photosensitization performance for PDT treatment.

In conclusion, this work revealed interesting aspects to be considered in future research concerning the PDT application of BODIPY derivatives. Some suggestions for studies to be carried out in order to support the conclusions reached and complement the work done would be:

- Optimize the experimental conditions of phototoxicity of BODIPY **4** with regard to concentration and incubation and irradiation time.
- Assess the potential of BODIPY **4** as a photosensitizer in *in vivo* studies.

Chapter 5

References

5. References

(1) Schmitt, A.; Hinkeldey, B.; Wild, M.; Jung, G. Synthesis of the Core Compound of the BODIPY Dye Class: 4,4′-Difluoro-4-Bora-(3a,4a)-Diaza-s-Indacene. *J. Fluoresc.* **2009**, *19* (4), 755–758. https://doi.org/10.1007/s10895-008-0446-7.

(2) Lakshmi, V.; Sharma, R.; Ravikanth, M. Functionalized Boron-Dipyrromethenes and Their Applications. *Rep. Org. Chem.* **2016**, *6*, 1–24. https://doi.org/10.2147/ROC.S60504.

(3) Zlatić, K.; Ayouchia, H. B. El; Anane, H.; Mihaljević, B.; Basarić, N.; Rohand, T. Spectroscopic and Photophysical Properties of Mono- and Dithiosubstituted BODIPY Dyes. *J. Photochem. Photobiol. A Chem.* **2020**, *388*, 112206. https://doi.org/10.1016/j.jphotochem.2019.112206.

(4) Bañuelos, J. BODIPY Dye, the Most Versatile Fluorophore Ever? *Chem. Rec.* **2016**, *16* (1), 335–348. https://doi.org/10.1002/tcr.201500238.

(5) Boens, N.; Verbelen, B.; Dehaen, W. Postfunctionalization of the BODIPY Core: Synthesis and Spectroscopy. *Eur. J. Org. Chem.* **2015**, *2015* (30), 6577–6595. https://doi.org/10.1002/ejoc.201500682.

(6) Clarke, R. G.; Hall, M. J. Recent Developments in the Synthesis of the BODIPY Dyes. In *Advances in Heterocyclic Chemistry*; Eric F.V. Scriven, C. A. R., Ed.; Academic Press, 2019; Vol. 128, pp 181–261. https://doi.org/10.1016/bs.aihch.2018.12.001.

(7) Liu, M.; Ma, S.; She, M.; Chen, J.; Wang, Z.; Liu, P.; Zhang, S.; Li, J. Structural Modification of BODIPY: Improve Its Applicability. *Chin. Chem. Lett.* **2019**, *30* (10), 1815–1824. https://doi.org/10.1016/j.cclet.2019.08.028.

(8) Boens, N.; Leen, V.; Dehaen, W. Fluorescent Indicators Based on BODIPY. *Chem. Soc. Rev.* **2012**, *41* (3), 1130–1172. https://doi.org/10.1039/c1cs15132k.

(9) Ni, Y.; Wu, J. Far-Red and near Infrared BODIPY Dyes: Synthesis and Applications for Fluorescent PH Probes and Bioimaging. *Org. Biomol. Chem.* **2014**, *12* (23), 3774–3791. https://doi.org/10.1039/c3ob42554a.

(10) Loudet, A.; Burgess, K. BODIPY Dyes and Their Derivatives: Syntheses and Spectroscopic Properties. *Chem. Rev.* **2007**, *107* (11), 4891–4932. https://doi.org/10.1021/cr078381n.

(11) Ulrich, G.; Ziessel, R.; Harriman, A. The Chemistry of Fluorescent Bodipy Dyes: Versatility Unsurpassed. *Angew. Chemie - Int. Ed.* **2008**, *47* (7), 1184–1201. https://doi.org/10.1002/anie.200702070.

(12) Tao, J.; Sun, D.; Sun, L.; Li, Z.; Fu, B.; Liu, J.; Zhang, L.; Wang, S.; Fang, Y.; Xu, H. Tuning the Photo-Physical Properties of BODIPY Dyes: Effects of 1, 3, 5, 7- Substitution on Their Optical and Electrochemical Behaviours. *Dyes Pigments* **2019**, *168*, 166–174. https://doi.org/10.1016/j.dyepig.2019.04.054.

(13) Boens, N.; Verbelen, B.; Ortiz, M. J.; Jiao, L.; Dehaen, W. Synthesis of BODIPY Dyes through Postfunctionalization of the Boron Dipyrromethene Core. *Coord. Chem. Rev.* **2019**, *399*, 213024. https://doi.org/10.1016/j.ccr.2019.213024.

(14) Maity, A.; Ghosh, U.; Giri, D.; Mukherjee, D.; Maiti, T. K.; Patra, S. K. A Water-Soluble BODIPY Based "OFF/ON" Fluorescent Probe for the Detection of Cd^{2+} Ions with High Selectivity and Sensitivity. *Dalton Trans.* **2019**, *48* (6), 2108–2117. https://doi.org/10.1039/c8dt04016h.

(15) Kaur, P.; Singh, K. Recent Advances in the Application of BODIPY in Bioimaging and Chemosensing. *J. Mater. Chem. C* **2019**, *7* (37), 11361–11405. https://doi.org/10.1039/c9tc03719e.

(16) Bai, J.; Qian, Y. Construction of an NIR and Lysosome-Targeted Quinoline-BODIPY Photosensitizer and Its Application in Photodynamic Therapy for Human Gastric Carcinoma Cells. *Dyes Pigments* **2020**, *181*, 108615. https://doi.org/10.1016/j.dyepig.2020.108615.

(17) Kue, C. S.; Ng, S. Y.; Voon, S. H.; Kamkaew, A.; Chung, L. Y.; Kiew, L. V.; Lee, H. B. Recent Strategies to Improve Boron Dipyrromethene (BODIPY) for Photodynamic Cancer Therapy: An Updated Review. *Photochem. Photobiol. Sci.* **2018**, *17* (11), 1691–1708. https://doi.org/10.1039/c8pp00113h.

(18) Moreira, X.; Santos, P.; Faustino, M. A. F.; Raposo, M. M. M.; Costa, S. P. G.; Moura, N. M. M.; Gomes, A. T. P. C.; Almeida, A.; Neves, M. G. P. M. S. An Insight into the Synthesis of Cationic Porphyrin-Imidazole Derivatives and Their Photodynamic Inactivation Efficiency against *Escherichia Coli*. *Dyes Pigments* **2020**, *178*, 108330. https://doi.org/10.1016/j.dyepig.2020.108330.

(19) Collado, D.; Casado, J.; González, S. R.; Navarrete, J. T. L.; Suau, R.; Perez-Inestrosa, E.; Pappenfus, T. M.; Raposo, M. M. M. Enhanced Functionality for Donor-Acceptor Oligothiophenes

by Means of Inclusion of BODIPY: Synthesis, Electrochemistry, Photophysics, and Model Chemistry. *Chem. - A Eur. J.* **2011**, *17* (2), 498–507. https://doi.org/10.1002/chem.201001942.

(20) Poddar, M.; Misra, R. Recent Advances of BODIPY Based Derivatives for Optoelectronic Applications. *Coord. Chem. Rev.* **2020**, *421*, 213462. https://doi.org/10.1016/j.ccr.2020.213462.

(21) Ivaniuk, K.; Pidluzhna; Stakhira, P.; Baryshnikov, G. V.; Kovtun, Y. P.; Hotra, Z.; Minaev, B. F.; Ågren, H. BODIPY-Core 1,7-Diphenyl-Substituted Derivatives for Photovoltaics and OLED Applications. *Dyes Pigments* **2020**, *175*, 108123. https://doi.org/10.1016/j.dyepig.2019.108123.

(22) Ullah, N.; Mansha, M.; Khan, I.; Qurashi, A. Nanomaterial-Based Optical Chemical Sensors for the Detection of Heavy Metals in Water: Recent Advances and Challenges. *Trends Anal. Chem.* **2018**, *100*, 155–166. https://doi.org/10.1016/j.trac.2018.01.002.

(23) Udhayakumari, D. Chromogenic and Fluorogenic Chemosensors for Lethal Cyanide Ion. A Comprehensive Review of the Year 2016. *Sens. Actuators B Chem.* **2018**, *259*, 1022–1057. https://doi.org/10.1016/j.snb.2017.12.006.

(24) Udhayakumari, D.; Naha, S.; Velmathi, S. Colorimetric and Fluorescent Chemosensors for Cu^{2+}. A Comprehensive Review from the Years 2013-15. *Anal. Methods* **2017**, *9* (4), 552–578. https://doi.org/10.1039/c6ay02416e.

(25) Bell, T. W.; Hext, N. M. Supramolecular Optical Chemosensors for Organic Analytes. *Chem. Soc. Rev.* **2004**, *33* (9), 589–598. https://doi.org/10.1039/b207182g.

(26) Kaur, B.; Kaur, N.; Kumar, S. Colorimetric Metal Ion Sensors – A Comprehensive Review of the Years 2011–2016. *Coord. Chem. Rev.* **2018**, *358*, 13–69. https://doi.org/10.1016/j.ccr.2017.12.002.

(27) You, L.; Zha, D.; Anslyn, E. V. Recent Advances in Supramolecular Analytical Chemistry Using Optical Sensing. *Chem. Rev.* **2015**, *115* (15), 7840–7892. https://doi.org/10.1021/cr5005524.

(28) Santos-Figueroa, L. E.; Moragues, M. E.; Raposo, M. M. M.; Batista, R. M. F.; Costa, S. P. G.; Ferreira, R. C. M.; Sancenón, F.; Martínez-Máñez, R.; Ros-Lis, J. V.; Soto, J. Synthesis and

Evaluation of Thiosemicarbazones Functionalized with Furyl Moieties as New Chemosensors for Anion Recognition. *Org. Biomol. Chem.* **2012**, *10* (36), 7418–7428. https://doi.org/10.1039/c2ob26200b.

(29) Martínez-Máñez, R.; Sancenón, F. Fluorogenic and Chromogenic Chemosensors and Reagents for Anions. *Chem. Rev.* **2003**, *103* (11), 4419–4476. https://doi.org/10.1021/cr010421e.

(30) García, J. M.; García, F. C.; Serna, F.; De La Peña, J. L. Fluorogenic and Chromogenic Polymer Chemosensors. *Polym. Rev.* **2011**, *51* (4), 341–390. https://doi.org/10.1080/15583724.2011.616084.

(31) Quang, D. T.; Kim, J. S. Fluoro- and Chromogenic Chemodosimeters for Heavy Metal Ion Detection in Solution and Biospecimens. *Chem. Rev.* **2010**, *110* (10), 6280–6301. https://doi.org/10.1021/cr100154p.

(32) Christie, R. M. *Colour Chemistry*, 2nd ed.; Royal Society of Chemistry: Cambridge, England, 2015.

(33) Valeur, B.; Leray, I. Design Principles of Fluorescent Molecular Sensors for Cation Recognition. *Coord. Chem. Rev.* **2000**, *205* (1), 3–40. https://doi.org/10.1016/s0010-8545(00)00246-0.

(34) Formica, M.; Fusi, V.; Giorgi, L.; Micheloni, M. New Fluorescent Chemosensors for Metal Ions in Solution. *Coord. Chem. Rev.* **2012**, *256* (1–2), 170–192. https://doi.org/10.1016/j.ccr.2011.09.010.

(35) Suganya, S.; Naha, S.; Velmathi, S. A Critical Review on Colorimetric and Fluorescent Probes for the Sensing of Analytes via Relay Recognition from the Year 2012–17. *ChemistrySelect* **2018**, *3* (25), 7231–7268. https://doi.org/10.1002/slct.201801222.

(36) Roy, P.; Jha, A.; Yasarapudi, V. B.; Ram, T.; Puttaraju, B.; Patil, S.; Dasgupta, J. Ultrafast Bridge Planarization in Donor-π-Acceptor Copolymers Drives Intramolecular Charge Transfer. *Nat. Commun.* **2017**, *8* (1). https://doi.org/10.1038/s41467-017-01928-z.

(37) Kundu, P.; Banerjee, D.; Maiti, G.; Chattopadhyay, N. Dehydrogenation Induced Inhibition of Intramolecular Charge Transfer in Substituted Pyrazoline Analogues. *Phys. Chem. Chem. Phys.* **2017**, *19* (19), 11937–11946. https://doi.org/10.1039/c7cp01121k.

(38) Misra, R.; Bhattacharyya, S. P. *Intramolecular Charge Transfer: Theory and Applications*; Wiley-VCH: Weinheim, Germany, 2018.

(39) Yoshihara, T.; Druzhinin, S. I.; Zachariasse, K. A. Fast Intramolecular Charge Transfer with a Planar Rigidized Electron Donor/Acceptor Molecule. *J. Am. Chem. Soc.* **2004**, *126* (27), 8535–8539. https://doi.org/10.1021/ja049809s.

(40) Shao, J.; Lin, H.; Lin, H. Rational Design of a Colorimetric and Ratiometric Fluorescent Chemosensor Based on Intramolecular Charge Transfer (ICT). *Talanta* **2008**, *77* (1), 273–277. https://doi.org/10.1016/j.talanta.2008.06.035.

(41) Cheng, D.; Liu, X.; Xie, Y.; Lv, H.; Wang, Z.; Yang, H.; Han, A.; Yang, X.; Zang, L. A Ratiometric Fluorescent Sensor for Cd^{2+} Based on Internal Charge Transfer. *Sensors* **2017**, *17* (11), 1–10. https://doi.org/10.3390/s17112517.

(42) Wu, D.; Chen, L.; Lee, W.; Ko, G.; Yin, J.; Yoon, J. Recent Progress in the Development of Organic Dye Based Near-Infrared Fluorescence Probes for Metal Ions. *Coord. Chem. Rev.* **2018**, *354*, 74–97. https://doi.org/10.1016/j.ccr.2017.06.011.

(43) Okda, H. E.; El Sayed, S.; Otri, I.; Ferreira, R. C. M.; Costa, S. P. G.; Raposo, M. M. M.; Martínez-Máñez, R.; Sancenón, F. A Simple and Easy-to-Prepare Imidazole-Based Probe for the Selective Chromo-Fluorogenic Recognition of Biothiols and Cu(II) in Aqueous Environments. *Dyes Pigments* **2019**, *162*, 303–308. https://doi.org/10.1016/j.dyepig.2018.10.017.

(44) Huang, L.; Zhang, J.; Yu, X.; Ma, Y.; Huang, T.; Shen, X.; Qiu, H.; He, X.; Yin, S. A Cu^{2+}-Selective Fluorescent Chemosensor Based on BODIPY with Two Pyridine Ligands and Logic Gate. *Spectrochim. Acta - Part A Mol. Biomol. Spectrosc.* **2015**, *145*, 25–32. https://doi.org/10.1016/j.saa.2015.02.109.

(45) Xue, Z.; Liu, T.; Liu, H. Naked-Eye Chromogenic and Fluorogenic Chemosensor for Mercury (II) Ion Based on Substituted Distyryl BODIPY Complex. *Dyes Pigments* **2019**, *165*, 65–70. https://doi.org/10.1016/j.dyepig.2019.01.061.

(46) Maity, A.; Sil, A.; Nad, S.; Patra, S. K. A Highly Selective, Sensitive and Reusable BODIPY Based 'OFF/ON'' Fluorescence Chemosensor for the Detection of Hg^{2+} Ions. *Sens. Actuators B Chem.* **2018**, *255*, 299–308. https://doi.org/10.1016/j.snb.2017.08.016.

(47) Gu, Z.; Cheng, H.; Shen, X.; He, T.; Jiang, K.; Qiu, H.; Zhang, Q.; Yin, S. A BODIPY Derivative for Colorimetric Fluorescence Sensing of Hg^{2+}, Pb^{2+} and Cu^{2+} Ions and Its Application in Logic Gates. *Spectrochim. Acta - Part A Mol. Biomol. Spectrosc.* **2018**, *203* (2017), 315–323. https://doi.org/10.1016/j.saa.2018.05.094.

(48) Lo Presti, M.; Martínez-Máñez, R.; Ros-Lis, J. V.; Batista, R. M. F.; Costa, S. P. G.; Raposo, M. M.; Sancenón, F. A Dual Channel Sulphur-Containing a Macrocycle Functionalised BODIPY Probe for the Detection of Hg(II) in a Mixed Aqueous Solution. *New J. Chem.* **2018**, *42* (10), 7863–7868. https://doi.org/10.1039/c7nj04699e.

(49) Wang, L.; Ding, H.; Ran, X.; Tang, H.; Cao, D. Recent Progress on Reaction-Based BODIPY Probes for Anion Detection. *Dyes Pigments* **2020**, *172*, 107857. https://doi.org/10.1016/j.dyepig.2019.107857.

(50) Mahapatra, A. K.; Maji, R.; Maiti, K.; Adhikari, S. S.; Das Mukhopadhyay, C.; Mandal, D. Ratiometric Sensing of Fluoride and Acetate Anions Based on a BODIPY-Azaindole Platform and Its Application to Living Cell Imaging. *Analyst* **2014**, *139* (1), 309–317. https://doi.org/10.1039/c3an01663c.

(51) Wu, H.; Guo, X.; Yu, C.; Wong, W. Y.; Hao, E.; Jiao, L. Highly Photostable Ketopyrrolyl-BODIPYs with Red Aggregation-Induced Emission Characteristics for Ultrafast Wash-Free Mitochondria-Targeted Bioimaging. *Dyes Pigments* **2020**, *176*, 108209. https://doi.org/10.1016/j.dyepig.2020.108209.

(52) Terai, T.; Nagano, T. Small-Molecule Fluorophores and Fluorescent Probes for Bioimaging. *Pflugers Arch. Eur. J. Physiol.* **2013**, *465* (3), 347–359. https://doi.org/10.1007/s00424-013-1234-z.

(53) Nagano, T. Development of Fluorescent Probes for Bioimaging Applications. *Proc. Japan Acad. Ser. B Phys. Biol. Sci.* **2010**, *86* (8), 837–847. https://doi.org/10.2183/pjab.86.837.

(54) Freidus, L. G.; Pradeep, P.; Kumar, P.; Choonara, Y. E.; Pillay, V. Alternative Fluorophores Designed for Advanced Molecular Imaging. *Drug Discov. Today* **2018**, *23* (1), 115–133. https://doi.org/10.1016/j.drudis.2017.09.008.

(55) Kolemen, S.; Akkaya, E. U. Reaction-Based BODIPY Probes for Selective Bio-Imaging. *Coord. Chem. Rev.* **2018**, *354*, 121–134. https://doi.org/10.1016/j.ccr.2017.06.021.

(56) Kowada, T.; Maeda, H.; Kikuchi, K. BODIPY-Based Probes for the Fluorescence Imaging of Biomolecules in Living Cells. *Chem. Soc. Rev.* **2015**, *44* (14), 4953–4972. https://doi.org/10.1039/c5cs00030k.

(57) Ni, Y.; Zeng, L.; Kang, N. Y.; Huang, K. W.; Wang, L.; Zeng, Z.; Chang, Y. T.; Wu, J. *meso*-Ester

and Carboxylic Acid Substituted BODIPYs with Far-Red and Near-Infrared Emission for Bioimaging Applications. *Chem. - A Eur. J.* **2014**, *20* (8), 2301–2310. https://doi.org/10.1002/chem.201303868.

(58) Liu, P.; Mu, X.; Zhang, X. D.; Ming, D. The Near-Infrared Fluorophores and Advanced Microscopy Technologies Development and Application in Bioimaging. *Bioconjug. Chem.* **2020**, *31* (2), 260–275. https://doi.org/10.1021/acs.bioconjchem.9b00610.

(59) Zhang, T.; Ma, C.; Sun, T.; Xie, Z. Unadulterated BODIPY Nanoparticles for Biomedical Applications. *Coord. Chem. Rev.* **2019**, *390*, 76–85. https://doi.org/10.1016/j.ccr.2019.04.001.

(60) Zeng, L.; Jiao, C.; Huang, X.; Huang, K. W.; Chin, W. S.; Wu, J. Anthracene-Fused BODIPYs as Near-Infrared Dyes with High Photostability. *Org. Lett.* **2011**, *13* (22), 6026–6029. https://doi.org/10.1021/ol202493c.

(61) Yi, X. M.; Wang, F. L.; Qin, W. J.; Yang, X. J.; Yuan, J. L. Near-Infrared Fluorescent Probes in Cancer Imaging and Therapy: An Emerging Field. *Int. J. Nanomedicine* **2014**, *9* (1), 1347–1365. https://doi.org/10.2147/IJN.S60206.

(62) Alamudi, S. H.; Chang, Y. T. Advances in the Design of Cell-Permeable Fluorescent Probes for Applications in Live Cell Imaging. *Chem. Commun.* **2018**, *54* (97), 13641–13653. https://doi.org/10.1039/c8cc08107g.

(63) Gao, T.; He, H.; Huang, R.; Zheng, M.; Wang, F. F.; Hu, Y. J.; Jiang, F. L.; Liu, Y. BODIPY-Based Fluorescent Probes for Mitochondria-Targeted Cell Imaging with Superior Brightness, Low Cytotoxicity and High Photostability. *Dyes Pigments* **2017**, *141*, 530–535. https://doi.org/10.1016/j.dyepig.2017.03.009.

(64) Chen, T.; Chen, Z.; Liu, R.; Zheng, S. A NIR Fluorescent Probe for Detection of Viscosity and Lysosome Imaging in Live Cells. *Org. Biomol. Chem.* **2019**, *17* (26), 6398–6403. https://doi.org/10.1039/c9ob01222b.

(65) Su, D.; Teoh, C. L.; Gao, N.; Xu, Q. H.; Chang, Y. T. A Simple Bodipy-Based Viscosity Probe for Imaging of Cellular Viscosity in Live Cells. *Sensors* **2016**, *16* (9), 1397. https://doi.org/10.3390/s16091397.

(66) Li, L. L.; Li, K.; Li, M. Y.; Shi, L.; Liu, Y. H.; Zhang, H.; Pan, S. L.; Wang, N.; Zhou, Q.; Yu, X. Q.

BODIPY-Based Two-Photon Fluorescent Probe for Real-Time Monitoring of Lysosomal Viscosity with Fluorescence Lifetime Imaging Microscopy. *Anal. Chem.* **2018**, *90* (9), 5873–5878. https://doi.org/10.1021/acs.analchem.8b00590.

(67) Wu, D.; Sedgwick, A. C.; Gunnlaugsson, T.; Akkaya, E. U.; Yoon, J.; James, T. D. Fluorescent Chemosensors: The Past, Present and Future. *Chem. Soc. Rev.* **2017**, *46* (23), 7105–7123. https://doi.org/10.1039/c7cs00240h.

(68) Cao, J.; Zhao, C.; Wang, X.; Zhang, Y.; Zhu, W. Target-Triggered Deprotonation of 6-Hydroxyindole-Based BODIPY: Specially Switch on NIR Fluorescence upon Selectively Binding to Zn^{2+}. *Chem. Commun.* **2012**, *48* (79), 9897–9899. https://doi.org/10.1039/c2cc35080g.

(69) Gao, M.; Tang, B. Z. Fluorescent Sensors Based on Aggregation-Induced Emission: Recent Advances and Perspectives. *ACS Sensors* **2017**, *2* (10), 1382–1399. https://doi.org/10.1021/acssensors.7b00551.

(70) Hong, Y.; Lam, J. W. Y.; Tang, B. Z. Aggregation-Induced Emission: Phenomenon, Mechanism and Applications. *Chem. Commun.* **2009**, *29*, 4332–4353. https://doi.org/10.1039/b904665h.

(71) Mao, L.; Liu, Y.; Yang, S.; Li, Y.; Zhang, X.; Wei, Y. Recent Advances and Progress of Fluorescent Bio-/Chemosensors Based on Aggregation-Induced Emission Molecules. *Dyes Pigments* **2019**, *162*, 611–623. https://doi.org/10.1016/j.dyepig.2018.10.045.

(72) Baysec, S.; Minotto, A.; Klein, P.; Poddi, S.; Zampetti, A.; Allard, S.; Cacialli, F.; Scherf, U. Tetraphenylethylene-BODIPY Aggregation-Induced Emission Luminogens for Near-Infrared Polymer Light-Emitting Diodes. *Sci. China Chem.* **2018**, *61* (8), 932–939. https://doi.org/10.1007/s11426-018-9306-2.

(73) Vu, T. T.; Badre, S.; Dumas-Verdes, C.; Vachon, J. J.; Julien, C.; Audebert, P.; Senotrusova, E. Y.; Schmidt, E. Y.; Trofimov, B. A.; Pansu, R. B.; Clavier, G.; Meallet-Renault, R. New Hindered BODIPY Derivatives: Solution and Amorphous State Fluorescence Properties. *J. Phys. Chem. C* **2009**, *113* (27), 11844–11855. https://doi.org/10.1021/jp9019602.

(74) Tang, B. Z.; Qin, A. *Aggregation-Induced Emission: Fundamentals*; John Wiley & Sons: New Jersey, USA, 2014.

(75) Chen, Y.; Lam, J. W. Y.; Kwok, R. T. K.; Liu, B.; Tang, B. Z. Aggregation-Induced Emission:

Fundamental Understanding and Future Developments. *Mater. Horiz.* **2019**, *6* (3), 428–433. https://doi.org/10.1039/c8mh01331d.

(76) Kuimov, A. D.; Becker, C. S.; Koskin, I. P.; Zhaguparov, D. E.; Sonina, A. A.; Shundrina, I. K.; Sherin, P. S.; Kazantsev, M. S. 2-((9H-Fluoren-9-Ylidene)Methyl)Pyridine as a New Functional Block for Aggregation Induced Emissive and Stimuli-Responsive Materials. *Dyes Pigments* **2020**, *181*, 108595. https://doi.org/10.1016/j.dyepig.2020.108595.

(77) Niu, G.; Zhang, R.; Shi, X.; Park, H.; Xie, S.; Kwok, R. T. K.; Lam, J. W. Y.; Tang, B. Z. AIE Luminogens as Fluorescent Bioprobes. *TrAC - Trends Anal. Chem.* **2020**, *123*, 115769. https://doi.org/10.1016/j.trac.2019.115769.

(78) Baglan, M.; Ozturk, S.; Gür, B.; Meral, K.; Bozkaya, U.; Bozdemir, O. A.; Atilgan, S. Novel Phenomena for Aggregation Induced Emission Enhancement: Highly Fluorescent Hydrophobic TPE-BODIPY Couples in Both Organic and Aqueous Media. *RSC Adv.* **2013**, *3* (36), 15866–15874. https://doi.org/10.1039/c3ra40791h.

(79) Bui, H. T.; Mai, D. K.; Kim, B.; Choi, K. H.; Park, B. J.; Kim, H. J.; Cho, S. Effect of Substituents on the Photophysical Properties and Bioimaging Application of BODIPY Derivatives with Triphenylamine Substituents. *J. Phys. Chem. B* **2019**, *123* (26), 5601–5607. https://doi.org/10.1021/acs.jpcb.9b04782.

(80) Liu, Z.; Jiang, Z.; Yan, M.; Wang, X. Recent Progress of BODIPY Dyes With Aggregation-Induced Emission. *Front. Chem.* **2019**, *7*, 1–16. https://doi.org/10.3389/fchem.2019.00712.

(81) Hu, R.; Lager, E.; Aguilar-Aguilar, A.; Liu, J.; Lam, J. W. Y.; Sung, H. H. Y.; Williams, I. D.; Zhong, Y.; Wong, K. S.; Peña-Cabrera, E.; Tang, B. Z. Twisted Intramolecular Charge Transfer and Aggregation-Induced Emission of BODIPY Derivatives. *J. Phys. Chem. C* **2009**, *113* (36), 15845–15853. https://doi.org/10.1021/jp902962h.

(82) Qian, J.; Tang, B. Z. AIE Luminogens for Bioimaging and Theranostics: From Organelles to Animals. *Chem.* **2017**, *3* (1), 56–91. https://doi.org/10.1016/j.chempr.2017.05.010.

(83) Cherumukkil, S.; Vedhanarayanan, B.; Das, G.; Praveen, V. K.; Ajayaghosh, A. Self-Assembly of BODIPY-Derived Extended π-Systems. *Bull. Chem. Soc. Jpn.* **2018**, *91* (1), 100–120. https://doi.org/10.1246/bcsj.20170334.

(84) Abrahamse, H.; Hamblin, M. R. New Photosensitizers for Photodynamic Therapy. *Biochem. J.*

2016, *473* (4), 347–364. https://doi.org/10.1042/BJ20150942.

(85) Li, X.; Lee, S.; Yoon, J. Supramolecular Photosensitizers Rejuvenate Photodynamic Therapy. *Chem. Soc. Rev.* **2018**, *47* (4), 1174–1188. https://doi.org/10.1039/c7cs00594f.

(86) Celli, J. P., Spring, B. Q., Rizvi, I., Evans, C. L., Samkoe, K. S., Verma, S., Hasan, T. Imaging and Photodynamic Therapy: Mechanisms, Monitoring, and Optimization. *Chem. Rev.* **2010**, *110* (5), 2795–2838. https://doi.org/10.1021/cr900300p.

(87) Castano, A. P.; Demidova, T. N.; Hamblin, M. R. Mechanisms in Photodynamic Therapy: Part One - Photosensitizers, Photochemistry and Cellular Localization. *Photodiagnosis Photodyn. Ther.* **2004**, *1* (4), 279–293. https://doi.org/10.1016/S1572-1000(05)00007-4.

(88) Awuah, S. G.; You, Y. Boron Dipyrromethene (BODIPY)-Based Photosensitizers for Photodynamic Therapy. *RSC Adv.* **2012**, *2* (30), 11169–11183. https://doi.org/10.1039/c2ra21404k.

(89) Lan, M.; Zhao, S.; Liu, W.; Lee, C. S.; Zhang, W.; Wang, P. Photosensitizers for Photodynamic Therapy. *Adv. Healthc. Mater.* **2019**, *8* (13), 1–37. https://doi.org/10.1002/adhm.201900132.

(90) Turksoy, A.; Yildiz, D.; Akkaya, E. U. Photosensitization and Controlled Photosensitization with BODIPY Dyes. *Coord. Chem. Rev.* **2019**, *379*, 47–64. https://doi.org/10.1016/j.ccr.2017.09.029.

(91) Agazzi, M. L.; Ballatore, M. B.; Durantini, A. M.; Durantini, E. N.; Tomé, A. C. BODIPYs in Antitumoral and Antimicrobial Photodynamic Therapy: An Integrating Review. *J. Photochem. Photobiol. C Photochem. Rev.* **2019**, *40*, 21–48. https://doi.org/10.1016/j.jphotochemrev.2019.04.001.

(92) Agostinis, P.; Berg, K.; Cengel, K. A.; Foster, T. H.; Girotti, A. W.; Gollnick, S. O.; Hahn, S. M.; Hamblin, M. R.; Juzeniene, A.; Kessel, D.; Korbelik, M.; Moan, J.; Mroz, P.; Nowis, D.; Piette, J.; Wilson, B. C.; Golab, J. Photodynamic Therapy of Cancer: An Update. *CA. Cancer J. Clin.* **2011**, *61* (4), 250–281. https://doi.org/10.3322/caac.20114.

(93) Jiang, Z.; Shao, J.; Yang, T.; Wang, J.; Jia, L. Pharmaceutical Development, Composition and Quantitative Analysis of Phthalocyanine as the Photosensitizer for Cancer Photodynamic Therapy. *J. Pharm. Biomed. Anal.* **2014**, *87*, 98–104. https://doi.org/10.1016/j.jpba.2013.05.014.

(94) Nguyen, V. N.; Yim, Y.; Kim, S.; Ryu, B.; Swamy, K. M. K.; Kim, G.; Kwon, N.; Kim, C. Y.; Park, S.; Yoon, J. Molecular Design of Highly Efficient Heavy-Atom-Free Triplet BODIPY Derivatives for Photodynamic Therapy and Bioimaging. *Angew. Chemie - Int. Ed.* **2020**, *59* (23), 8957–8962. https://doi.org/10.1002/anie.202002843.

(95) Zhao, J.; Xu, K.; Yang, W.; Wang, Z.; Zhong, F. The Triplet Excited State of BODIPY: Formation, Modulation and Application. *Chem. Soc. Rev.* **2015**, *44* (24), 8904–8939. https://doi.org/10.1039/c5cs00364d.

(96) Kamkaew, A.; Lim, S. H.; Lee, H. B.; Kiew, L. V.; Chung, L. Y.; Burgess, K. BODIPY Dyes in Photodynamic Therapy. *Chem. Soc. Rev.* **2013**, *42* (1), 77–88. https://doi.org/10.1039/c2cs35216h.

(97) Watley, R. L., Awuah, S. G., Bio, M., Cantu, R., Gobeze, H. B., Nesterov, V. N., You, Y. Dual Functioning Thieno-pyrrole Fused BODIPY Dyes for NIR Optical Imaging and Photodynamic Therapy: Singlet Oxygen Generation without Heavy Halogen Atom Assistance. *Chem. Asian J.* **2015**, *10* (6), 1335–1343. https://doi.org/10.1002/asia.201500140.

(98) Durantini, A. M.; Heredia, D. A.; Durantini, J. E.; Durantini, E. N. BODIPYs to the Rescue: Potential Applications in Photodynamic Inactivation. *Eur. J. Med. Chem.* **2018**, *144*, 651–661. https://doi.org/10.1016/j.ejmech.2017.12.068.

(99) Rice, D. R.; Gan, H.; Smith, B. D. Bacterial Imaging and Photodynamic Inactivation Using Zinc(II)-Dipicolylamine BODIPY Conjugates. *Photochem. Photobiol. Sci.* **2015**, *14* (7), 1271–1281. https://doi.org/10.1039/c5pp00100e.

(100) Carmello, J. C.; Pavarina, A. C.; Oliveira, R.; Johansson, B. Genotoxic Effect of Photodynamic Therapy Mediated by Curcumin on *Candida Albicans*. *FEMS Yeast Res.* **2015**, *15* (4), 1–23. https://doi.org/10.1093/femsyr/fov018.

(101) Piskorz, J.; Dlugaszewska, J.; Porolnik, W.; Teubert, A.; Mielcarek, J. Boron-Dipyrromethene Derivatives Bearing *N*-Alkyl Phthalimide and Amine Substituents of Potential Application in the Photoinactivation of Bacteria. *Dyes Pigments* **2020**, *178*, 108322. https://doi.org/10.1016/j.dyepig.2020.108322.

(102) Gonçalves, R. C. R.; Pina, J.; Costa, S. P. G.; Raposo, M. M. M. Synthesis and Characterization of Aryl-Substituted BODIPY Dyes Displaying Distinct Solvatochromic Singlet Oxygen Photosensitization Efficiencies. *Dyes Pigments* **2021**, *196,* 109784.

https://doi.org/10.1016/j.dyepig.2021.109784.

(103) Pinto, S. C. S.; Gonçalves, R. C. R.; Costa, S. P. G.; Raposo, M. M. M. Synthesis and Characterization of a *meso*-Anthracene-BODIPY Derivative for Colorimetric Recognition of Cu^{2+} and Fe^{3+}. *Chem. Proc.* **2020**, *3* (1), 79, Seijas, J. A. and Tato, M. P. V. (Eds), MDPI, Basel, Switzerland. https://doi.org/10.3390/ecsoc-24-08292.

(104) Okda, H. E.; El Sayed, S.; Ferreira, R. C. M.; Gonçalves, R. C. R.; Costa, S. P. G.; Raposo, M. M. M.; Martínez-Máñez, R.; Sancenón, F. *N,N*-Diphenylanilino-Heterocyclic Aldehyde-Based Chemosensors for UV-Vis/NIR and Fluorescence Cu(II) Detection. *New J. Chem.* **2019**, *43* (19), 7393–7402. https://doi.org/10.1039/c9nj00880b.

(105) Gonçalves, R.; Nogueira, M.; Costa, S. P. G.; Raposo, M. M. M.; Functionalized BODIPY derivatives as potential fluorescent labels. *Proceedings* **2019**, *9*(1), 36; Seijas, J. A. and Tato, M. P. V. (Eds), MDPI, Basel, Switzerland, (ISBN 978-3-03897-547-2). https://doi.org/10.3390/ecsoc-22-05701

(106) Miyaura, N.; Suzuki, A. Palladium-Catalyzed Cross-Coupling Reactions of Organoboron Compounds. *Chem. Rev.* **1995**, *95* (7), 2457–2483. https://doi.org/10.1021/cr00039a007.

(107) Magde, D.; Wong, R.; Seybold, P. G. Fluorescence Quantum Yields and Their Relation to Lifetimes of Rhodamine 6G and Fluorescein in Nine Solvents: Improved Absolute Standards for Quantum Yields. *Photochem. Photobiol.* **2002**, *75* (4), 327. https://doi.org/10.1562/0031-8655.

(108) Jin, X.; Wang, S.; Yin, W.; Xu, T.; Jiang, Y.; Liao, Q.; Xia, X.; Liu, J. A Highly Sensitive and Selective Fluorescence Chemosensor for Fe^{3+} Based on Rhodamine and Its Application *in Vivo* Imaging. *Sens. Actuators B Chem.* **2017**, *247*, 461–468. https://doi.org/10.1016/j.snb.2017.03.084.

(109) Sui, B.; Tang, S.; Liu, T.; Kim, B.; Belfield, K. D. Novel BODIPY-Based Fluorescence Turn-on Sensor for Fe^{3+} and Its Bioimaging Application in Living Cells. *ACS Appl. Mater. Interfaces* **2014**, *6* (21), 18408–18412. https://doi.org/10.1021/am506262u.

(110) Dhiman, N.; Awasthi, R.; Sharma, B.; Kharkwal, H.; Kulkarni, G. T. Lipid Nanoparticles as Carriers for Bioactive Delivery. *Front. Chem.* **2021**, *9*. https://doi.org/10.3389/fchem.2021.580118.

(111) Zhu, H.; Fan, J.; Du, J.; Peng, X. Fluorescent Probes for Sensing and Imaging within Specific Cellular Organelles. *Acc. Chem. Res.* **2016**, *49* (10), 2115–2126. https://doi.org/10.1021/acs.accounts.6b00292.

(112) Ballabio, A. The Awesome Lysosome. *EMBO Mol. Med.* **2016**, *8* (2), 73–76. https://doi.org/10.15252/emmm.201505966.

(113) Ballabio, A.; Bonifacino, J. S. Lysosomes as Dynamic Regulators of Cell and Organismal Homeostasis. *Nat. Rev. Mol. Cell Biol.* **2020**, *21* (2), 101–118. https://doi.org/10.1038/s41580-019-0185-4.

(114) Tatenaka, Y.; Kato, H.; Ishiyama, M.; Sasamoto, K.; Shiga, M.; Nishitoh, H.; Ueno, Y. Monitoring Lipid Droplet Dynamics in Living Cells by Using Fluorescent Probes. *Biochemistry* **2019**, *58* (6), 499–503. https://doi.org/10.1021/acs.biochem.8b01071.

(115) DiDonato, D.; Brasaemle, D. L. Fixation Methods for the Study of Lipid Droplets by Immunofluorescence Microscopy. *J. Histochem. Cytochem.* **2003**, *51* (6), 773–780. https://doi.org/10.1177/002215540305100608.

(116) Spandl, J.; White, D. J.; Peychl, J.; Thiele, C. Live Cell Multicolor Imaging of Lipid Droplets with a New Dye, LD540. *Traffic* **2009**, *10* (11), 1579–1584. https://doi.org/10.1111/j.1600-0854.2009.00980.x.

(117) Zhang, L.; Chen, Y.; Jiang, J. Solid State Fluorescent Functionalized-Triphenylamine BODIPY Detector for HCl Vapor with High Stability and Absolute Fluorescent Quantum Yield. *Dyes Pigments* **2016**, *124*, 110–119. https://doi.org/10.1016/j.dyepig.2015.09.005.

(118) Zhang, Y. P.; Teng, Q.; Yang, Y. S.; Cao, J. Q.; Xue, J. J. Aggregation-induced Emission Properties of Triphenylamine Chalcone Compounds. *J. Fluoresc.* **2021**, *31* (3), 807–815. https://doi.org/10.1007/s10895-021-02711-6.

(119) Montalti, M.; Credi, A.; Prodi, L.; Gandolfi, M. T. *Handbook of Photochemistry*, 3rd Editio.; CRC Press: Boca Raton, USA, 2006.

(120) Zhang, T.; Brumboiu, I. E.; Grazioli, C.; Guarnaccio, A.; Coreno, M.; De Simone, M.; Santagata, A.; Rensmo, H.; Brena, B.; Lanzilotto, V.; Puglia, C. Lone-Pair Delocalization Effects within Electron Donor Molecules: The Case of Triphenylamine and Its Thiophene-Analog. *J. Phys. Chem. C* **2018**, *122* (31), 17706–17717. https://doi.org/10.1021/acs.jpcc.8b06475.

(121) Rongrong, H.; Azael Gómez Durán, C. F.; Lam, J. W. Y.; Belmonte-Vázquez, J. J.; Deng, C.; Chen, S.; Ye, R.; Peña-Cabrera, E.; Zhong, Y.; Sing Wong, K.; Zhong T. B. Synthesis, Solvatochromism, Aggregation-Induced Emission and Cell Imaging of Tetraphenylethene-Containing BODIPY Derivatives with Large Stokes Shifts. *Chem. Commun.* **2012**, *48* (81), 10099–10101. https://doi.org/10.1039/c2cc35188a.

(122) Lager, E.; Liu, J.; Aguilar-Aguilar, A.; Tang, B. Z.; Peña-Cabrera, E. Novel *meso*-Polyarylamine-BODIPY Hybrids: Synthesis and Study of Their Optical Properties. *J. Org. Chem.* **2009**, *74* (5), 2053–2058. https://doi.org/10.1021/jo802519b.

(123) Sasaki, S.; Drummen, P. C.; Konishi, G. Recent Advances in Twisted Intramolecular Charge Transfer (TICT) Fluorescence and Related Phenomena in Materials Chemistry. *J. Mater. Chem. C* **2016**, *4*, 2731–2743. https://doi.org/10.1039/c5tc03933a.

(124) An, B.; Kwon, S.; Jung, S.; Park, S. Y. Enhanced Emission and Its Switching in Fluorescent Organic Nanoparticles. *J. Am. Chem. Soc.* **2002**, *124* (48), 14410–14415.

(125) Horiuchi, H.; Tanaka, T.; Yoshimura, K.; Sato, K.; Kyushin, S.; Matsumoto, H.; Hiratsuka, H. Enhancement of Singlet Oxygen Sensitization of Tetraphenylporphyrin by Silylation. *Chem. Lett.* **2006**, *35* (6), 662–663. https://doi.org/10.1246/cl.2006.662.

(126) Jha, G.; Sahu, P. K.; Panda, S.; Singh, D. V.; Patole, S.; Mohapatra, H.; Sarkar, M. Synthesis, Photophysical Studies on Some Anthracene–Based Ionic Liquids and Their Application as Biofilm Formation Inhibitor. *ChemistrySelect* **2017**, *2* (8), 2426–2432. https://doi.org/10.1002/slct.201601964.

(127) Macey, M. G. *Flow Cytometry: Principle and Applications*; Humana Press: New Jersey, USA, 2007.

(128) McKinnon, K. M. Flow Cytometry: An Overview. *Curr. Protoc. Immunol.* **2018**, *120*. https://doi.org/10.1002/cpim.40.